

TOPICAL REVIEW • OPEN ACCESS

Recent advances in radiation-hardened fiber-based technologies for space applications

To cite this article: Sylvain Girard *et al* 2018 *J. Opt.* **20** 093001

View the [article online](#) for updates and enhancements.




IOP | ebooksTM

Bringing you innovative digital publishing with leading voices to create your essential collection of books in STEM research.

Start exploring the [collection](#) - download the first chapter of every title for free.

Topical Review

Recent advances in radiation-hardened fiber-based technologies for space applications

Sylvain Girard¹ , Adriana Morana¹, Ayoub Ladaci^{1,2,3}, Thierry Robin², Luciano Mescia³, Jean-Jacques Bonnefois⁴, Mathieu Boutillier⁵, Julien Mekki⁵, Armelle Paveau⁶, Benoît Cadier², Emmanuel Marin¹, Youcef Ouerdane¹ and Aziz Boukenter¹

¹ Univ Lyon, UJM St Etienne, CNRS, IOGS, Laboratoire Hubert Curien, UMR5516, F-42000 St Etienne, France

² iXBlue Photonics, Rue Paul Sabatier, F-22300, Lannion, France

³ Polytechnic University of Bari, Via E. Orabona, 4, 70125 Bari, Italy

⁴ iXblue, 34 Rue de la Croix de Fer, F-78100 Saint-Germain-en-Laye, France

⁵ CNES, 18 Avenue Edouard Belin, F-31400 Toulouse, France

⁶ Airbus Defense and Space, Toulouse, France

E-mail: sylvain.girard@univ-st-etienne.fr

Received 20 February 2017, revised 9 July 2018

Accepted for publication 10 July 2018

Published 1 August 2018



CrossMark

Abstract

In this topical review, the recent progress on radiation-hardened fiber-based technologies is detailed, focusing on examples for space applications. In the first part of the review, we introduce the operational principles of the various fiber-based technologies considered for use in radiation environments: passive optical fibers for data links, diagnostics, active optical fibers for amplifiers and laser sources as well as the different classes of point and distributed fiber sensors: gyroscopes, Bragg gratings, Rayleigh, Raman or Brillouin-based distributed sensors. Second, we describe the state of the art regarding our knowledge of radiation effects on the performance of these devices, from the microscopic effects observed in the amorphous silica glass used to design fiber cores and cladding, to the macroscopic response of fiber-based devices and systems. Third, we present the recent advances regarding the hardening (improvement of the radiation tolerance) of these technologies acting on the material, device or system levels. From the review, the potential of fiber-based technologies for operation in radiation environments is demonstrated and the future challenges to be overcome in the coming years are presented.

Keywords: optical fibers, space, fiber-based sensors, radiation effects, fiber optic gyroscope, rare-earth doped amplifiers

(Some figures may appear in colour only in the online journal)



Original content from this work may be used under the terms of the [Creative Commons Attribution 3.0 licence](https://creativecommons.org/licenses/by/3.0/). Any further distribution of this work must maintain attribution to the author(s) and the title of the work, journal citation and DOI.

Glossary

AOCS

Altitude and orbit control

ASE

Amplified spontaneous emission

ASPICS	Application specific photonic integrated circuits	NBOHC	Nonbridging oxygen hole center
BPF	Band pass filter	NIF	National Ignition Facility
BOTDA	Brillouin optical time domain analyzer	NSSDC	NASA Space Science Data Coordinated Archive
BOTDR	Brillouin OTDR	OFDR	Optical frequency domain reflectometry
CEA	Commissariat à l'énergie atomique et aux énergies alternatives	OFS	Optical fiber sensor
CERN	European Organization for Nuclear Research	OTDR	Optical time domain reflectometry
CL	Cathodoluminescence	PBGF	Photonic bandgap fibers
CML	Confocal microscopy of luminescence	PbP	Point-by-point
CNES	Centre National d'Etudes Spatiales	PCE	Power conversion efficiency
CW	Continuous wave	PhM	Phase mask
DE	Double-ended	PIN	Positive intrinsic negative
DFB D	istributed feedback laser	PMF	Polarization-maintaining optical fiber
DOFS	Distributed OFS	PM-LMA	Polarization-maintaining large mode area
EDRS	European data relay system	PSC	Pure silica core
EDFA	Erbium-doped fiber amplifier	RDTs	Raman distributed temperature sensor
EDFS	Erbium-doped fiber source	REDFA	Rare-earth-doped fiber amplifier
EDX	Energy dispersive x-ray	RF	Radio frequency
EPR	Electron paramagnetic resonance	RIA	Radiation-induced attenuation
ESA	European Space Agency	RI-BFS	Radiation-induced Brillouin frequency shift
EYDFA	Erbium-ytterbium-doped fiber amplifier	RI-BWS	Radiation-induced Bragg wavelength shift
EYDFS	Erbium-ytterbium-doped fiber source	RIE	Radiation-induced emission
FBG	Fiber Bragg grating	RIP	Refractive index profile
FOG	Fiber optic gyroscope	RIRIC	Radiation-induced refractive index change
FUT	Fiber under test	RT	Room temperature
GEO	Geostationary Earth orbit	SAA	South Atlantic anomaly
GLPC	Germanium lone pair center	SBS	Stimulated Brillouin scattering
GCR	Galactic cosmic rays	SE	Single-ended
GSFC	Goddard Space Flight Center	SEE	Single event effect
IR	Infrared	SMF	Single-mode optical fiber
ISS	International Space Station	SMOS	Soil moisture and ocean salinity
LADEE	Lunar Atmosphere and Dust Environment Explorer	SNR	Signal to noise ratio
LED	Light emitting diode	STE	Self-trapped excitons
LEO	Low Earth orbit	STH	Self-trapped holes
LHC	Large Hadron Collider	TID	Total ionizing dose
LIDAR	Light detection and ranging	TIR	Total internal reflection
LLCD	Lunar Laser Communications Demonstration	TNID	Total nonionizing dose
LMJ	Laser Mégajoule	UV	Ultraviolet
MCVD	Modified chemical vapor deposition	WDM	Wavelength division multiplexed
MEO	Medium Earth orbit		
MIRAS	Microwave imaging radiometer with aperture synthesis		
MMF	Multimode optical fiber		
MOF	Microstructured optical fiber		
NASA	National Aeronautics and Space Administration		

1. Introduction

There is growing interest in studying the potential of fiber-based technologies for integration in harsh or severe environments, in particular those associated with radiation constraints. The considered environments can either be natural,

such as space [1], or man-made such as those associated with fusion-related facilities [2–4], nuclear power plants [5] or high-energy physics facilities [6]. The first studies in the 1970s [7, 8] were mainly devoted to the characterization of the transmission degradation of optical fibers under irradiation, as this effect had been limiting their use for data transfer. The origins of this degradation were investigated and the radiation-induced attenuation (RIA) phenomenon, caused by the generation of optically active point defects in silica-based cores and the cladding of optical fibers [9, 10] was identified. In this topical review paper, an overview of the main parameters influencing the RIA levels and kinetics is given, explaining the observed differences in the radiation responses of the various classes of optical fibers, and showing how, by making appropriate choices during the fiber design and manufacturing, it has been possible to conceive radiation-tolerant or radiation-hardened optical fiber architectures for almost all targeted applications. The recent results obtained for rare-earth-doped optical fibers by coupling theoretical and experimental approaches are detailed, as these active fibers play a key role in the radiation response of fiber optic gyroscopes and the high-power fiber sources that are used, and will be more widely exploited for inter- and intra-satellite communications in the near future. More recently, radiation vulnerability and hardening studies have been conducted to evaluate the feasibility of using new generations of powerful fiber-based sensors in various harsh environments. These sensors are either point (FBGs) or distributed (Raman, Rayleigh or Brillouin), allowing a wide range of parameters, such as temperature, strain, liquid level or dose, to be monitored. An overview of the recently acquired knowledge is given, highlighting the remaining scientific challenges and the increasing impact of two other radiation-induced phenomena: radiation-induced emission (RIE) and radiation-induced refractive-index changes (RIRIC).

A variety of radiation environments exist. The principal ones of interest are listed in table 1 and the main parameters used to define such harsh environments are listed hereafter:

- Nature of particles: depending on the impacting particles, the relative contributions of ionization and displacement damage processes in silica differ [9, 11, 12] and so does the radiation response of silica-based optical fibers [13]. Usually, for optical-fiber-based technologies, ionization processes govern the radiation response [14, 15]. However, for environments associated with very high neutron fluences ($>10^{16}$ n cm⁻²) or heavy ions, a specific displacement damage contribution clearly appears in the optical and structural signatures of silica-based fibers and glass [16–18].
- Total ionizing dose (TID): TID is expressed in gray (Gy), and the dose corresponds to the quantity of energy ($1 \text{ Gy} = 1 \text{ J kg}^{-1}$) deposited in the considered material. In our case and throughout this review, Gy(SiO₂) is then used. An older unit is still widely used by a large fraction of the radiation effect community and especially space engineers, namely the rad: $1 \text{ Gy} = 100 \text{ rad}$.
- Dose rate: the dose rate corresponds to the speed of dose deposition within the material. It is then expressed in Gy(SiO₂) s⁻¹ for optical fibers. The dose rate strongly varies between the studied harsh environments from 10⁻⁵ to 10⁻³ Gy h⁻¹ in the case of space missions [19] up to more than a GGy h⁻¹ during the ignition shot at a megajoule class laser facility [20].
- Temperature: for a number of applications, radiation is not the sole constraint to consider when designing fiber-based optical systems. The temperature of the irradiation will strongly affect the device radiation response too. Temperatures range from very low for space missions to high, especially when considering the future generation of nuclear power plants whose sensors must be able to operate at temperatures as high as 800 °C for reactor core monitoring.
- Other constraints: many other constraints can also be present. As an example, in nuclear waste storage facilities, the waste will release hydrogen in the atmosphere [21]. This gas presence has to be taken into account when evaluating the performance of fibers or fiber sensors, as hydrogen strongly interacts with silica-based fibers [22]. Another example is possible operation in vacua, water or other liquids instead of air. In the case of multiple constraints, a vulnerability study that considers these mixed factors simultaneously is yet to be done, as the interactions between these various parameters are generally still too complex to be modeled or predicted.

Describing all these environments is outside the scope of this article. In the next paragraphs, we first recall the advantages of using fiber-based technologies under irradiation and then briefly review their possible space applications as well as the radiation constraints associated with such programs.

1.1. Advantages of fiber-based technologies in such environments

Silica-based optical fibers present a lot of advantages for operation in these harsh environments. Of course, the well-known advantages of optical fibers for telecommunications are also interesting for applications that have to operate under irradiation: their low attenuation level, high bandwidth, multiplexing capability, etc [28]. In addition to these advantages, others are more specifically operated in harsh environments. First, optical fibers are quasi-immune to most electromagnetic perturbations as their core and cladding are made of pure or doped silica glass, which is a dielectric material. This advantage is crucial for data links or diagnostics operating in megajoule class lasers, as during ignition experiments, very high parasitic currents will be generated in the coaxial cables [20, 29]. Second, fiber-based devices are usually lightweight, reliable, and crucially advantageous for integration into a spacecraft or to reduce the amount of nuclear waste in nuclear facilities. Third, with appropriate coatings, optical fibers can resist high temperatures [30]: telecom-grade acrylate-coated optical fibers can operate up to 80 °C, those with a high-temperature acrylate coating up to 180 °C, those with Ormocer up to 200 °C, and those with a

Table 1. The main characteristics of radiation environments and targeted applications for fiber-based systems.

Environment of interest	Nature of particles (direct or secondary)	Dose range Gy(SiO ₂)	Dose rate range	Temperature range	Main applications for fibers	References (and references herein)
Space	x-rays, γ -rays, protons, heavy ions, electrons	Up to 10 kGy (usually < 1 kGy)	10^{-5} to 10^{-3} Gy h ⁻¹	-200 °C to 300 °C	Data transfer, fiber lasers, gyroscopes, fiber sensing	[19]
Large Hadron Collider (LHC)	Neutral hadrons, photons, electrons and muons	Up to 100 kGy	Up to 0.1 Gy h ⁻¹	Room temperature (RT)	Data transfer, distributed sensing (dose, temperature), point sensing (humidity)	[23]
ITER	γ -rays, neutrons	Up to 10 MGy, up to 10^{18} n cm ⁻²	1 kGy h ⁻¹ and 10^{12} - 10^{14} n (cm ⁻² .s ⁻¹)	From RT to 400 °C	Data transfer, plasma diagnostics, sensing	[24]
LMJ, NIF	γ -rays, x-rays, 14 MeV neutrons	<1 kGy	>MGy s ⁻¹	RT	Data transfer laser and plasma diagnostics	[20]
Nuclear reactor core	Neutrons, γ -rays	GGy levels up to 10^{20} n cm ⁻²	Up to 10^{15} n (cm ⁻² .s ⁻¹)	From RT to up to 800 °C	Fiber sensing (temperature)	[25]
Nuclear industries	γ -rays	<10 MGy dose levels	Up to 10 kGy h ⁻¹	From RT to 400 °C	Sensing (temperature, liquid level, etc)	[26]
Nuclear waste storage	γ -rays	Up to 10 MGy	Up to 10 Gy h ⁻¹	From RT to 90 °C	Data transfer, distributed sensing	[21]
Medicine	x-rays, protons	10 mGy to 50 Gy	<1 Gy s ⁻¹	RT	Radiotherapy, proton-therapy, beam monitoring, dosimetry	[27]

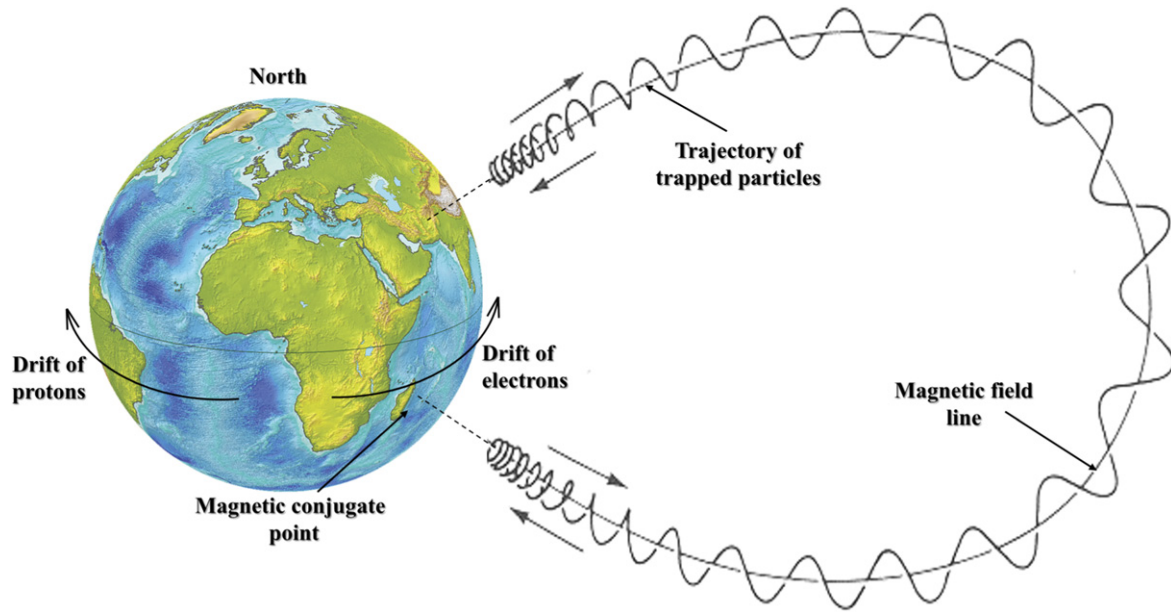


Figure 1. Near-Earth region magnetic field. Electron and proton populations are trapped in a gyration, bounce and drift movement. More details about the space environment can be found in [32].

polyimide coating up to 300 °C. It is also possible to use metal-based coatings, extending the maximal temperature of operation up to 400 °C (aluminum, copper) and 800 °C for gold-coated fibers.

1.2. Space environment

Spacecraft are exposed to a complex and aggressive environment whose characteristics depend on the targeted mission profile. Several review papers and short-courses have been devoted to the description of space-associated constraints [1, 31] such as space debris, meteoroids, strong thermal variations, vacua and energetic particles. The spacecraft, materials, devices and systems within them have to survive these constraints without their performance degrading.

As far as missions in Earth's orbit are concerned, three different environment profiles are distinguished:

- Low Earth orbit (LEO): altitude below 2 000 km, with polar inclination. LEO is the standard orbit for Earth observation satellites.
- Medium Earth orbit (MEO): altitude between 2 000 km and ~36 000 km at which most navigation systems satellites are located.
- Geostationary Earth orbit (GEO): altitude of ~36 000 km, this orbit is mainly used for telecommunication satellites.

The energetic particles that affect fiber-based technologies mainly originate from three sources: galactic and extra-galactic cosmic rays (GCR), solar energetic particles and trapped particles. The relative contributions of these different sources to the material or device degradation depend both on the mission orbit characteristics and on the basic mechanisms of the degradation associated with the tested device technology. Fiber-based devices mostly degrade through ionizing

processes, and therefore, the role of solar particles and trapped particles such as electrons and protons, has been shown to be preponderant.

Indeed GCR, due to their high atomic number and high energy, can strongly influence the amplitude of single event effects (SEE) in microelectronics, but will have a negligible impact on fiber-based systems as their associated flux of ~ 4 particles $\text{cm}^{-2} \text{s}^{-1}$ on average remains low, its intensity being anti-correlated to solar activity.

Solar energetic particles, originating either from solar flares or coronal mass ejections, as well as trapped particles, may damage fiber-based systems. Both events generate protons, electrons, neutrons, γ -rays, x-rays and heavy ions. These events are characterized by high fluxes of particles over a short period of time. The event frequency is influenced by the solar activity cycle, with a period of roughly 11 years. The energies of these particles are variable, but are anyway softer than GCR.

The Earth's magnetic field keeps electrons and protons trapped around the Earth, with the population distributions illustrated in figure 1 [32].

Particle movement follows the magnetic lines and is made of various components: drift, gyration and bounce. The proton belt mainly concerns LEO orbits. In this region, the main radiation effects are therefore TID and displacement damage. The proton spectrum extends up to energies of 500 MeV (larger energies are found in the core of radiation belts), while for MEO and GEO, the proton energies remain below 10 MeV and a few MeV, respectively. Higher fluxes of trapped protons are localized in geographic zones associated with weaker magnetic fields, noted at both Earth's poles and at the south Atlantic anomaly (SAA). The SAA region is associated with a lower magnetic flux due to the 11° tilt of the magnetic field with regards to the Earth's rotation axis, offset by 500 km towards the north Pacific. MEO and GEO orbits

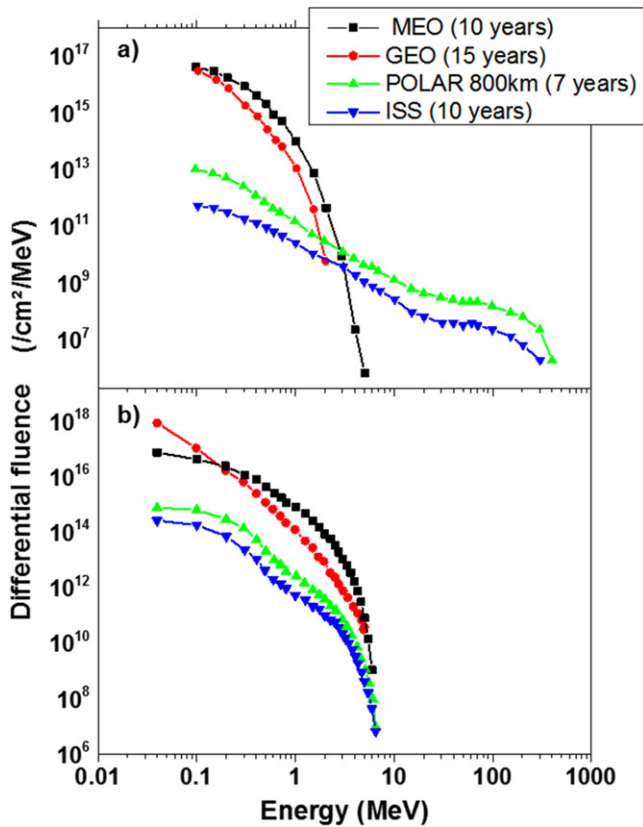


Figure 2. Trapped electron (a) and proton (b) fluences for different mission profiles and orbits. Adapted from [31].

are dominated by the electron belt, making materials and devices especially exposed to risks related to ionizing dose and charging effects here.

Radiation constraints also evolve with the technology. As an example, recent technical progress has led to the use of electric propulsion in GEO spacecraft, resulting in an increased duration to reach GEO orbit and also a longer time spent in radiation belts. This evolution is then accompanied by an increase of the TID received during the satellite on this orbit. Figure 2 presents the fluences of trapped (a) electrons and (b) protons at different orbits and for varying mission profiles [31]:

- Polar orbit (800 km), mission duration of 7 years
- International Space Station (ISS), mission duration of 10 years
- Medium Earth orbit (MEO), mission duration of 10 years
- Geostationary Earth orbit (GEO), mission duration of 15 years

To estimate the impact of these radiation contributions on the performance of a mission profile, environment models are mandatory. Such models have been developed by space researchers. One can cite the AE8 and AP8 models for trapped particles [33, 34]. These models were developed at the Aerospace Corporation for the NSSDC at NASA/GSFC, based on data from satellites flown in the 1960s and early 1970s. Improved models, the AE9 and AP9, are today under validation [35–38]. In addition, some local models have been

developed to cover the issues encountered with the AE8 and AP8, such as OPAL from ONERA, covering high-energy protons at low altitudes [39] and IGE-2006, as specific models covering electrons in GEO orbit [31]. ESCC-E-ST-10-04 [40] from ESA intends to assist in the consistent application of space environment engineering to space products through the specification of required or recommended methods, data and models to the problem of ensuring best performance, problem avoidance or the survivability of a product in space. The modeling of trapped radiation around other planets within the solar system, such as Jupiter, is today a major challenge, since solar system exploration has become a strong objective for space agencies [41].

The metrics used to measure the cumulative doses deposited inside a material while exposed to space radiation are TID and the total nonionizing dose (TNID). While the TNID effect can be considered as negligible for optical fibers in space, when those waveguides are exposed to TID, their optical absorption increases due to the generation of radiation-induced defects. Figure 3 illustrates the effects of aluminum shielding on the TID deposited inside Si-based material [42–44].

As shown in figure 3, spacecraft shielding reduces the TID at component level, however, a compromise between the additional weight embedded on the spacecraft due to shielding materials and the radiation effect on components such as optical fibers always has to be attained.

1.3. Space applications for fiber-based technologies

Various fiber-based systems are already embedded in spacecraft, and the potential for the use of many more is currently under investigation [45, 46]. The needs of these optical technologies concern various applications for different missions. Usually, the systems developed in the framework of space programs are defined as payloads. One example of payload using optical fibers concerns the light detection and ranging (LIDAR) system on the SWARM mission. This LIDAR exploits a fiber laser emitting at 1082.908 nm, single frequency (linewidth <30 kHz) and polarized. This system is used to characterize the Earth's magnetic fields [41]. Platform equipment is also being used, such as fiber optic gyroscopes (FOGs). Such equipment is based on the Sagnac effect, which will be detailed later in this review and which uses various classes of optical fibers, including rare-earth-doped optical fibers (REDFs). Numerous FOGs, such as the Astrix® family, are currently flying and present state-of-the-art performance [47, 48].

Another main field of applications concerns optical datalinks, both intra-satellite and inter-satellite (or in-orbit to ground). Concerning intra-satellite datalinks, the data can either be analog or digital. An example of the first case is the microwave imaging radiometer with an aperture synthesis (MIRAS) optical harness developed for the in-soil moisture and ocean salinity (SMOS) mission. It distributes a 56 MHz clock signal to 69L-band receivers (carrier wavelength 1300 nm, Corning SMF28 fiber) [49, 50].

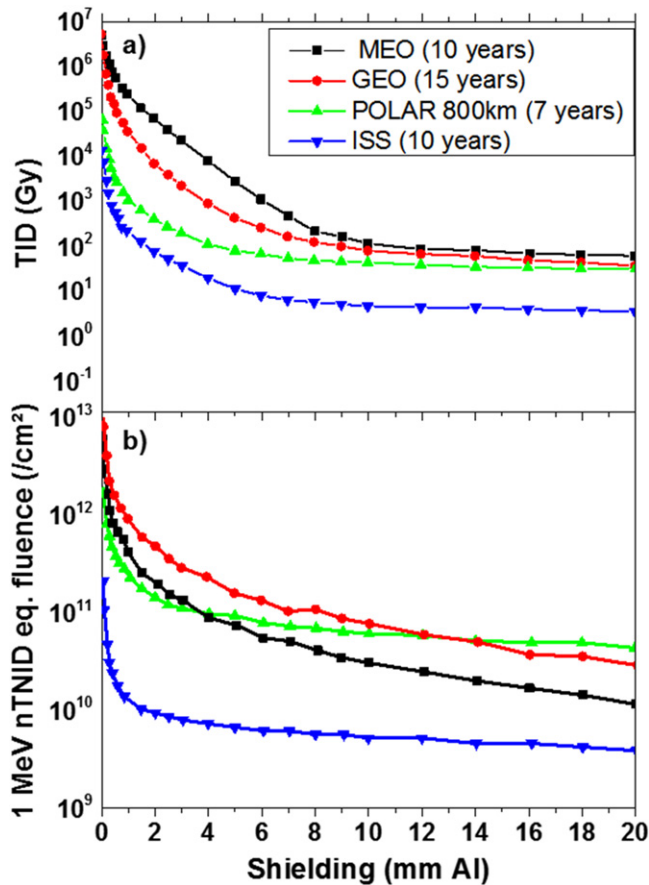


Figure 3. The total ionizing dose (TID) and (b) total nonionizing dose (TNID) calculated for a simple geometry (solid sphere) as a function of Al shielding thickness for the various mission profiles presented in figure 2. Adapted from [31].

Concerning inter-satellites or in-orbit to ground transmissions, we can cite the Lunar Laser Communications Demonstration (LLCD) project. The LLCD consists of a space terminal on the NASA Lunar Atmosphere and Dust Environment Explorer (LADEE) spacecraft and three ground terminals on Earth. Together, they demonstrate the feasibility of transferring up to 622 Mbps of data from the Moon using a space terminal of reduced weight, requiring less power and occupying a volume smaller than comparable radio frequency systems [51]. The EDRS (European Data Relay System) accelerates the transmission of data from low-orbiting satellites, such as the Sentinels, to the end-user on the ground. This is achieved by locking onto satellites with a laser beam as they pass below, and immediately relaying the information to European ground stations via a high-speed radio beam [52].

The emerging fields of applications mainly concern data transmissions. In telecommunications payloads, the introduction of fiber-based systems could lead to some technological breakthroughs. For inter-satellites and orbit-to-ground transmissions, LLCD demonstrates concept feasibility and some advantages. However, to take over RF systems, fiber-based systems must be able to procure higher bandwidth and therefore a good signal-to-noise ratio (SNR). High-power emitting laser sources are required here, with a minimum of a few Watts. The development of high-power erbium-

ytterbium-doped optical amplifiers (EYDFAs) represents the main challenge for such applications. This aspect will be discussed in more detail later in this review.

Another potential field of application for fiber-based technologies is spacecraft monitoring with distributed optical fiber sensors (DOFSs). These sensors can provide cartographies of temperature, radiation and mechanical constraints during missions. The huge potential of this DOFS technology explains why the recent advances and future challenges regarding radiation vulnerability and hardening are discussed here—even though, to the best of our knowledge, these devices have not yet been implemented in space missions.

2. Fiber-based technologies

In this chapter, we describe the operational principles and characteristics of the fiber-related technologies that are today characterized by irradiation in view of their integration into harsh environments. We first review the various classes of optical fibers, their main characteristics and the specifics necessary to understand their radiation responses. Second, the fiber Bragg grating (FBG) technology [53] is introduced, as this temperature point and/or strain sensor is today the most studied optical fiber sensor (OFS) under irradiation. Third, we introduce the distributed OFS technologies that exploit one of the light scattering phenomena (Brillouin, Rayleigh or Raman) to convert the optical fiber into a sensing element [54]. Combined with the reflectometry technique, these OFSs open the way to distributed measurements of temperature, strain [55, 56] or even radiation in harsh environments [57, 58]. This part is then followed by a description of optical devices exploiting the amplification properties of the REDFs to provide optical sources or amplifiers such as erbium or erbium-ytterbium-doped fiber sources (EDFS, EYDFS) or amplifiers (EDFA, EYDFA) [59]. These devices are the key elements of FOGs, which are a major example of space technology ensuring the inertial navigation of satellites [60]. The operation principles of the FOG are then briefly described.

There exists a large variety of optical fibers and not all will be covered by this article, which is limited to those having been evaluated under irradiation. In particular, we focus the paper on silica-based optical fibers which guide light by total internal reflection (TIR). This class of fibers represents the quasi totality of the fibers studied in the last few decades. However, some preliminary results regarding plastic optical fibers (POFs) and infrared-material-based fibers can be found in [61–65], respectively. Describing in detail the operation principles of optical fibers is outside the scope of the present review (see [28] for more details), but we recall here the main TIR fiber characteristics that will play a role in defining the performance of these waveguides when they are exposed to radiation.

These components have an optical core, made of pure or doped silica, with a refractive-index larger than that of the surrounding glass known as cladding. To ensure the mechanical hardness of the waveguide, silica material is

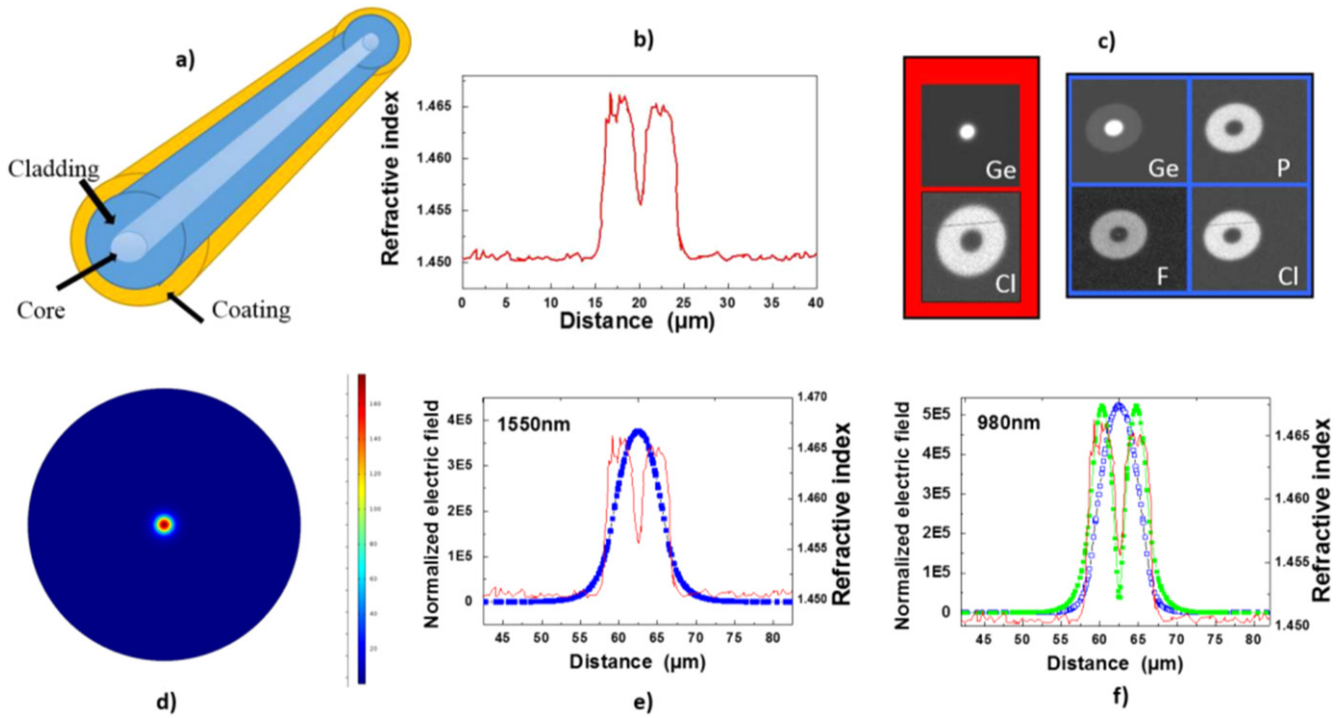


Figure 4. An illustration of (a) a telecom-grade SMF structure, (b) the RIP of this fiber, (c) 2D chemical analysis of this fiber by electron microprobe analysis, (d) a COMSOL simulation of the fundamental mode at 1550 nm, (e) a comparison between the RIP and the radial distribution of the LP_{01} mode, (f) radial distributions of the allowed LP_{01} and LP_{11} modes at 980 nm.

embedded into the coating, usually a polymer such as acrylate or polyimide, but it can also be done using a metal such as copper, aluminum or gold to allow the fiber to be used at higher temperatures. A typical fiber structure is given in figure 4(a). To modify the glass refractive index and then tune the fiber refractive-index profile (RIP) (see figure 4(b) for the typical RIP of a telecom-grade optical fiber), the glass is doped with chemical elements—or dopants—allowing the silica index to increase (germanium, phosphorus, aluminum, nitrogen) or decrease (fluorine, boron). Figure 4(c) illustrates the 2D dopant distributions measured in two telecom-grade fibers by electron microprobe analysis (EMPA). Such compositions allow the step-index single-mode fibers (SMFs), such as the one in figure 4(b), to be defined. The control of the fiber guiding properties, meaning the characteristics of the allowed guided modes at the wavelengths of interest, is achieved by defining its RIP. Knowing these profiles, the radial power distributions of the guided modes can be calculated. A 2D illustration of the fundamental LP_{01} mode has been simulated with COMSOL Multiphysics and is given in figure 4(d), and its radial distribution is compared in figure 4(e) with the fiber RIP. An important outcome of this comparison is that for SMFs only part of the light is guided into the core—an evanescent part of this mode propagates in the fiber cladding. The confinement factor (the ratio of power confined in the core versus the cladding) depends on the RIP but also strongly on the signal wavelength. As the wavelength decreases, the confinement factor increases up to a certain wavelength—the cut-off wavelength—where an additional guided mode of higher order appears and the SMFs then

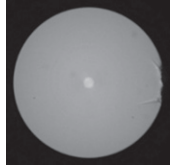

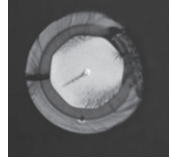
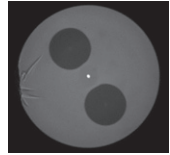
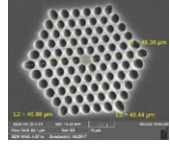
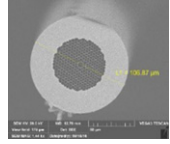
become bimodal (usually around $1.2\ \mu\text{m}$ for telecom-grade fibers). Figure 4(f) illustrates the two guided modes in the same fiber at 980 nm.

From figure 4, it clearly appears that the radiation response of an optical fiber will be complex. Indeed at the material level, the differently doped layers constituting the fiber can exhibit different radiation behavior, and the contribution of each layer to the radiation-induced changes of the fiber optical properties will depend on the fiber light guidance properties too.

2.1. Classes of optical fibers and applications

Several classes of optical fibers can be distinguished in terms of their radiation responses and application domains; their main characteristics are listed in table 2. SMF and multimode (MMF) optical fibers are of primary importance as they are used for data transfer, diagnostics and sensing in harsh environments. REDFs, or active fibers, are crucial too as they allow IR-fiber-based lasers or amplifiers to be designed. This class of fibers is particularly studied for space applications, as RE-doped fiber amplifiers and sources (REDFA and REDFs) are developed for a variety of optical functions [66], including FOGs. The radiation response of polarization maintaining optical fibers (PMFs) is of interest too, especially for space and military applications, as they are a key component of the FOG Sagnac coil. Since 2000, various architectures of microstructured optical fibers (MOFs) have become commercially available. Some of those still guide light by TIR, and they usually consist of a silica-based core surrounded by

Table 2. The main characteristics of silica-based optical fibers considered for integration in radiation environments.

Fiber categories	Typical core diameter	Typical cladding diameter	SEM or EDX picture	Key references about their radiation response
Telecom and OFS grade SMF	<10 μm	125 μm		[69–78]
Telecom and OFS grade MMF	From 50 to 100 μm	125 μm		[69, 71–74, 76–85]
REDFs	<10 μm	125 μm , ErYb fibers can have a double clad (DC) structure		[85–94]
PMF	<10 μm	125 μm		[74, 95–97]
MOF	<20 μm	125 μm		[98–100]
PBGF	<10 μm	125 μm		[18, 63, 64]

cladding microstructured with longitudinal holes. The interest in this class of optical fibers is that it can be made with a unique glass, e.g. pure-silica, be endlessly single-mode or have a large mode area for high-power devices [67]. It is also possible to use a photonic band-gap effect to guide the light in a fiber with an air core and microstructured cladding [68]. In

this case, the main interest is to have up to 98% of the light guided in air (or in another gas). If this last fiber appears very promising for operation under steady-state γ -rays [63], the cost of this technology still appears to be too high and its reliability too low for consideration as the principal candidate for most radiation-oriented applications.

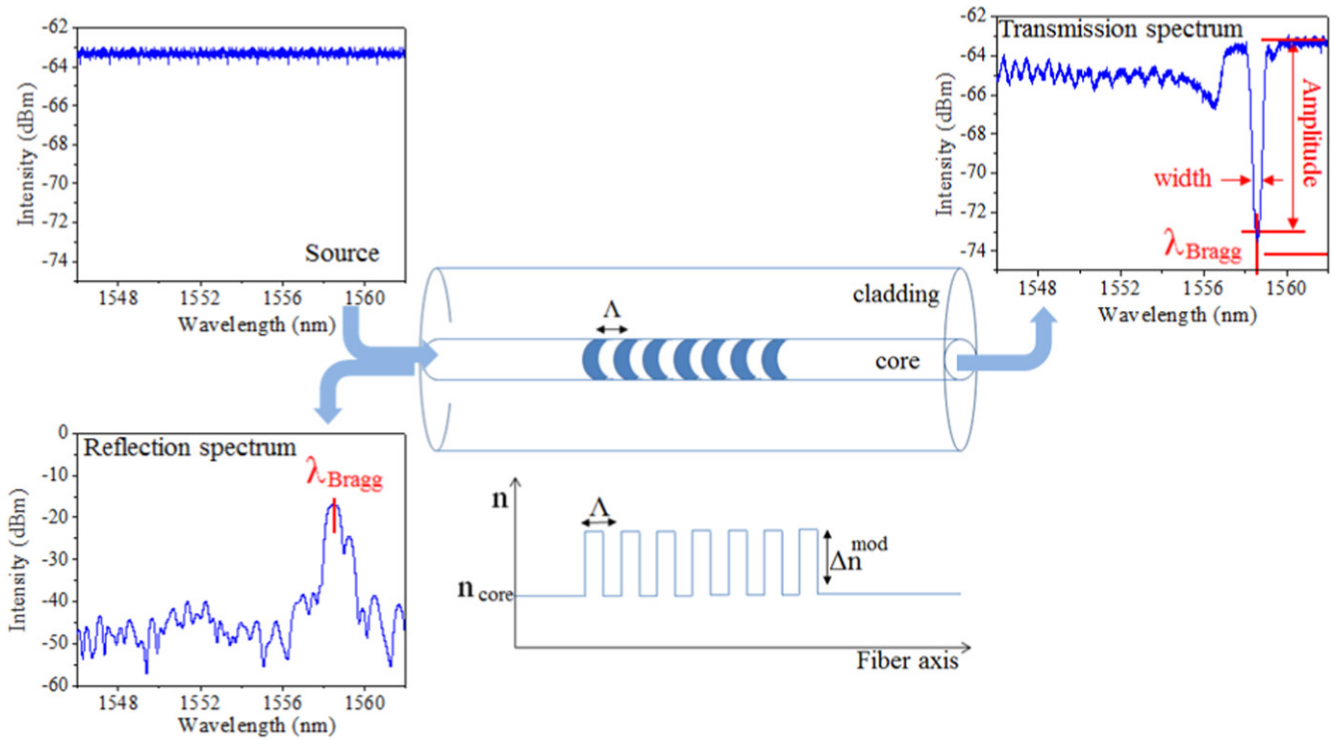


Figure 5. The schema of an FBG written in an SMF. As an example, the white light spectrum of the source injected inside the fiber core and the measured transmission and reflection spectra of the FBG are illustrated. At the center of the figure the FBG is schematically represented as a modulation of the refractive index as a function of the fiber axis. The three main parameters to define an FBG are given: Bragg wavelength, FBG peak amplitude and width.

2.2. Point sensors: fiber Bragg gratings

FBGs consist of a periodic perturbation of the core refractive index associated with a period (Λ) typically from $0.5 \mu\text{m}$ up to a few μm . Such a structure couples light from a forward-propagating mode to the backward counter-propagating mode. The coupling occurs at specific wavelengths, named Bragg wavelengths. These wavelengths are defined by equation (1) [101]:

$$\lambda_{Bragg} = \frac{2n_{eff}\Lambda}{m} \quad (1)$$

where n_{eff} is the effective refractive index of the propagating core mode and m is an integer number, called order. So, the transmission and reflection spectra of an FBG show a narrow dip or a narrow peak centered at λ_{Bragg} , respectively, as shown in figure 5.

2.2.1. FBG inscription technique. Since the first observation of an FBG in 1978 by Hill *et al* [102], several techniques have been developed and optimized for grating fabrication. The most used today are the point by point (PbP), the phase-mask (PhM) and the free space interferometry technique. The first one was established by Malo *et al*, in 1993 [103]. The PbP technique consists of generating each grating fringe, one after the other, by focusing the laser light at a point of the core, locally increasing its refractive index, and finally by translating the fiber or the laser beam by a distance corresponding to the grating period Λ , parallel to the fiber axis. The other common technique was developed by Hill

et al in 1993 [104]. This one uses a phase-mask (PhM) made with a material transparent to the laser wavelength and with one-dimensional surface relief. For the FBG inscription, the fiber is placed almost in contact with the PhM, with the grating corrugations normal to the fiber axis, while the PhM is perpendicular to the laser beam. The PhM spatially modulates the phase and diffracts the laser beam by forming an interference pattern, which causes a refractive index modulation in the fiber core. Indeed, the FBGs written through the PhM technique are highly reproducible, but at a well-defined and fixed spatial period, implying the use of a specific PhM for each grating architecture. To overcome this last constraint, more flexible methods have been identified to produce interference patterns, such as Lloyd’s mirror. However, the fine reproducibility of the final FBG is somehow difficult to control. For both techniques, the inscription laser beam can be emitted in the ultraviolet (UV) or infrared (IR) spectral regions. However, whereas UV light can be a continuous wave or pulsed in the time domain of a nanosecond or femtosecond, the IR laser pulse duration has to be a picosecond or femtosecond to efficiently produce FBGs in silica-based fibers. Due to the small energy of the IR photons, the phenomena originating the gratings can only be multi-photons, and consequently a high power density is required.

2.2.2. FBG-based sensors. FBGs are efficient strain and temperature point sensors [105]. Indeed, the Bragg wavelength λ_{Bragg} depends linearly on the axial strain (ϵ) applied to the

waveguide with no evidence of the hysteresis effect, as reported in equation (2) [101]:

$$\lambda_{Bragg}(\varepsilon) = \lambda_{Bragg}^{unstrained} + C_{\varepsilon} \cdot \varepsilon. \quad (2)$$

Typically, the strain sensitivity (C_{ε}) of a grating with a Bragg wavelength peaking at 1550 nm is about 1 pm $\mu\varepsilon^{-1}$. The grating temperature response, instead, is linear only over a small range of about 100 °C around RT:

$$\lambda_{Bragg}(T) = \lambda_{Bragg}(T_0) + C_T \cdot (T - T_0). \quad (3)$$

The temperature sensitivity C_T is about 10 pm °C⁻¹ for a bare grating at 1550 nm and is not significantly dependent on the FBG type [106]. However, this coefficient depends on the pre- or post-treatment the FBG undergoes [107], and, above all, on the selected fiber coating and packaging. For example, this sensitivity coefficient C_T can be increased by embedding the FBG in a metal plate or by using a metal coating: the thermal expansion of the metal transfers a strain to the fiber core, which affects the period and also the refractive index through the thermo-elastic effect [108].

Consecutive thermal treatments can nevertheless entail hysteresis. As demonstrated by several studies—performed above all on the most classical grating type, known as type I UV-FBG—during thermal treatment a grating can undergo degradation, which manifests itself as a reduction in the peak reflectivity and bandwidth as well as a Bragg wavelength shift towards the blue. During treatment, the decay is first rapid and then the rate decreases. A few models [109, 110], depending on the pre-treatment performed on the gratings, have been proposed to explain this degradation and allow the determination of recipes to obtain a stable FBG for application requirements. If the FBG has to be stable at the temperature T_O for an operating time t_O , after its inscription it has to undergo treatment at an annealing temperature T_A , higher than T_O , with a duration t_A that depends on the grating type and the parameters T_O , t_O and T_A [110]. The first model was proposed by Erdogan and only applies to gratings written in H₂-free fibers [109].

2.2.3. FBG classification. The first classification of FBGs separates them into two main groups, known as type I and type II, according to the basic mechanisms governing the FBG inscription. This classification is completed by specifying the spectral domain of the inscription laser, either UV or IR, as shown in figure 6.

The fabrication of type I gratings results from color center or point defect formation. These gratings cannot withstand operation temperatures higher than 600 °C, since at such temperatures all the defects at the origin of the refractive index periodic modulation Δn^{mod} are bleached. During the inscription, n_{eff} and Δn^{mod} increase and consequently λ_{Bragg} shifts towards the red, while the FBG peak reflectivity and width increase [111, 112].

A type I-UV FBG inscription is only possible thanks to the photo-sensitivity of the silica-based matrix of the fiber core. To ensure sufficient photosensitivity, the core has to be

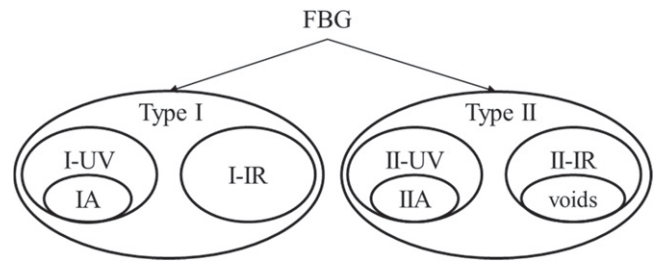


Figure 6. FBG classification.

doped with specific elements, such as Ge. In germanosilicate fibers, the FBG formation is associated with the generation of some specific Ge-related defects such as GeE' and GeH centers [113]. To further increase the fiber photosensitivity, H₂-loading can be performed before the grating inscription. For this, the selected fiber is maintained in a vessel containing the gas and ensuring its diffusion into the silica matrix at kinetics fixed by the fiber geometry, the selected pressure and temperature. The induced refractive index increase ranges between 10⁻⁵ and 10⁻³ for H₂-free Ge-doped fibers, whereas it reaches 10⁻² for H₂-loaded ones [102].

Type I-IR FBG inscription only occurs for a pulse peak intensity beyond a threshold, since the refractive index increase is induced by multi-photon processes. This threshold depends on the fiber composition, the selected writing technique, the laser system alignment accuracy and other laser-related parameters. This threshold is at about 2 × 10¹³ W cm⁻² (femtosecond laser operating at 800 nm) for a Ge-doped fiber with the PhM technique [114, 115]. When the pulse energy, and consequently the pulse peak intensity, increases beyond a threshold, type II FBGs are written. The growth rate of these FBGs is faster than that of type I. Moreover, they exhibit higher reflectivity and a larger peak width, resulting in a reduction of the effective grating length (typically from a few mm to 2 cm). These type II gratings are more thermally stable than type I but have reflection spectra of lower quality [116, 117].

The origin of type II-UV gratings is the laser damage induced at the fiber core-cladding interface [116], whereas for type II-IR FBGs, it is assumed to be related to silica densification induced by femtosecond radiation at a high power density. As an example, the pulse peak intensity threshold is at about 5 × 10¹³ W cm⁻² (a femtosecond laser operating at 800 nm) for a Ge-doped fiber and the PhM technique [117].

Concerning the UV-FBGs, two other groups can be highlighted:

- Type IA FBGs are written in highly photosensitive fibers, such as hydrogenated Ge-doped or B/Ge co-doped optical fibers, after prolonged UV exposure. They exhibit a large red-shift of the central wavelength during inscription. Such a shift can be associated with a large increase of the mean refractive index of the core, of about 2 × 10⁻² [118].
- Type IIA FBGs are regenerated gratings written in highly Ge-doped, B/Ge or Sn/Ge co-doped fibers, with or

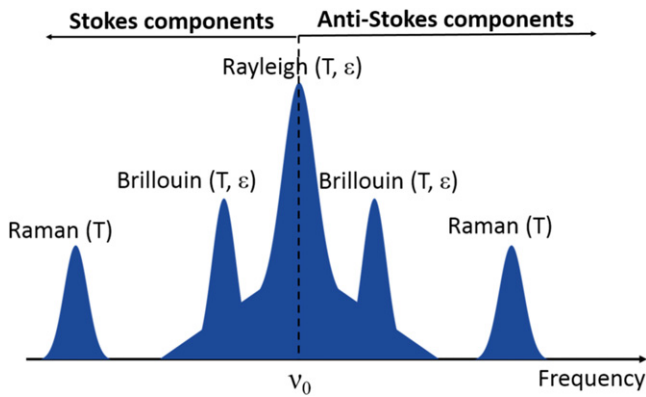


Figure 7. The spectrum of the scattered signal as a function of the frequency. ν_0 is the frequency of the incident light.

without H₂-loading and characterized by a UV-light-induced negative refractive index change [119]. By increasing the accumulated laser energy on a pre-existing type I grating [120] or by subjecting the latter to a thermal treatment at a high temperature such as 700 °C [121], the type I grating is erased, until the starting point of the regeneration process is reached. A new grating will then appear with a blue-shift of the initial central wavelength.

Type IA gratings show lower temperature stability than type I, whereas type IIA gratings have better stability at high temperatures than type II. Finally, among type II-IR gratings, a particular group can be isolated, known as void-FBGs. These are PbP gratings written by focusing the femtosecond IR laser at successive positions along the fiber. Around the area where the laser is focalized, the silica refractive index increases, whereas in the center it decreases in such a way that a micro-void is assumed to form in the core and that this void is surrounded by high-density silica [122]. The void-gratings exhibit the same high thermal stability of type II FBGs [123].

2.3. Distributed sensors

2.3.1. Operational principles. The laser light injected into a silica-based fiber can be transmitted, absorbed or scattered by the material. Two types of scattering, illustrated in figure 7, are distinguished [124]:

- Elastic, if the scattered and incident lights have the same wavelength; this is the case, for example, for Rayleigh scattering and Fresnel reflections [125].
- Inelastic, if a wavelength change is recorded, as is the case in Raman and Brillouin phenomena. When the scattered photon has a frequency (ν_S) lower than the incident photon (ν_0), because the latter gives energy to the system, the scattering is known as Stokes; if the scattered photon absorbs energy from the system, it will have a frequency (ν_{AS}) that is higher than the incident photon, and in this case the scattering is known as anti-Stokes.

The silica properties differ when the environment surrounding the fiber changes. Local temperature, strain, vibration or acoustic wave changes will affect the scattered

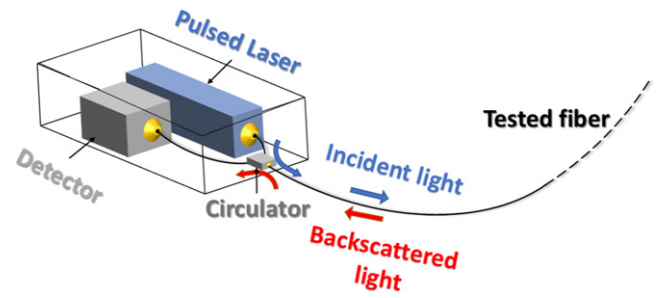


Figure 8. Schema of an OTDR.

signals in a predictable way. Then, by measuring the modifications of the Rayleigh, Raman or Brillouin signatures, the evolution of external constraints applied to the waveguide can be monitored. DOFSs are able to probe numerous points along the fiber length, by recording the intensities of the signals scattered from different fiber parts. To identify which position corresponds to the acquired scattering trace, most of these sensors are based on reflectometry techniques, such as optical time domain reflectometry (OTDR) [126]. A typical DOFS scheme is given in figure 8.

A pulsed signal is injected at one end of the fiber and guided along the waveguide. After interaction with the silica material, the backscattered signal is recorded; the time ‘ t ’ needed by the incident signal to reach a point at a distance z along the fiber and by the backscattered one to go back to the interrogator allows the position z to be determined, through:

$$z = \frac{v_g t}{2} \tag{4}$$

where v_g is the group velocity of propagated light. Consequently, for this technique, the spatial resolution directly depends on the pulse width duration; i.e. a 10 ns pulse is associated with a spatial resolution of ~ 1 m.

2.3.2. Rayleigh-based DOFS. Rayleigh scattering is an elastic phenomenon caused by random fluctuations in the RIP, due to small variations in density or dopant concentration. Each fiber is characterized by its own Rayleigh signature or trace, giving the backscattered light amplitude as a function of distance. Such a signature is random and static but locally changes when an external stimulus, such as temperature or strain, is applied. This is the basis of the operation principle of a Rayleigh-based DOFS: a temperature and/or strain variation applied to a segment of the fiber length can be measured by comparing the Rayleigh signatures acquired before (reference) and after applying the constraint.

Different techniques to measure the backscattered Rayleigh signal exist:

- The simplest one is the OTDR, which measures the backscattered signal intensity [126]: the external parameter value is obtained by the ratio of the scattered intensity in the new state and in that of [127]. For example, for temperature sensors, this ratio linearly depends on temperature with a sensitivity of about $0.015\% \text{ } ^\circ\text{C}^{-1}$ between RT and 800 °C.

- A very efficient technique is the optical frequency domain reflectometer (OFDR) [128]. In this case, the light of a tunable laser source is injected into the two arms of an interferometer: the reference light is split between the two orthogonal polarization states, while the light in the measurement arm is reflected from the fiber under test (FUT). Analysis of the interference patterns between the measurement light and the two polarization states leads to a complex reflection coefficient of the FUT as a function of wavelength. Finally, the Rayleigh scatter as a function of length is calculated via a Fourier transform.

To measure an external parameter, the two Rayleigh scatter functions recorded on a short fiber segment in two different states, for example at RT and at another temperature, and the Fourier transform in the frequency domain have to undergo a cross-correlation, whose result is a peak. The shift of this peak is proportional to the temperature or strain variation, according to equation (5):

$$\frac{\Delta\lambda}{\lambda} = -\frac{\Delta\nu}{\nu} = C_T \cdot \Delta T + C_\varepsilon \cdot \Delta\varepsilon \quad (5)$$

where C_T is the temperature coefficient, of about $6.5 \times 10^{-6} \text{ }^\circ\text{C}^{-1}$, C_ε is the strain coefficient, of about $0.8 \mu\varepsilon^{-1}$ for a germanosilicate fiber, and ΔT and $\Delta\varepsilon$ are the temperature and strain variations, respectively.

2.3.3. Brillouin-based DOFS. Brillouin scattering is the inelastic scattering of a photon from fluctuations in the density of the medium, with the creation (Stokes component) or the annihilation (anti-Stokes component) of an acoustic phonon. The frequency of the scattered light is shifted with respect to the excitation line by a quantity named the Brillouin frequency and defined in equation (6) [129]:

$$\nu_B = \frac{2n_{eff}V_a}{\lambda_0} \quad (6)$$

where n_{eff} is the effective refractive index of the propagating mode, V_a is the acoustic speed of silica (about 5800 m s^{-1}), which depends on the density, and λ_0 is the wavelength of the incident light. The Brillouin frequency of a silica-based fiber ranges from 9 to 13 GHz, depending on its composition and its RIP. Since the acoustic speed depends on temperature and strain, a variation of these external parameters gives rise to a Brillouin frequency shift ($\Delta\nu_B$). The relationship between $\Delta\nu_B$ and the temperature variation ΔT or a strain $\Delta\varepsilon$ is linear, indeed:

$$\Delta\nu_B = C_T \Delta T + C_\varepsilon \Delta\varepsilon \quad (7)$$

where C_ε and C_T are the strain and temperature coefficients, of about $0.05 \text{ MHz } \mu\varepsilon^{-1}$ and $1 \text{ MHz } ^\circ\text{C}^{-1}$, respectively, for a germanosilicate fiber.

Different techniques allow the Brillouin frequency to be measured. The Brillouin optical time-domain reflectometry (BOTDR) is a single-ended (SE) device, indeed as for all OTDRs, a laser pulse is injected into a fiber end and the spontaneously backscattered signal is detected by the same fiber end. Another technique is based on the stimulated Brillouin signal and is called Brillouin optical time-domain

analysis (BOTDA) [130]. This device is double-ended (DE); indeed a pulsed light and a continuous light counter-propagate in the fiber and interact in order to create a beat pattern, which causes a periodic fluctuation in the density and consequently an acoustic wave. By scanning one of the two frequencies, one of the beams will be amplified when the difference between the frequencies of the two signals coincides with the Brillouin frequency.

2.3.4. Raman-based DOFS. Raman scattering is inelastic scattering, due to the interaction of a photon on molecules with the creation and annihilation of an IR phonon [131]. The phonon that is emitted or absorbed, respectively in Stokes and anti-Stokes Raman scattering, has a frequency $\Delta\nu$ of about $1.3 \times 10^{13} \text{ Hz}$ for the fused silica.

Raman-based DOFSs are not sensitive to strain and measure only temperature. Indeed, the cross sections for Stokes and anti-Stokes scattering depend differently on the temperature T . Consequently, this sensor operational principle is based on the intensity ratio of the anti-Stokes signal to the Stokes signal, $R(T, z)$, which depends on the position along the fiber length z and on the temperature T at such a point, according to equation (8) [132]:

$$R(T, z) = \left(\frac{\nu_{AS}}{\nu_S}\right)^4 \cdot \exp\left(-\frac{h \cdot \Delta\nu}{k_B \cdot T}\right) \cdot \exp\left(-\int_z^0 (\alpha(\nu_{AS}, u) - \alpha(\nu_S, u)) du\right) \quad (8)$$

where k_B is Boltzmann's constant. The first factor takes into account the different frequencies of the anti-Stokes and Stokes signals, ν_{AS} and ν_S , respectively; the second one contains the dependence on the temperature, whereas the last one includes the differential losses, due to the different attenuations α at the two frequencies of the two signals. In the absence of ionizing radiation, the differential losses are constant, so they can be neglected. Therefore, the temperature can easily be calculated by comparing the ratio $R(T, z)$ at point z at an unknown temperature T , with the one recorded at a reference temperature (T_0):

$$T(z) = \left(\frac{1}{T_0} - \frac{k_B}{h \cdot \Delta\nu} \cdot \ln\left(-\frac{R(T, z)}{R(T_0, z)}\right)\right)^{-1} \quad (9)$$

2.3.5. Performance of various DOFS technologies. Table 3 compares the performance of different DOFSs in terms of spatial resolution, sensing range, strain and/or temperature measurement accuracy. The table gives typical values, accessible at the time at which these technologies were evaluated under irradiation; however, more detailed studies on these performances have recently been published [133, 134]. As the development of DOFSs is a very active research field, performance is continuously optimized, thanks to the building of new sensor architectures and signal processing approaches. An important remark is that for most of today's applications in harsh environments, it appears to be mandatory to combine at

Table 3. The main characteristics of DOFSs.

Scattered signal	Technique	Spatial resolution	Sensing range	Temperature accuracy	Strain accuracy
Rayleigh	OTDR	1 m	~100 km	15 °C	1 $\mu\epsilon$
	OFDR	From 1 cm to 10 μm	From 2 km to 10 m	0.1 °C	
Brillouin	BOTDR	1 m	~20–50 km	10 °C	60 $\mu\epsilon$
	BOTDA	<50 cm	~100 km	1 °C	20 $\mu\epsilon$
Raman	OTDR	<50 cm	~100 km	1 °C	—

least two technologies to simultaneously measure the strain and temperature distributions on two different fibers [135].

2.4. EDFA and EDFS

2.4.1. Applications for RE-based devices. During the last decade, a revolution in the space industry has been observed. New space launch ventures such as Space X, Virgin Galactic and Blue Origin and advances in nano-satellites, such as the CubeSat, are bringing the focus back to the space industry. This revolution is well underway, and private companies, national space agencies and governmental organizations are investing in the design of new satellite constellations that aim to answer specific scientific questions covering a broad range of fields including weather and climate on Earth, space weather and cosmic rays, planetary exploration and much more. Moreover, giants such as Virgin, Qualcomm, Space X, Google, Airbus, Samsung and LeoSat are placing big bets on new mega-constellations in LEO to provide broadband Internet service around the world, Internet connectivity in remote or underserved areas, as well as the most secure and high-performance data network on Earth [136–140].

Observation and scientific missions will require larger data transfer capacity. As an example, Earth-viewing systems and planetary probes can generate a lot of image data to be exchanged between more remote spacecraft and the ground stations on or near Earth. Such data transfer has to be done at the appropriate time of request and within brief time slots, resulting in a high data transfer rate. Moreover, the next generation of fast Internet will be based on new satellite systems requiring high-speed inter-satellite links. In this context, and considering that the desired data volumes cannot be accomplished using the available radio links, photonic technologies have become of great interest for the space payload [141]. In particular, since they enable a high data rate, secure links, decreased mass, size and electrical power, fiber optics systems are beginning to penetrate satellite technologies and they are expected to play a critical role in next generation space missions bridging the gap addressing different applications, including on-board photonic signal handling and processing.

Recent and planned developments of spaceborn optical communication systems are based on the eye-safe 1.55 μm telecom wavelength window. This wavelength allows low-loss transmission through both the fiber and the atmosphere. Moreover, it makes possible the use of suitably designed terrestrial high-bandwidth photonic components as well, as it

enables link capacities to be scaled by employing wavelength division multiplexed (WDM) technology. In order to leverage significant investment and the reliability heritage of terrestrial telecommunication systems, there is a strong motivation to use Er^{3+} -doped (EDFA) or $\text{Er}^{3+}/\text{Yb}^{3+}$ -codoped (EYDFA) fiber amplifiers and sources (EDFS) as an integral part of space optical communication terminals to boost and generate the optical signal and to enable long reach in free-space [142–147]. Moreover, optical fiber amplifiers are expected to be used to compensate for insertion losses between functional blocks of the payload.

2.4.2. Architecture of REDF amplifiers. In the context of space optical communications, there is no station between the transmitting and receiving terminals. So, a transmitter operating at 1.55 μm should be able to provide a stable average output signal power of several watts (>5 W) during long-term space missions. Figure 9 illustrates the scheme of a high-power laser transmitter for space communication [148–150]. The seed laser is a high-power 1.55 μm distributed feedback laser (DFB) operating in the continuous wave (CW) regime [151]. Pulses can be generated using an external intensity modulator (INT mod) with a high extinction ratio. A pulse-shaped control section is directly connected to the modulator to provide a wide range of pulse position modulation formats with the pulse duration typically ranging from 0.5 ns to 8 ns, and a low duty cycle essential to ensure high pulse energies. Moreover, since at a low pulse repetition frequency the pulse energies are near the saturation value, it is important to correct the corresponding pulse energy variation through a pre-pulse shaping function delivered by the control device. A low loss phase modulator (PHS mod) is used to control the laser linewidth at values lower than 6 GHz. This signal processing is indispensable for suppressing the stimulated Brillouin scattering (SBS) that occurs at longer pulse durations.

Depending on the mission scenario, the amplifying section can be designed using one or two sub-units in cascade connection. For short-range (<2000 km) high-speed LEO-to-ground downlinks, only one mid-power booster amplifier is used to directly amplify the output of the laser transmitter. For long-range (>30 000 km) GEO links, a mid-power booster amplifier (AMPL1) is used to pre-amplify the transmitter signal and to saturate the cascaded high-power amplifier (AMPL2). The mid-power booster amplifier is typically an EDFA pumped by an uncooled single mode

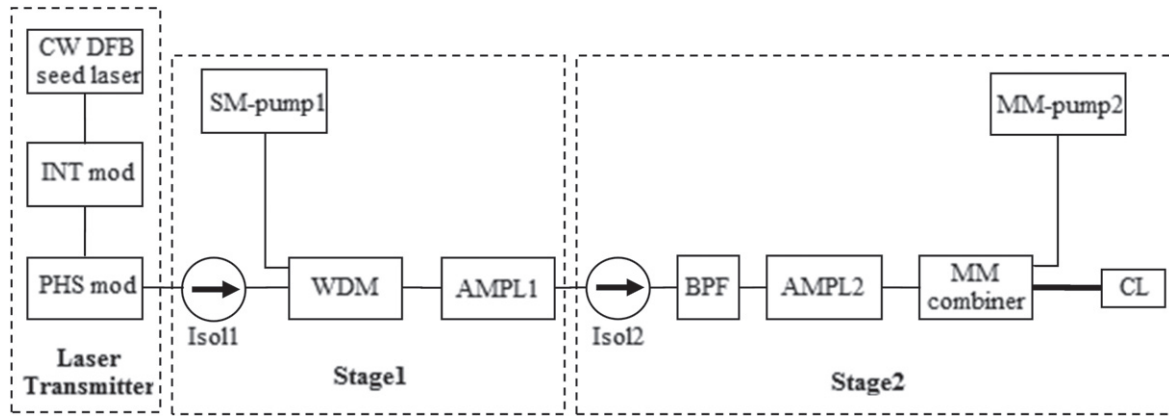


Figure 9. A schematic of the transmitting system based on optical fiber amplifiers.

980 nm pump laser diode (SM-pump1). This amplifier should be designed to achieve a low noise figure (~ 5 dB) and the high amplification gain of a small signal (>30 dB) in the wavelength range 1540–1560 nm. The polarization independent isolator (Iso1) has to be placed at the input to minimize the degradation of the noise figure and to prevent optical feedback reflections that could result in lasing. Moreover, a very high inversion level can be accomplished by using a short segment of erbium-doped fiber and 980 nm pumping.

The high power requirement (output signal power >5 W) is difficult to satisfy using EDFA since various nonlinearity impairments result in serious gain-saturation problems in both the C-band and L-band, especially when the output power increases. Co-doping with ytterbium Yb^{3+} sensitizer ions could be an effective way to solve problems concerning the delivery of high output power. In fact, the presence of Yb^{3+} ions makes an efficient indirect pumping mechanism possible for erbium ions, and reduces the formation of Er^{3+} clusters and cooperative upconversion processes among Er^{3+} ions, extends the range of the possible pump wavelength band between 800 nm and 1100 nm, and increases pump absorption by providing a peak absorption around 975 nm that is two orders of magnitude larger than the nonsensitized one. Moreover, considering that core pumping is not applicable to multiwatt amplifiers, double cladding fiber geometry is required (see illustration in table 2). Such a technique allows the propagation of much larger optical pump powers delivered by low-cost multimode pump diodes, without exciting nonlinear effects, as well as reducing the thermal loading density. Starting from these considerations, the high power amplifier (AMPL2) exhibits Er/Yb polarization maintaining a large mode area (PM-LMA) fiber amplifier. The use of a PM-LMA fiber is essential to achieve the required very high peak power and SBS free operation. A narrow band pass filter (BPF) is used to suppress the amplified spontaneous emission (ASE) generated during Stage1 ensuring the clean seeding of Stage2. The AMPL2 is pumped by multimode laser diodes (MM-pump2) operating at a wavelength within the range 915–940 nm. A high power and low loss multimode pump combiner (MM combiner) is used to launch the pump signal into the AMPL2. Moreover, pumping in a backward propagating configuration should

enable a lower ASE and hence increase the signal power in the output. Finally, a low-loss high-power polarizer collimator (CL) should be designed to ensure an output beam quality $M^2 < 1.1$.

2.4.3. Space constraints on REDF amplifiers. In contrast to terrestrial-based systems, the design and development of components and systems based on rare-earth-doped fibers for space applications require special treatment to face a number of challenges and performance trade-offs. In fact, because repairs cannot be made in space and the investments are enormous, meticulous analysis, study and testing need to be performed during each phase characterizing the whole construction process. Such activities are essential to eliminate expensive surprises after launch and to ensure that operational performance objectives are met. Very thorough and special tests need to be performed on the individual components and subsystems as well as the complete communication system, both separately and integrated, in the lab and under real-use conditions. It is well known that due to exposure to ionizing radiation, the long-term EDFA and EYDFA characteristics will deteriorate when they operate in the space radiation environment. As a result, a number of design challenges, including severe attenuation and performance degradation due to radiation, have to be taken into account during amplifier design and definition of the optimum parameters (pump power, fiber length, erbium and/or ytterbium concentration, etc). Moreover, in the case of booster and power amplifiers, the development of devices with high power conversion efficiency (PCE) is of prime importance. In fact, considering that satellite resources are typically well-defined and restricted, the design of fiber amplifiers for space applications has to comply with spacecraft electrical power resource specifications and component de-rating requirements. In this context, the availability of accurate numerical models is an invaluable tool (i) to evaluate the suitable amplifier configuration for controlling unwanted degradation mechanisms due to fiber exposure to ionizing radiation, (ii) to correctly predict the amplifier performance in terms of efficiency and power scaling capability, (iii) to maximize the PCE through optimization of the amplifier topology, pumping configuration and fiber parameters as numerical aperture, core size, fiber length,

cladding geometry and dopant concentration [143–146]. Moreover, the amplifier topology has to be engineered according to the wavelength channel plan and noise performance to achieve optimal trade-off between optical performance and electrical power requirements [148, 149].

Although radiation can degrade optical fiber performance, thermal loading inside the fiber can become a serious problem in booster and power amplifiers. Moreover, since higher optical signal attenuation improves heat generation, the radiation can further induce dramatic impairments of the amplifier in terms of efficiency, gain and noise figures. On the other hand, quantum defects due to the amplification of the 1550 nm signal using a 980 nm pump source generates further heat accumulation, which can become a serious concern, especially when high-power optical signals transit through short fiber amplifiers. The increased heat load has a number of undesirable consequences resulting in the deterioration of amplifier performance. As a consequence, the design and development of the optical fiber amplifiers has to comply with further constraints due to heat dissipation. This means that a specific functional test validating the thermal design of the unit has to be defined with the aim of demonstrating stable operation over the required module temperature range. Again, the quantum defect of the mismatch in the pump-to-signal wavelength still ultimately limits the potential for higher efficiency in the amplifier, which is the main power draw in a fiber laser. So, to overcome these drawbacks a new paradigm is required. The recent development of high-power fiber-coupled pump diodes at 1480 nm and 1530 nm offers the potential for significantly improved fiber amplifier power efficiency, and hence fiber laser transmitters in general [152]. However, their maturity and reliability has not yet been demonstrated at levels comparable to 980 nm pump diodes.

In conclusion, the requirements of high reliability and robustness make the evaluation of optical fiber boosters and power amplifier vulnerability to radiation a crucial point to be considered for ensuring system functionality over the satellite lifetime. Thus, the end-of-life performance has to be carefully defined in the context of mission environment constraints as well as the mission's operational specifications.

2.5. Fiber-optic gyroscopes

FOGs provide rotation speed measurements [153, 154]. When this technology is associated with accelerometers, FOGs can also provide inertial positioning, which is a crucial parameter in the monitoring of satellites. In space, various grades of gyroscope are used in a large variety of missions requiring measurement precision ranging from 1° h^{-1} to $0.0001^\circ \text{ h}^{-1}$. Some examples of FOG usage, sorted by gyroscope precision, are telecommunication satellite spin control, altitude and orbit control (AOCS) for electric propulsion and deep space exploration, AOCS for planetary landing, scientific satellite orientation, science missions, and Earth and space observation satellites. FOGs exploit the Sagnac effect [155, 156]: light traveling along a closed ring path in opposite directions allows the rotation to be detected with respect to inertial space (figure 10). Over one turn,

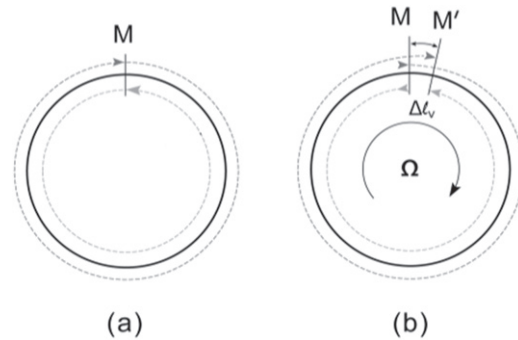


Figure 10. The principle of the Sagnac effect: (a) at rest, both opposite paths have equal length, (b) rotating at rate Ω , M moves to M' during the transit time, then the corotating path is more than one turn while the counterrotating one is less, yielding a path difference of $2\Delta L_v$.

as in the original experiment 104 years ago [157], the effect is extremely weak, but it can be increased using the numerous loops of a fiber coil as this Sagnac effect is proportional to the apparent surface of the coil. To fully exploit this cumulative behavior, modern commercial FOGs contain up to several fiber kilometers per coil [153].

The modern principle of FOG operation is the continuous tracking of the interferometric fringe position [154], which evolves with the coil's rotation rate. Modern FOG architecture is displayed in figure 11 and its basic subparts are listed hereafter:

- A broadband 1550 nm optical amplified spontaneous emission (ASE) source including a 980 nm pumping laser diode and an active Er-doped fiber [158, 159]. For a low to medium FOG performance, a superluminescent semiconductor diode at either $1.5 \mu\text{m}$ or $1.3 \mu\text{m}$ can be used as a cheaper and smaller replacement [160].
- Passive optical components such as couplers and isolators.
- A lithium niobate optical phase modulator, in an integrated-optic Y junction form [161, 162].
- A polarization-maintaining optical fiber coil of up to several kilometers [163].
- A high quantum efficiency PIN photodiode to convert the optical power returning from the interferometer into an electric signal.
- A digital electronic achieving a servo loop to track the optical fringe [164]. The two following parameters are of particular interest:

The fiber coil's optical spectrum transfer function and the erbium ASE optical spectrum; any mean wavelength modification at the detector's end linearly affects the FOG scale factor.

Fiber attenuation as the FOG noise rises while the optical power at the detector's end decreases.

3. Radiation effects on fiber-based technologies

Radiation effects on optical fibers have been investigated for more than 40 years for data transfer applications, and important knowledge has been acquired, even though the

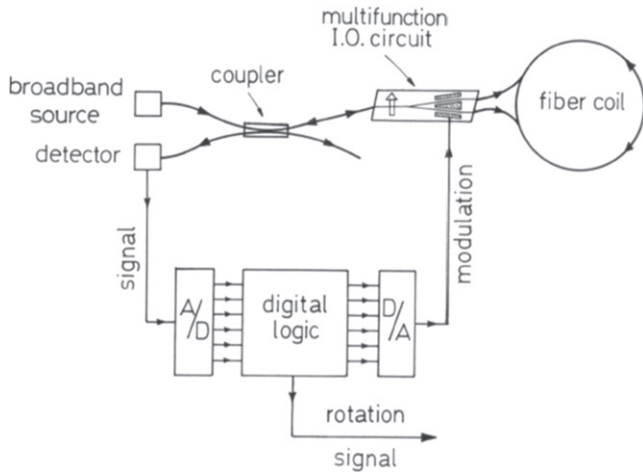


Figure 11. Modern architecture of the FOG.

microscopic mechanisms leading to this degradation are still partially unknown and too complex to yet be predicted by simulation. With the development of more and more sophisticated fiber sensor architecture, new types of degradation have been noticed, which are related to changes of the silica-based matrix structure rather than by the evolution of its optical properties. In this part, multi-scale radiation effects on optical fibers will first be described, reviewing our current knowledge on the main intrinsic and extrinsic parameters affecting their response to radiation.

3.1. Radiation effects on optical fibers

3.1.1. *Macroscopic effects: RIA, RIE, RIRIC.* Three main radiation effects are observed at the macroscopic scale when a silica-based optical fiber is exposed to radiation.

- The first one is radiation-induced attenuation (RIA). RIA is an excess of loss that appears during irradiation, growing with the dose and usually partially recovering after irradiation stops. Figure 12 illustrates the RIA growth in the spectral range 350–900 nm for a polymicro FVP-UVMI MMF under γ -rays at a dose rate of 11 Gy h^{-1} up to 200 Gy. The RIA growth kinetics are illustrated in the inset of figure 12 at 350 nm, 400 nm and 660 nm.

This figure illustrates the complex response of an optical fiber, highlighting the strong spectral dependence of these excess losses. Furthermore, for this PSC fiber, a clear absorption band can be seen peaking around 630 nm. In this case, the defect structure associated with this optical absorption band is known, namely the nonbridging oxygen hole centers (NBOHC) [166]. The RIA levels and kinetics depend on numerous parameters that will be detailed in section 3.3. RIA is often the main issue to consider when implementing an optical fiber in a harsh environment, as it degrades, in the worst case the SNR of the optical data links up to the loss of the guided signal after short distances of propagation. As an example, after an x-ray pulse of a few tens of nanoseconds, RIA levels as high as 2000 dB km^{-1} at

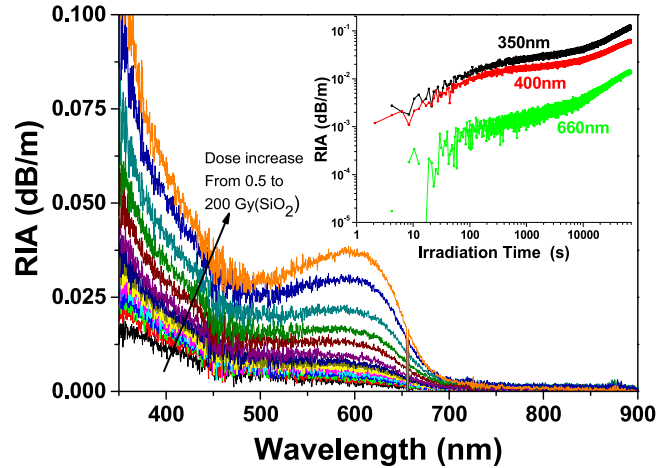


Figure 12. The spectral dependence of the RIA generated during the irradiation of a polymicro FVP-UVMI multimode optical fiber at RT, up to $200 \text{ Gy}(\text{SiO}_2)$ at a dose rate of 11 Gy h^{-1} . In the inset the RIA growth kinetics are illustrated at three particular wavelengths: 350, 400 and 660 nm. More details can be found in [165].

1550 nm (to be compared to 0.2 dB km^{-1} before irradiation) have been observed for Corning SMF28 fibers, meaning that 50% of the signal is absorbed in $\sim 1.5 \text{ m}$. For DOFSs, in which the optical fibers are the sensitive element, the RIA strongly decreases the available sensing length from kilometers down to a few meters for the most challenging environments. Usually, the RIA can be calculated as:

$$\alpha_{RIA}(\text{dB}/\text{km}) = -\frac{10}{L(\text{km})} \times \log(I/I_0) \quad (10)$$

where I and I_0 are the intensities of the transmitted signal at a given time and before irradiation starts, respectively. On the fiber market, some optical fibers are sold as radiation-hardened, as their composition has been adapted to limit the RIA level for a certain type of irradiation (usually steady-state γ -rays up to MGy dose level) and a certain range of wavelengths (usually IR operation within the telecommunication windows). Generally, this class of optical fibers comprises pure-silica core and fluorine-doped core optical fibers, both types with F-doped claddings. If for most applications RIA is a limiting issue that has to be mitigated, it should be noted that monitoring it in a radiation-sensitive optical fiber can be exploited for radiation detection or dosimetry applications, for example, at the DESY facility in Germany [57].

- The second one is radiation-induced emission (RIE). RIE acts as a parasitic light that superposes on the propagated signal, and originates from several sources.

If the energy of the incident particles is sufficient, Cerenkov light can be generated and guided in the optical fibers. This is the case for the example given in figure 13, with the RIE spectra acquired during and after the irradiation of a PSC MMF using a high dose rate x-ray facility, ASTERIX from CEA [167], which allows the dose rates encountered during ignition experiments to be reproduced [20]. In addition to Cerenkov, the radiation can also generate some additional

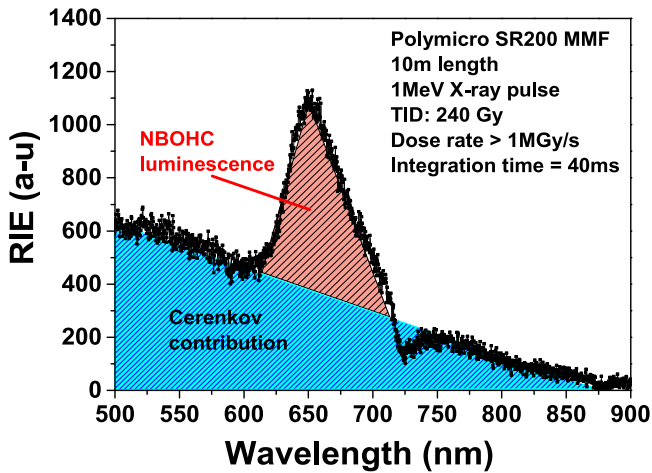


Figure 13. The spectral dependence of the RIE generated in a polymicro SR200 MMF during and just after (40 ms integration time) its irradiation with an x-ray pulse (240 Gy, > 1 MGy s⁻¹, RT). The fiber length was 10 m and the acquired spectrum is not corrected from the RIA effect, or by the function transfer of the used HR4000 spectrophotometer from OCEAN optics.

luminescence signals from pre-existing defects or new defects created during irradiation. This is also illustrated in figure 13 and provides evidence for the excitation of pre-existing or radiation-induced NBOHCs emitting around 650 nm during the first milliseconds following the x-ray pulse.

Regardless of its nature, RIE affects the SNR ratio, especially for systems operating in the visible domain, such as diagnostics, and in harsh environments associated with a high dose rate (this is particularly the case for megajoule class lasers). As for the RIA, in recent years, several studies have investigated how this luminescence, also called radio-luminescence, can be exploited to provide real-time monitoring of the dose rate (or particle flux) in high-energy physics facilities or for medical applications, radio- [168] or proton-therapy [169].

- The third one is radiation-induced refractive index change (RIRIC).

The observed refractive-index change arising from irradiation probably results from two mechanisms: the change in the α -SiO₂ glass density and the RIA. The contribution of the density ρ change to the refractive-index n can be explained by the Lorentz–Lorenz formula relying on the two parameters:

$$\frac{n^2 - 1}{n^2 + 2} = K\rho$$

where the proportionality constant K depends on the glass polarizability. The part of the RIRIC caused by point defects is described through the Kramers–Kronig relations, which define the relation between the refractive index and the absorption. Compaction or swelling leading to glass density modifications was first observed by Primak [170] in bulk pure-silica exposed to high fluences of fast neutrons (>10¹⁹ n cm⁻²) with a densification of about 3%. It is remarkable to note that, under the same conditions, silica in its α -quartz

form exhibits a density decrease of more than 10%. It was observed that neutrons change both types of silica into a common topological structure referred to as the metamict phase [171]. The RIRIC also affects the optical fiber waveguide structure, as shown in [25]. For fiber samples exposed to fluences above 10¹⁹ n cm⁻² at temperatures exceeding 290 °C, a linear compaction of 0.25% was observed; furthermore the densification effects of silica can be observed through the evolution of its Raman spectra for fluences above 10¹⁶ n cm⁻² in bulk silica [172].

3.1.2. Microscopic origins of the fiber degradation. A large number of studies have been conducted over the last 50 years and beyond in order to improve our knowledge about the nature of radiation-induced point defects, also called color centers (RICC), which are generated in pure or doped α -SiO₂ glasses under irradiation. Complete reviews are regularly done, resuming the evolution of our knowledge about this complex subject, see for example [9, 12 173–175] and the references therein. The α -SiO₂ building unit is a SiO₄ tetrahedron, as in the quartz crystalline structure. In this unit, the central silicon (Si) atom is bonded to four oxygen (O) atoms occupying the corners of the tetrahedron. Figure 14(a) illustrates the 2D continuous random network representation of an ideal pure-silica network, whereas figure 14(b) illustrates the same glass containing intrinsic and extrinsic point defects such as dangling bonds and oxygen deficiencies. If these defects can exist before irradiation, they are then called precursor sites. The concentration of precursor sites generally decreases through the trapping of radiolytic electrons and holes while the concentration of radiation-induced point defects increases.

This fundamental research is of primary importance, as the identification of the nature and properties of the point defects responsible for the RIA at the wavelength of interest is mandatory in order to imagine radiation hardening approaches. Historically, these studies have mainly been done by combining different experimental tools allowing the optical properties (absorption, luminescence) to be associated with their structure, accessible, for paramagnetic defects, through electron paramagnetic resonance (EPR) measurements. By combining these spectroscopic techniques with samples that have been submitted to an external constraint (radiation, temperature, hydrogen treatment, etc), it is possible to correlate the evolution of the concentration of a particular defect given by EPR with that of the observed absorption or luminescence bands. Even though very deep knowledge has been acquired for a number of defects, such as those related to pure silica, P- or Ge-related defects, this set of experiments presents some limitations, which explains why the structures and optical properties of some defects are still under investigation today. As an example, for most studies, EPR and luminescence measurements are usually done on irradiated samples, after the end of the irradiation. Then, they are only able to characterize the signatures of point defects that are stable at the temperature of the experiments, and none of the transient defects that are bleached shortly

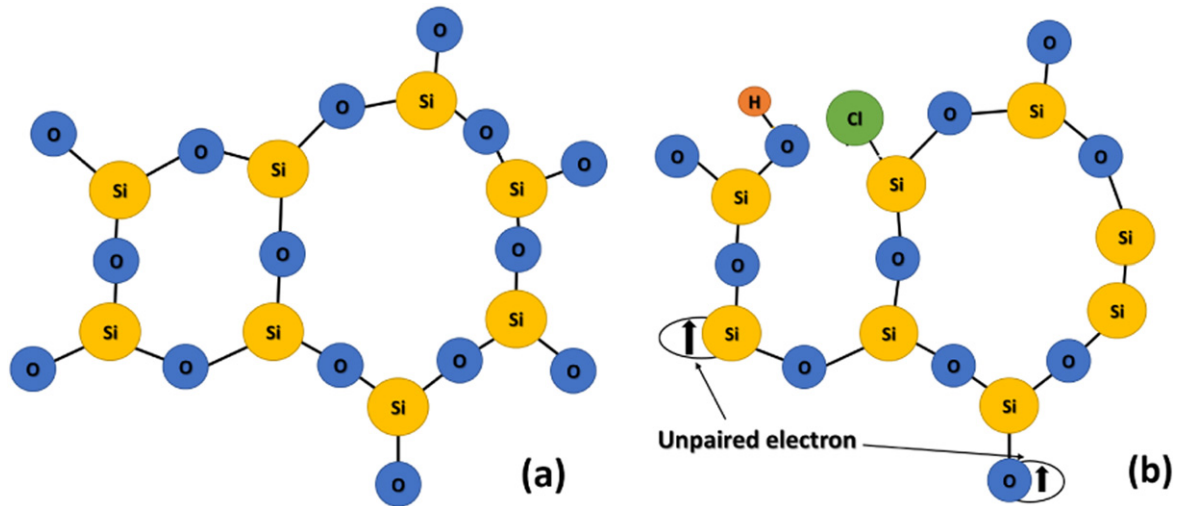


Figure 14. A 2D illustration of a silica continuous random network (a) undefected amorphous silica structure, (b) $a\text{-SiO}_2$ structure containing defects (here, SiE' center and NBOHC defects), either created during the fiber manufacturing process or by irradiation, as well as chlorine and hydroxyl impurities.

after the irradiation ends are measurable by these techniques. Furthermore, EPR and luminescence measurements are only applicable to paramagnetic defects and emitting centers, respectively, limiting the investigation to a reduced fraction of the defects that are absorbing within the silica gap.

Figure 15 gives an overview of the main absorption bands related to pure silica (figure 15(a)), Ge-related defects (figure 15(b)) and P-related defects (figure 15(c)). It should be emphasized that these bands have been observed in both bulk glasses and optical fibers. From this figure, several statements can be made:

- First, most known point defects that pre-exist the irradiation or are created during exposure are associated with absorption bands peaking in the ultraviolet–visible domain, at wavelengths below 800 nm ($E > 1.55$ eV). As a general rule, the RIA levels are lower in the near-IR part of the spectrum at wavelengths above 800 nm.
- Second, the contribution of various defects to the measured RIA will also depend on their localization in the fiber cross sections and on the amount of light that travels in this part of the fiber. The concentration of these defects is not always directly related to the dopant concentration, and the defect generation or bleaching efficiencies can be affected by other parameters such as the internal fiber stress, or through photobleaching effects. It then appears crucial to identify spectroscopic techniques, which allow spatial information to be obtained with a resolution that permits the characterization of the defect distribution over the fiber cross-section. The confocal microscopy of luminescence (CML) and cathodoluminescence (CL) has been investigated and its potential demonstrated in a series of publications [176–179]. An example of CL results is given in figure 16, which illustrates the case of a GeCe-codoped optical fiber. For this fiber, some of the defect distributions are correlated to the internal stress generated at the interfaces

between differently doped parts of the fiber rather than to its composition.

- The origin of the observed RIA levels in the IR is still under investigation. A detailed analysis of the contribution of the described UV-visible absorption bands reveals that the tails of these bands are not able to fully explain the losses in excess. This means that although no clear absorption bands are observable in the IR domain for Ge-doped and pure silica glass, some defects absorb in this spectral range and still have to be identified. In addition to this, in the IR domain and for SM optical fibers, it is also mandatory to consider the impact of the fiber guiding properties on the RIA spectral dependence.

3.1.3. Intrinsic and extrinsic parameters affecting the fiber response. Numerous parameters have been shown to influence the radiation response of optical fibers, especially regarding the RIA levels and kinetics. Table 4 reviews the main parameters.

The first category of parameters, labeled intrinsic parameters, relates to the fiber itself. The main one is the fiber composition. It is important to notice that both the composition of the fiber core and cladding play a key role in governing the RIA levels of the fibers. The fibers can mainly be categorized in three sets when considering moderate dose levels of steady state γ -rays (typically up to 100 kGy): radiation-sensitive, radiation-hardened and radiation-tolerant fibers. This classification strongly depends on the harsh environments of interest and it is important to notice that none of the existing optical fibers have been shown to be radiation resistant for any of the studied applications. In particular, this classification is not valid for transient exposures such as those associated with megajoule class lasers or some military applications.

- Among the radiation-sensitive optical fibers, all the fibers containing phosphorus (P), aluminum (Al) in either their

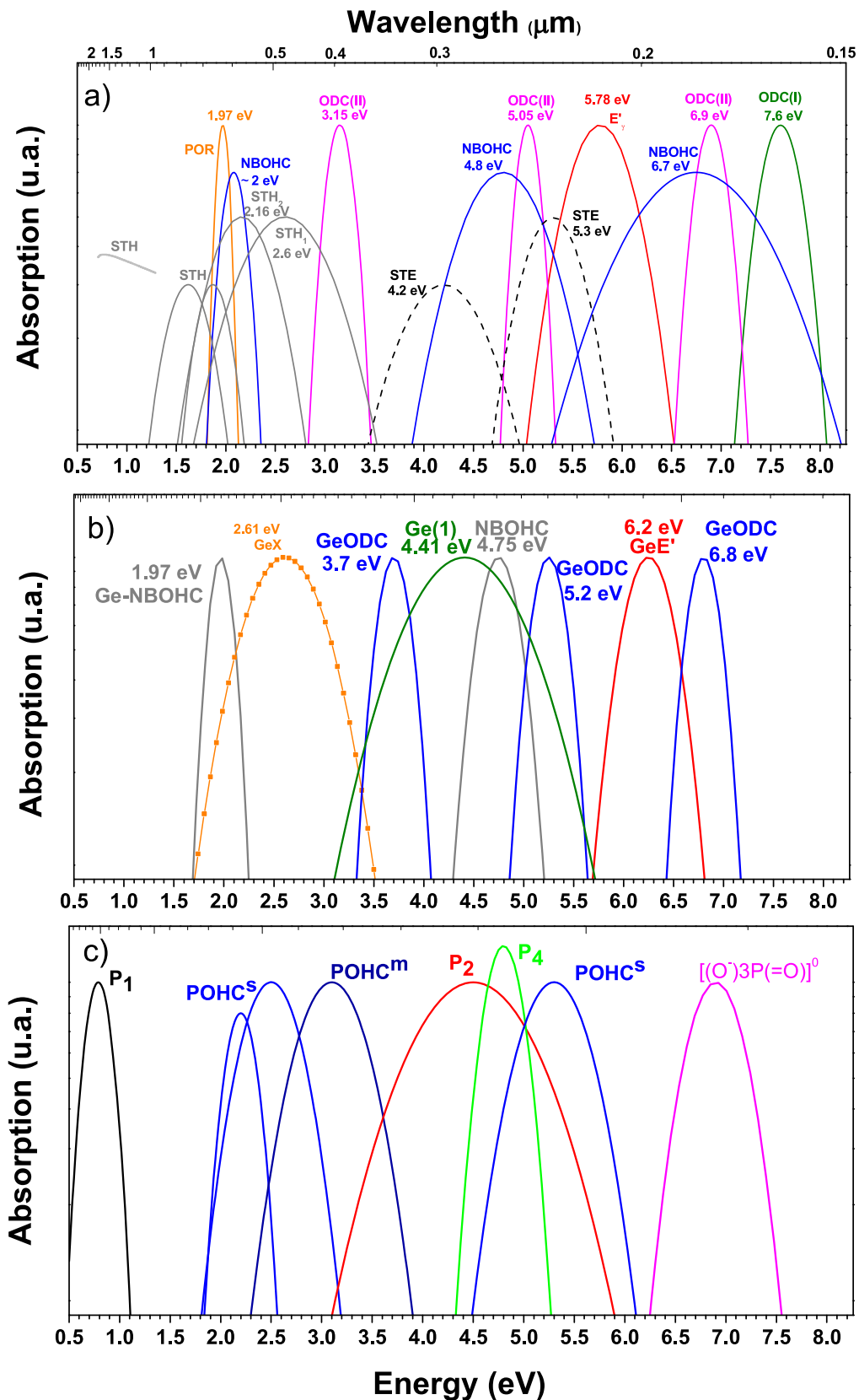


Figure 15. The main absorption bands associated with pure silica, Ge-doped $a\text{-SiO}_2$ and P-doped $a\text{-SiO}_2$.

core or cladding, or more recently lanthanum (La) or thulium (Tm) have been identified [181]. Usually these fibers are associated with very high RIA levels in both the

visible and IR parts of the spectrum and should be avoided for data-transfer. Finally, if these fibers are not suitable for most of the targeted applications in harsh

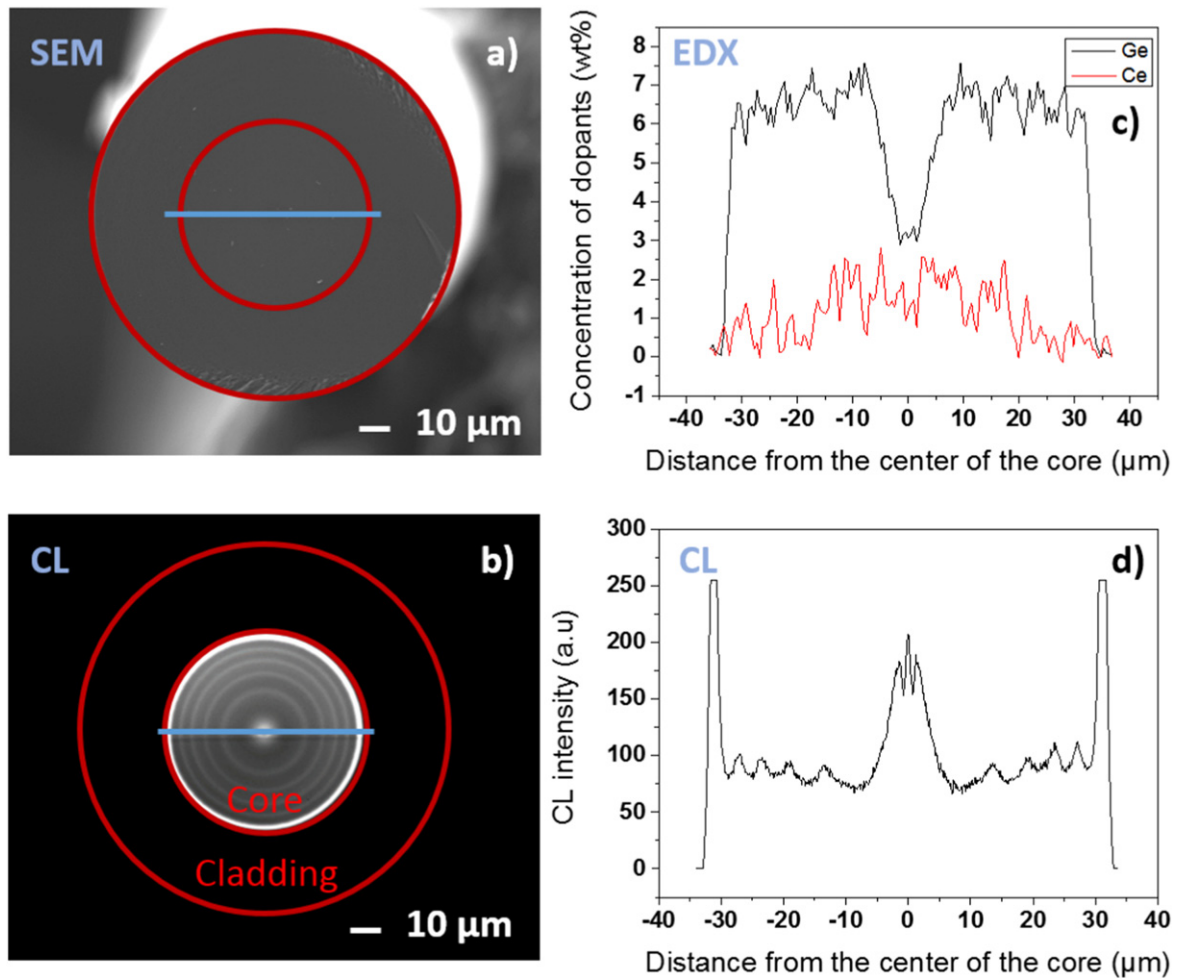


Figure 16. (a) An SEM image of a GeCe-codoped multimode optical fiber; (b) a panchromatic image acquired by the CL of the same fiber; (c) an EDX analysis of the Ge and Ce radial distribution along the blue line of (b); (d) the radial distribution of the emitting centers along the blue line.

environments, it should be noticed that they are promising candidates for radiation detection or dosimetry systems.

- Among the radiation-tolerant optical fibers, all the telecom-grade germanosilicate optical fibers without P in their core and cladding have been identified. These fibers are acceptable for a wide range of applications, including, for example, short length data links in spacecraft. These fibers are strongly sensitive to dose rate, temperature and photobleaching effects and may not be adapted for applications involving long lengths of optical fibers exposed to radiation.
- Regarding the radiation-hardened optical fibers, from previous research, pure-silica cores, fluorine-doped cores (both with F-doped cladding) and nitrogen-doped optical fibers are the most radiation-hardened optical fibers up to 100 kGy [209–212] for steady state irradiation. Optimization of these fibers is still possible to enhance their radiation resistance, but implies the fine control of their fabrication process parameters—in particular the glass stoichiometry and fictive temperature—in order to control the nature and concentration of the point defects responsible for their degradation, such as chlorine-related

impurities and self-trapped holes and excitons (STEs, STHs) [186, 213]. It should be noted that some of these fibers are today commercially available from manufacturers such as Fujikura [214], IXBlue Photonics [215] or Prysmian [216].

It is well known that part of the precursor sites, such as GLPCs and NBOHCs in germanosilicate and pure optical fibers, respectively, are partially induced during the process of drawing the preform into an optical fiber [84]. This has been clearly shown in [84, 188], but numerous studies have reported that changing the drawing conditions (temperature, strain, speed) in the usual range exploited for the design of MCVD specialty optical fibers does not allow the fiber radiation response to change significantly [191, 217]. If this limits the development of radiation hardening solutions, it appears to be an interesting feature in terms of hardening assurance as it indicates that the fiber radiation response will be quite robust against small process changes during drawing. A complete study of the drawing influence on the radiation response of telecom-grade optical fibers, drawn at larger speeds and tension still has to be performed, to the best of our knowledge. Regarding the coating, it does not seem to

Table 4. Intrinsic and extrinsic parameters affecting the fiber response.

Fiber parameters				
Parameters	Main cases	Impact on	Remark	Refs
Core composition	Common dopants: pure silica, Ge, P, F, B, N, Al, rare-earths, etc	Nature and concentration of defects → RIA levels and kinetics	Affects all fiber types, UV to IR domains	[83, 84, 180, 181]
Cladding composition	Common co-dopants: pure silica, Ge, P, F, B	Nature and concentration of defects → RIA levels and kinetics	Affects especially SMF	[182],
Impurities	Presence of impurities in core and cladding: OH groups and Cl-species	Nature and concentration of defects → RIA levels and kinetics	Affect mainly RIA of pure silica and F-doped fibers → major for rad-hard fibers	[183–185]
Fiber stoichiometry	Oxygen-deficient or oxygen-loaded fibers	Nature and concentration of defects → RIA levels and kinetics	Affect mainly RIA of pure silica and F-doped fibers → major for rad-hard fibers	[186, 187]
Drawing conditions	Speed, tension and temperature	Nature and concentration of defects → RIA levels and kinetics	Change the observed concentration of defects between preforms and fibers → RIA is not easily changed by varying these parameters in the range used for speciality fibers	[188–191]
Irradiation conditions				
Nature of particles	γ -rays, x-rays, neutrons, protons, electrons, heavy ions	Relative contribution of ionization and displacement effects → nature and concentration of defects → RIA	Affect all fibers used for data transfer. For distributed fiber-based sensors using reflectometry techniques, the potential RIRIC will impact the sensor performance too	[14, 192]
Dose (fluence)	From very low (medical application—a few μGy) to huge (nuclear industry GGy , $>10^{20} \text{ n cm}^{-2}$)	Nature and concentration of defects → RIA levels and kinetics structural changes → point and distributed sensors	Affect all fibers used for data transfer. For distributed fiber-based sensors. The dose dependence of the RIA can be very complex, often increasing with dose, sometimes with saturation behavior; sometimes the RIA decreases with dose	[75, 193, 194]
Dose rate (flux)	From very low (space) to huge (fusion-related facilities)	Nature and concentration of defects → RIA levels and kinetics structural changes	Usually RIA increases with the dose rate (rad-hard, telecom-grade fibers) or RIA is dose-rate insensitive (P-doped fibers). A very few papers have related the enhanced low-dose rate sensitivity (ELDRS) effect to fibers	[195–197]
Temperature	From low (space applications) to high ($800 \text{ }^\circ\text{C}$ for nuclear industry)	Nature and concentration of defects → RIA levels and kinetics structural changes	Temperature changes the efficiency of defect generation and bleaching. It is often assumed that increasing T reduces RIA, but this is not always correct	[198, 199]
Fiber profile of use				
Wavelength	Depends on the application, ranging from UV to near IR	Operational wavelength will fix the nature of the defect responsible for the RIA and then RIA levels and kinetics	If the application operates in a range of wavelengths (e.g. diagnostics), the most affected wavelength has to be considered for the vulnerability study	[200]

8

Table 4. (Continued.)

Fiber parameters				
Parameters	Main cases	Impact on	Remark	Refs
Injected power	Depends on the application, ranging from very low (a few μW) to very high (W for high- power lasers)	Can increase the bleaching rate of some point defects, can also lead to photodarkening in RE-doped fibers	Photobleaching is very difficult to predict as it is strongly defect-dependent	[201–203]
Pre-loading with gas	The presence of gas (hydrogen, deuterium) strongly affects the fiber response	Nature and concentration of defects \rightarrow RIA levels and kinetics	Pre-loading sounds an efficient hardening technique \rightarrow its efficiency strongly depends on the fiber profile of use	[204–206]
Pre-irradiation	Pre-irradiation can change the fiber radiation response	Nature and concentration of defects \rightarrow RIA levels and kinetics	The impact of fiber pre-irradiation is strongly fiber and application-dependent	[207, 208]

directly influence the RIA, but its nature can impact the hardening approaches in some harsh environments [218], and also influence the response of some of fiber sensors such as those exploiting the FBG [219, 220] or OFDR technologies [221].

For a given fiber, its vulnerability will strongly depend on the constraints associated with the application. Among the main constraints that can affect the radiation response, the main ones are the nature of the radiation: x-rays, γ -rays, neutrons, protons, the dose (or fluence), the dose rate (or flux) and also the temperature during the irradiation. For some specific environments, such as the one associated with nuclear waste repositories, other constraints have to be considered such as hydrogen presence [21]. For most optoelectronic devices, such as image sensors and LEDs, the nature of irradiation has a strong influence on the device response: neutrons usually affect devices more through displacement damage. In the case of optical fibers, it has been shown that for fission (<1 MeV) or fusion (14 MeV) neutrons, up to a fluence of 10^{15} n cm⁻², the main degradation mechanism remains ionization [14]. Above this fluence threshold, some effects specific to the displacement damage start to appear, both in terms of optically active point defects [17, 85] and structural modifications [18]. Regarding the dose and dose rate, the amount of radiation damage usually increases with these parameters. The dose dependence of the RIA can follow various kinetics from linear increase, power law dependence or even more complex schemes, which are explained by the competition during irradiation between the generation of point defects and their recovery through thermal- or photobleaching processes [194, 222, 223]. Regarding the temperature impact on the fiber response, especially RIA, changing the temperature affects the efficiencies of both the creation and bleaching processes of radiation-induced color centers and then strongly affects both the RIA levels and kinetics. An important point is that contrary to what is usually stated in the literature, it is not always true that increasing the temperature of irradiation will decrease the RIA levels [198]. This statement is usually deduced from the thermal treatment performed after the end of irradiation, which gives insights into the temperature effect on the bleaching process efficiency only. Clearly, the combined effects of temperature and radiation should be investigated in more detail in the future.

Finally, the fiber operation conditions also clearly impact its radiation response, and this is the main factor to be exploited to improve its radiation tolerance. The main parameter is the selected signal wavelength. Usually, it is more favorable, if possible, to operate it in the IR part of the spectrum where fewer of the point defects are absorbing than in the UV-visible domain [200]. For steady state γ -rays, the minimum RIA is around 1–1.2 μ m in most classes of optical fibers [72]. It is important to note that the origin of IR-RIA still needs to be fully understood. If in some cases these IR losses can be explained by the tails of the absorption bands of point defects associated with the absorption bands peaking in the visible or near-IR domains (such as the STHs [185, 224, 225]), for most fiber types (Ge-doped, P-doped,

etc), it has been shown that this is not the case and that additional unknown absorption bands have to be added to reproduce the RIA spectral dependences [72]. Another phenomenon that can change the fiber behavior under irradiation is the power level of the injected signal through the photobleaching effect. For some optical fibers, it has been shown that increasing the light power level in the optical fiber reduces RIA levels during irradiation and accelerates the recovery processes post-irradiation [203]. The photobleaching efficiency then strongly depends on the radiation-induced point defect(s) responsible for the RIA. As a consequence, photobleaching depends on the fiber type and application characteristics (wavelength, temperature, etc) but can be very efficient for some fibers such as germanosilicate optical types [201]. As a consequence of photobleaching, the radiation tests on optical fibers have to be done using a very low light power (typically well below 1 μ W) to establish the worst case scenario [226, 227]. In case the tests are intended to perform a comparison between the potential of different optical fibers for a given application, the best procedure consists of testing the optical fibers at the targeted light power of the application (for example mW power level) as the fiber ranking done at low power level (<1 μ W) may not be representative of that obtained when application requirements are followed.

3.1.4. Modeling of radiation-induced attenuation. One of the main difficulties regarding the radiation vulnerability study of optical fibers and OFSs concerns the representability of the available irradiation facilities to reproduce the constraints associated with the targeted environments. This is particularly true for space, where the dose rate is very low, the mission duration very long and the temperature varies over a large range. This is also an issue when new facilities or industries are built with environments (dose, dose rate, temperature) not covered by the existing radiation test facilities, e.g. megajoule class lasers [20]. The accessible accelerated results have to be associated with models that allow the expected fiber degradation to be extrapolated in the application conditions from the radiation test data. As it exists for microelectronic components, predictive simulation tools are needed to determine the RIA levels and kinetics throughout the whole mission duration. Today, several empirical or semi-empirical models have been developed to predict the growth and decay kinetics of RIA versus the dose or time after irradiation based on a limited set of radiation test results on the chosen optical fiber. Despite their intrinsic limitations, these tools are successfully used for space applications allowing the evaluation of the fiber RIA at a low dose rate from high dose rate results. Usually these models do not consider thermal effects and are adapted to the case of telecom-grade optical fibers or some radiation-hardened passive and polarization maintaining optical fibers [228]. A selection of some of these models is listed in table 5. Particular attention has also been devoted to the building of models which allow the behavior of

Table 5. A selection of RIA models.

Type of model	Authors	References
Power law	Griscom <i>et al</i>	[193]
Saturating exponentials	Friebele <i>et al</i>	[231]
Stretched exponential fit	Devine	[232]
Series of growth and decay events	Liu <i>et al</i>	[233]
Saturated exponential curves with other different parameters	Kyoto <i>et al</i> Levy	[234, 235]
β th order dispersive kinetic model	Gilard <i>et al</i>	[222, 236]
First order fractal kinetics	Maskhov <i>et al</i>	[223]
First and second order fractal kinetics	Griscom <i>et al</i>	[194]
Kinetic model	Borgermans <i>et al</i>	[79]
Nth order kinetic model	Friebele <i>et al</i>	[237]

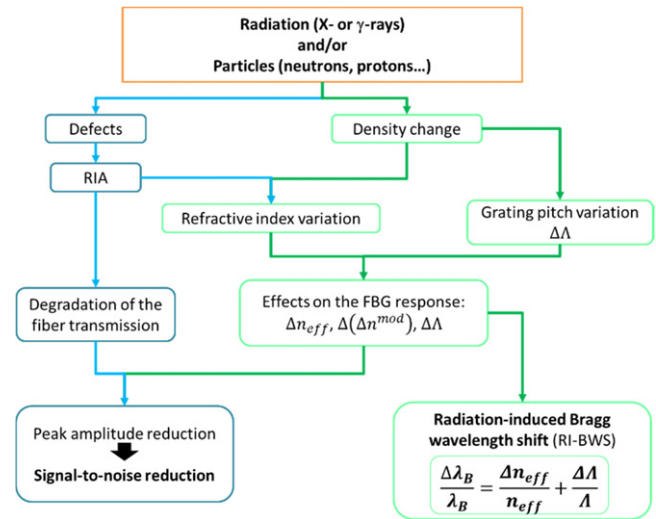


Figure 17. Schema describing how radiation influences the FBG response.

rare-earth optical fibers and related systems to be predicted for space applications [229], including thermal effects [230].

3.2. Point sensors: FBG

One key advantage of these point or distributed fiber sensing technologies remains the fact that only their sensitive part, being the sensing fiber, is exposed to radiation, whereas it is possible to install its interrogation part hundreds of meters or kilometers away. As a consequence, in all the performed studies, the performance of these sensors is characterized when only the sensing fiber is irradiated, not the interrogator parts, as these electronic-based devices would surely be more radiation-sensitive than the fibers.

3.2.1. Basic mechanisms. As already explained in section 3.1.1, harsh environments, such as space, are characterized by the presence of radiation and particles, which can induce defects and density change through ionization or displacement damage processes. Radiation affects the FBG response in two main ways, as highlighted in the diagram of figure 17.

First, the absorption bands related to the radiation-induced point defects degrade the optical fiber transmission. Then, even if at the basis of the FBG-based sensors there is a wavelength measurement, the RIA degrades the grating performance by decreasing the SNR, until the peak appears undetectable [238]. To avoid this issue, small pieces of photosensitive fiber, with gratings written on them, can be spliced onto radiation-hardened optical fibers for the signal transmission [239], or else the gratings have to be written directly on the radiation-resistant fibers at the Bragg wavelengths. However, a very important outcome of past studies is that the choice of radiation-hardened optical fibers does not ensure the design of radiation-tolerant FBGs, as demonstrated in [219].

Second, both the RIA and the density change can cause RIRIC, through the Kramers–Kronig dispersion relation and the Lorentz–Lorenz equation, respectively [240]. Therefore, the effective refractive index, the index modulation amplitude

and the period of the grating can change because of the radiation, inducing a reduction of the peak amplitude and a radiation-induced Bragg wavelength shift (RI-BWS, $\Delta\lambda_{Bragg}$). The peak amplitude reduction degrades the SNR; the RI-BWS can be defined as the sum of two contributions:

$$\frac{\Delta\lambda_{Bragg}}{\lambda_{Bragg}} = \frac{\Delta n_{eff}}{n_{eff}} + \frac{\Delta\Lambda}{\Lambda}, \quad (11)$$

and it entails an error on the sensing parameter measurement; i.e. an RI-BWS of 10 pm corresponds to a temperature error of 1 °C, for an FBG with a temperature sensitivity coefficient of 10 pm °C⁻¹. Figure 18 reports the x-ray-induced effects on the Bragg peak of a type I-UV FBG. Figure 18(a) shows the grating reflection spectra recorded during irradiation, whereas figure 18(b) highlights the induced peak shift and amplitude reduction.

For most cases—above all for type I-UV FBGs—under ionizing radiation the Bragg peak shifts towards the higher wavelengths with saturating behavior. Neglecting the effects on density and then $\Delta\Lambda$, the red-shift corresponds to an increase of n_{eff} , which can be explained by an increase of absorption at wavelengths shorter than λ_B . The saturating behavior can result from a limited concentration of precursor defects or competition between defect generation and recovery. In the first case, the saturation level should be dose-rate independent [241, 242].

3.2.2. Parameters affecting the FBG response. The RI-BWS depends on several parameters, as reported in table 6.

3.3. Distributed sensors

Mostly, three classes of DOFSs have been investigated under irradiation: those based on Rayleigh, Brillouin and Raman scattering phenomena, described in section 2.3. For each of these technologies, several sensing schemes have been developed allowing the sensing performance to be tuned with respect to the targeted application in terms of probed length,

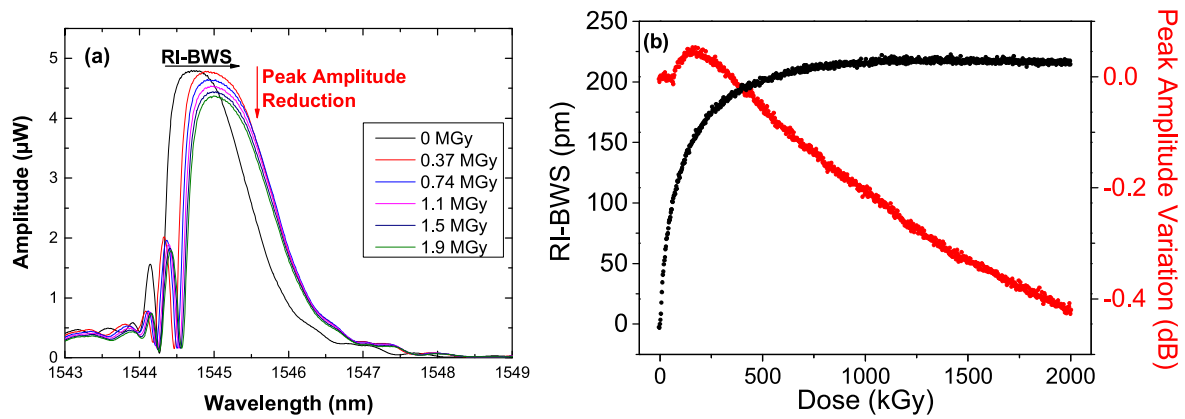


Figure 18. (a) The reflection spectra of a type I-UV FBG recorded under x-rays at RT with a 120 Gy s^{-1} dose-rate. (b) RI-BWS (black points) and peak amplitude variation (red points) as a function of the accumulated dose.

spatial resolution and sensitivity. In some cases, the choices made to develop the interrogator part can also modify the sensor vulnerability, even by keeping the same optical fiber as the sensitive element, as will be illustrated with the RDTS example.

3.3.1. Basic mechanisms. For sure, the RIA will affect all fiber-based technologies by reducing the available sensing length as the TID increases. Before irradiation, for most of the described technologies, sensing over kilometers or tens of kilometers is feasible, whereas during and after irradiation the available length for sensing will decrease by a factor that depends on the considered harsh environment, the nature of the fiber and its profile of use. As an example, fixing an arbitrary dynamic range of 10 dB for the sensor and based on the RIA measurements given in [73] for Ge-doped fibers, [249] for P-doped fibers and [73] for pure silica core or F-doped fibers, figure 19 illustrates the decrease of the sensing length with the γ -ray dose for an OFS operating around 1550 nm, either in single-ended (SE) or double-ended (DE) schemes. As can be seen, at MGy dose levels, even with radiation-hardened optical fibers, the available sensing length is strongly reduced, being less than one kilometer for all fiber types in these irradiation conditions. The use of DE sensors reduces this sensing range by a factor of two. For radiation-sensitive optical fibers, such as phosphosilicate ones, the RIA is so important that it prevents their use in DOFSs for doses exceeding 1 kGy. For the given example, the considered fiber presents an RIA of 10 dB m^{-1} after a dose smaller than 10 kGy [249].

In addition to RIA issues, it has been shown that radiation can change the structure of the pure or doped amorphous silica glass, this effect being more obvious at high fluences of neutrons, causing displacement damage [16]. By changing the fiber refractive index, the signature of the scattering mechanisms is affected in a way that usually induces an error in the evaluation of the measurand (temperature, applied strain, etc), as we have already highlighted for FBG-based sensors.

3.3.2. Macroscopic radiation response of Raman, Rayleigh and Brillouin-based sensors

3.3.2.1. Raman-based sensors. Several studies have been carried out to characterize RDTS performance under irradiation. The first studies [132, 250] provided evidence that in addition to a reduction of the sensing length with the dose, RIA causes a dramatic error in the temperature evaluation done by an SE-RDTS. This error is due to the difference in the RIA values at the Stokes and anti-Stokes wavelengths, also noted differential RIA or ΔRIA . The attenuation spectra before and after a 6 MGy dose are shown in figure 20(a) for a radiation-hardened pure silica core optical fiber (PSC-MMF) [82]. The probe wavelength (at 1064 nm) and the associated Stokes and anti-Stokes signals are indicated, highlighting that these different signals are differently affected by radiation [82]. This differential RIA, ΔRIA , causes an error in the evaluation of the ratio between the Stokes and anti-Stokes intensities, exploited to calculate the temperature. Its impact is shown in figure 20(b): when a 6 MGy irradiated optical fiber is used as the sensitive element of an SE-RDTS, the ΔRIA causes a direct error on the temperature estimation, and the amplitude of this error increases with the fiber distance, reaching 30°C after a short length of about 100 m. Even if this error can be reduced by an appropriate choice of fiber [251] or by applying a correction procedure [252], standard SE-RDTS is not adapted to operate in radiation-rich environments.

For sensors exploiting a DE scheme, the negative impact of the ΔRIA can be avoided at the cost of doubling the RIA impact on the sensing length [250]. A recent work has been published, demonstrating that such a DE-RDTS can be used to monitor the temperature around 350°C in a nuclear facility at doses of a few kGy using metal-coated PSC optical fibers [253].

3.3.2.2. Brillouin-based sensors. Several studies have been performed to characterize the radiation performance of Brillouin-based sensors [254, 255]. Here again the RIA limits the possible sensing range, for example from several kilometers down to a few hundredths of a meter for doses exceeding 1 MGy using a radiation-hardened optical fiber.

Table 6. The most important parameters affecting the RI-BWS.

Fiber parameters				
Parameters	Main cases	Impact on BWS	Remark	Refs
Fiber composition	Pure silica, Ge, F, B, Al, N, Ce	Nature and concentration of defects → photosensitivity	No correlation between the radiation hardness of a fiber and that of a grating written on it	[219]
Pre-treatment	H ₂ -loading	Nature and concentration of other extrinsic defects → photosensitivity	The hydrogen increases the fiber sensitivity to the laser light → it also increases the FBG radiation sensitivity → RI-BWS saturates at higher levels and at higher doses for FBGs written on loaded fibers than on unloaded ones	[243, 244]
Irradiation conditions				
Nature of particles	γ-rays, x-rays, neutrons, protons, electrons, heavy ions	Relative contribution of ionization and displacement effects → relative contribution of defects and densification	Preliminary results reveal different FBG behavior at equivalent doses when comparing x-ray, proton and electron tests	[220]
Dose (fluence)	From very low (space application—a few Gy) to huge (nuclear industry GGy, >10 ²⁰ n cm ⁻²)	Concentration of defects and phenomenon of densification	The higher the dose, the larger the induced BWS	[240]
Dose rate (flux)	From very low (space) to huge (fusion-related facilities)	Kinetics of defects → competition between defect generation and annealing	For type I FBGs, the larger the dose-rate the larger the induced BWS. For void-FBGs, no dependence on the dose-rate	[245, 246]
Temperature	From low (space applications) to high (800 °C for nuclear industry)	Kinetics of defects → competition between defect generation and annealing	The higher the irradiation temperature, the smaller the induced BWS	[247]
FBG writing conditions				
Type of grating	Types reported in figure 6	Nature of the periodic structure of the refractive index → defect precursors and structural arrangement	Type I-UV gratings are more radiation-sensitive than type I-IR varieties. Type IA FBGs are more sensitive than type I	[106, 248]
Writing laser	Laser wavelength and pulse width	Nature and concentration of defects in the different fringe of the periodic structure of the refractive index	For example, type I gratings written with cw laser at 244 nm are less radiation-sensitive than those written with the pulse lased at 248 nm	[106]
Post-treatment	Annealing	Recombination of defects and precursors, structural relaxation	A post-inscription short thermal treatment at high temperatures (15 min at 750 °C) significantly reduces the RI-BWS: from 60 pm down to 10 pm for an untreated and a pre-treated type II-IR FBG	[107, 243]
	Pre-irradiation	Defect precursor depletion	Pre-irradiation will reduce the grating sensitivity	

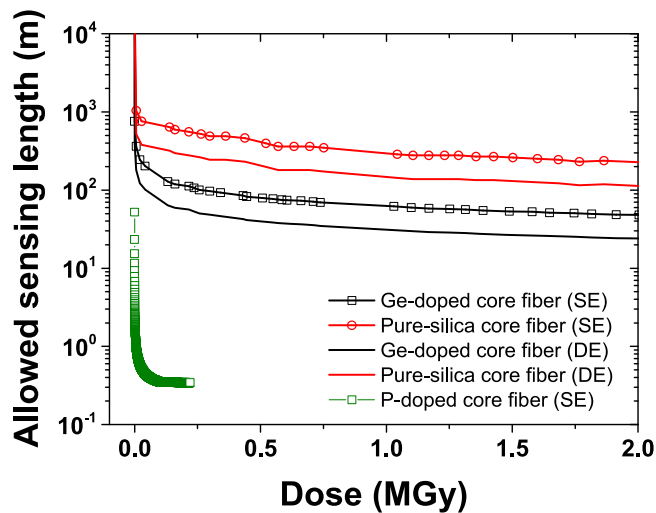


Figure 19. An illustration of the OFS sensing length decrease versus the dose for the main classes of optical fibers and a sensor having a 10 dB dynamic range at 1550 nm: telecom-grade, radiation-hardened and radiation-sensitive. The RIA data used to build this figure has been extracted from [73, 249].

Figure 21(a) illustrates the decrease of the Brillouin peak amplitude of a radiation-hardened pure silica core SMF during γ -ray irradiation at a dose rate of $\sim 1 \text{ kGy h}^{-1}$, when using a BOTDA [82]. Although the irradiation run was carried out for 160 h, the signal was no more exploitable after ~ 80 h due to a too small SNR. An analysis of the Brillouin signature after ~ 53 h of irradiation reveals that the peak amplitude value was reduced by more than 90%. Another radiation effect on the Brillouin-based sensor performance is the shift of the Brillouin frequency, hereafter named RI-BFS. This is due to the radiation-induced effects on the acoustic speed, through the density, and to the RIRIC. Figure 21(b) reports the RI-BFS as a function of the fiber length for these specific irradiation conditions (53 h). An RI-BFS toward lower frequencies is observed during γ -ray exposure at 1 kGy h^{-1} up to 53 h; its value remains almost constant along the fiber and is equal to $(-1.8 \pm 0.4) \text{ MHz}$. This RI-BFS cannot be distinguished from shifts caused by the measurands of interest (temperature, strain) and then causes a direct error of $1.5 \text{ }^\circ\text{C}$, for example, in the case of temperature monitoring.

The amplitudes and the kinetics of this RI-BFS depend on many parameters such as the fiber composition and the irradiation conditions. Today, the best identified optical fibers for Brillouin sensing at an MGy dose range are those with pure silica or fluorine-doped cores. In addition, to be associated with the lowest RIA levels in the near-IR range of wavelengths, these fibers also present the lowest RI-BFS, of a few MHz (equivalent to a few $^\circ\text{C}$ error) [82, 255].

3.3.2.3. Rayleigh-based sensors. Several studies have been performed to characterize the performance of Rayleigh-based sensors in radiation-rich environments. The two main categories of sensors are those based on the OTDR technique, and those operating in the frequency domain, OFDR [57, 256–259]. From the available results, it seems that

except for some very specific environments, such as those associated with very high neutron fluences, the Rayleigh signature remains almost unaffected by radiation and that reducing the fiber sensing length with RIA remains the main degradation parameter to be followed. Exploiting the interesting radiation tolerance of Rayleigh sensing, several sensors have been investigated. Some of them use radiation-sensitive optical fibers for radiation detection and dosimetry, while others exploit radiation-tolerant or radiation-hardened optical fibers for distributed sensing.

- OTDR/OFDR radiation sensors: associating these technologies with a radiation sensitive optical fiber, such as phosphorus, aluminum or REDFs, it is possible to make a distributed radiation detector with ODTR or OFDR sensors. The OTDR is an efficient tool to design dosimetry systems while the OFDR is associated with a more complex response to RIA [57, 249, 260–262]. For distributed dose measurements, the RIA is measured all along the fiber and knowing its dose dependence, the dose profile along the fiber is deduced with a typically one meter resolution. The first demonstration of such an approach was a dosimetry system deployed at the Tesla Test Facility (TTF) using an OTDR probing a multimode phosphosilicate optical fiber at 850 nm [263]. Today, another use of OTDR based-systems is under qualification at CERN, in view of its deployment at the LHC [249, 264].
- OFDR temperature sensors: for temperature sensing, the OFDR sensors associated with radiation-hardened optical fibers are able to operate up to very high doses of γ -rays [258, 259, 265] and neutron fluences up to $10^{17} \text{ n cm}^{-2}$ [17].
- OFDR liquid level sensor: in the context of post-Fukushima research, recent architecture for a water-level sensor to be implemented in nuclear pools has been demonstrated in [266] allowing the liquid level to be measured with a spatial resolution better than 1 cm or 3 cm in targeted normal and accidental conditions, respectively.

3.4. Rare-earth-doped fibers, EDFA and EDFS

Considering the interest of researchers in employing EDFAs and EDFs in space missions, most radiation studies have been performed at low γ -ray or x-ray doses ($< 1 \text{ kGy}(\text{SiO}_2)$) or low fluences of protons since the end of the 1970s. The first important outcome of these studies was to discover that REDF-based components are quite sensitive to radiation. An important decrease of the amplifier optical gain and an alteration of the noise figure are observed. These effects were sufficiently large to limit EDFA integration in space. Furthermore, these studies demonstrate that a few meters (typically less than 20 m) of the selected active REDF can explain the high EDFA radiation vulnerability. As a consequence, most of the past studies were then devoted to RE-doped fiber characterization in order to identify the best fiber types to increase the tolerance of EDFA or EDFs first, and second to

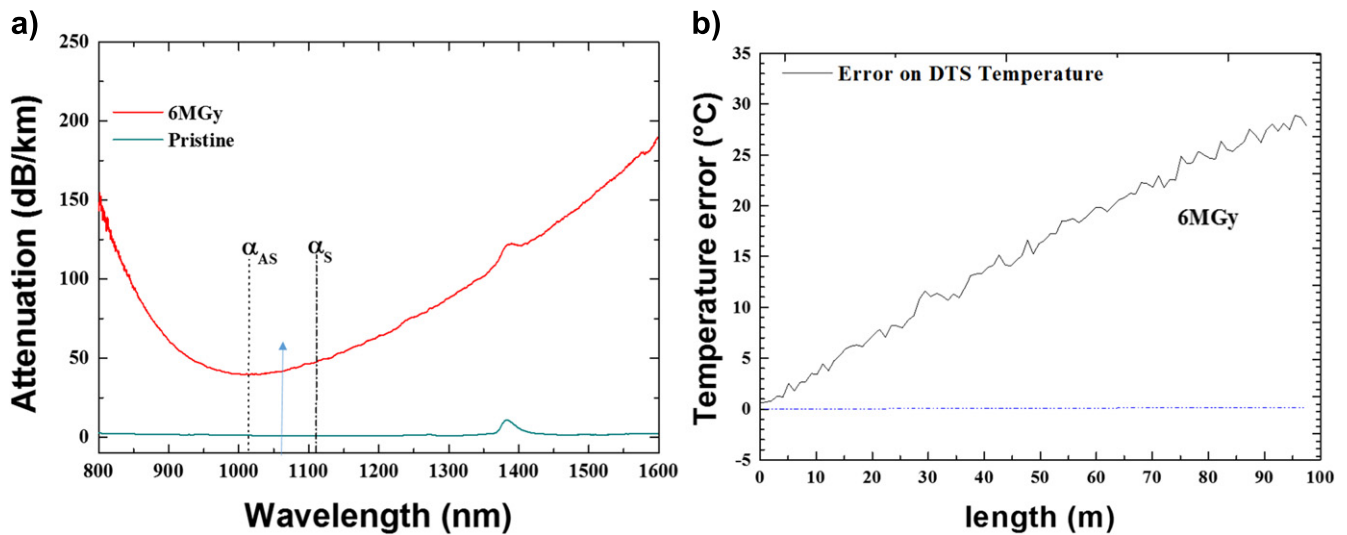


Figure 20. (a) The RIA spectra before and after irradiation at 6 MGy in a PSC MMF. The Stokes and anti-Stokes wavelengths as well as the probe laser light wavelength of the used SE-RDTS are highlighted; (b) an illustration of the error in the temperature measurement by this SE-RDTS using the PSC MMF pre-irradiated at 6 MGy. Reproduced with permission from [82].

understand the basic mechanisms at the origin of the high radiation sensitivities of REDFs compared to telecom-grade passive optical fibers. Among the different types of RE-doped fibers, erbium (Er) and Er/ytterbium (Er/Yb)-doped fibers are the most studied [267–271], but other RE elements have also been considered in the past [92, 272] or are today being investigated as promising technologies for future applications [273]. Characterizing the radiation response of REDFs appears to be more complex than the characterization of the transmission degradation of passive optical fibers. Indeed, the response of REDFs can be investigated under passive configurations (white light source and spectrophotometer, the configuration called P_{MIN} in section 4.4) similar to those used for passive fibers. However, as most of the applications used these waveguides in an active scheme, in which the rare-earth ions are pumped in the near-IR to generate amplified signals in the IR, the most representative results are those obtained in active configurations [274–277]. These studies first reveal the high sensitivity of commercial RE-doped optical fibers at both pump and signal wavelengths. This excess of losses clearly limits their use as lasers or amplifiers, but their high radiation sensitivity could be exploited for dosimetry applications [151].

3.4.1. Basic mechanisms. Spectroscopic measurements reveal that excess losses measured at the pump and signal wavelengths in REDFs are better explained by the nature of the matrix co-dopants (Al, P) added to facilitate RE incorporation rather than by the presence of RE ions [278]. These co-dopants are added to facilitate rare-earth incorporation while reducing the quenching effects. In the case of Er-Yb-codoped optical fibers, phosphorus is often used to increase the transfer efficiency from Yb^{3+} to Er^{3+} ions [278]. However, both Al and P dopants are associated with point defects responsible for an important RIA increase at both the pump and signal wavelengths [279, 280].

Furthermore, radiation at a space level seems to be associated with limited changes in the spectroscopic properties of RE ions [86], whereas at larger doses ($>6\text{MGy}$), changes of the ion spectroscopic properties also have to be considered to fully understand the properties of the RE-doped glass [281, 282].

3.4.2. EDFA macroscopic response. Under irradiation, EDFAs designed without hardening strategies suffer from strong gain degradation even at low doses. Figure 22 illustrates the gain decrease measured for an EDFA under x-rays at RT. In the used irradiation conditions, the EDFA gain decreases from 24 dB down to 14 dB after a dose of 3 kGy. The noise figure is also altered by irradiation, and simulation shows an increase from 6.5 dB up to 10 dB after the same dose. In the same figure the RIA spectra of the Er-doped fiber measured at different doses are also illustrated, highlighting the very high RIA levels at both the pump and signal wavelengths, exceeding 1 dB m^{-1} . These excess losses are mainly responsible for the EDFA and EYDFA gain and noise figure degradations.

3.4.3. Parameters affecting the EDF response. Numerous parameters can affect the response of the EDFA or EDFs. Among them, all those previously described in section 3.1.3 that affect the RIA levels in passive optical fibers also have an impact on the induced losses in RE-doped fibers. They are summarized in figure 23.

Of primary importance is the REDF composition, which has a clear impact on the nature of codopants or additional RE ions (such as cerium) used to optimize the amplification process. In addition to the fabrication process, the opto-geometric parameters have a strong influence too. As an example, for an ErYb-doped optical fiber, the double cladding, where the pump signal is propagating before being absorbed by the rare-earth ions, can strongly contribute to the

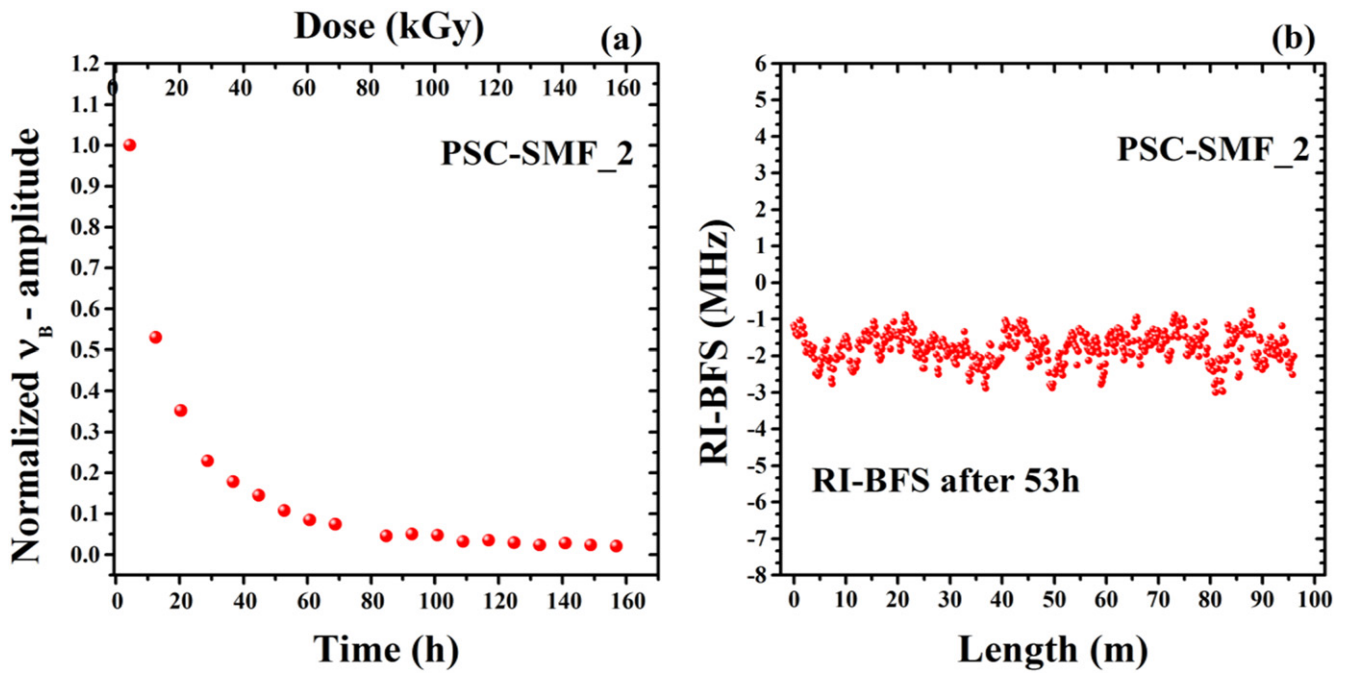


Figure 21. (a) The normalized Brillouin peak amplitude response versus the irradiation time for a radiation-hardened pure silica core single-mode optical fiber; (b) radiation-induced Brillouin frequency shift (RI-BFS) as a function of the same fiber length after an irradiation dose of 53 kGy. Reproduced with permission from [82].

gain degradation if it appears to be too radiation-sensitive and absorb the pump before its interaction with the RE ions embedded in the fiber core. The conditions of irradiation (dose, dose rate, temperature) influence the nature, growth and decay kinetics of point defects and then the RIA at the wavelengths of interest. From the available literature, it seems that ionization processes govern fiber degradation; as a consequence equivalent low doses of γ -rays, x-rays or protons seem to lead to the same degradation levels [270]. In the case of EDFA (or EFDS), the architecture choices also greatly impact the device radiation response.

- The EDFA radiation response depends on the pumping wavelength. It may appear advantageous to use a 1480 nm pump wavelength, as the RIA around this wavelength is lower than at 980 nm [283] so the gain reduction is minimized. However, to the best of our knowledge, no space-qualified diodes exist at 1480 nm, unlike those of 980 nm, explaining why all current EDFA architecture intended for space operates at 980 nm.
- The EDFA pumping scheme also influences its radiation response. Depending on the selected architecture (backward, forward, bidirectional), the pump and signal wavelengths present different RIA levels and kinetics and are also differently affected by additional phenomena such as photobleaching. The EDFA optimization will depend on each application case and will surely benefit from new simulation tools [145].
- The active fiber length is of primary importance. Without considering radiation, this length is optimized to obtain the best gain, usually by simulation, for a given optical fiber. Fibers with a higher concentration of rare-earth ions allow the EDFA to be designed with a smaller length of

active fiber, but can present quenching effects that limit the application process. As a general rule, as shown by Gusarov *et al* [284], the shorter the fiber length, the better the amplifier radiation response. Recently, a more systematic study on a possible broadband radiation-resistant EDFA was performed in [285].

- The pump power also strongly affects the relative contributions of point defect generation and bleaching mechanisms. A pump at a sufficient power level can induce both a darkening of the glass by creating point defects and simultaneously favor the bleaching of absorbing species through photobleaching [286]. Competition between these phenomena is complex and has been studied in detail in [93]. At the device level, the observed gain degradation can then be pump-power-dependent, rendering it mandatory to perform radiation tests in conditions representative of the application.
- Active fiber pre-treatment: As will be discussed in more detail in section 4.1.2 on hardening techniques, it is possible to change the active fiber radiation response and then the EDFA response by pre-treating the waveguide, with gas loading as an example. Every pre-treatment which allows the nature, concentration and kinetics of the point defects responsible for the RIA around the pump and signal wavelengths to be changed will affect the EDFA radiation response, either in a positive or negative way.

3.5. Gyroscopes

Commercial space FOGs have to deal with radiation at doses up to 1 kGy for 2 to 20 year missions with strong variability due to different orbits and shielding configurations. The

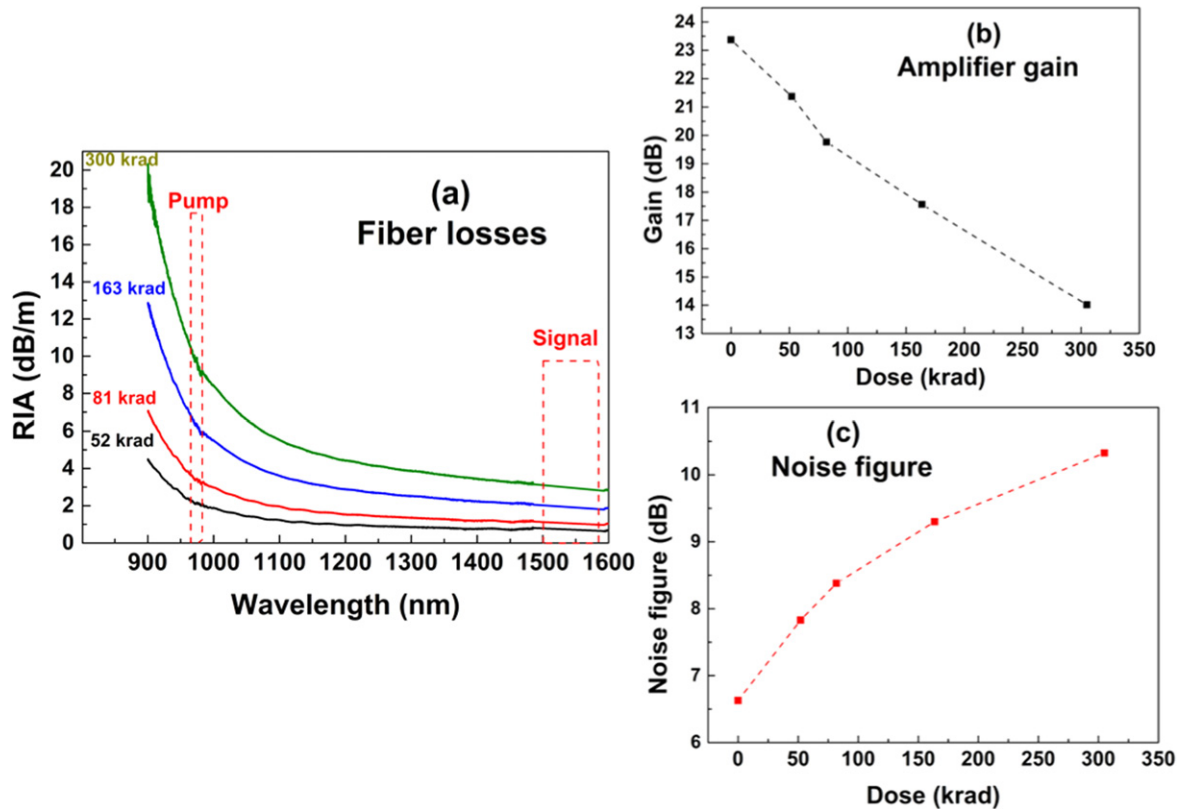


Figure 22. (a) An illustration of the radiation-induced attenuation (RIA) spectra measured in an erbium-doped optical fiber at different doses: 0.5, 0.8, 1.6 and 3 kGy; (b) the evolution of the EDFA gain versus the deposited dose (experimental results); (c) the evolution of the EDFA noise figure versus the deposited dose (simulation results [90]).

various FOG subassemblies react differently to radiation, as detailed hereafter.

- Electronics: radiation effects are obviously very important for the design of the digital part of the FOG servo loop. They are outside the scope of the present review.
- Laser diode and PIN photodiode: although the pump laser diode includes both a semiconductor laser and an FBG, neither the laser nor the photodiode display any significant degradation under proton and/or gamma exposure. The radiation-induced threshold current variation of the laser diode [287] remains negligible for the FOG design. Regarding space needs, those components are considered as radiation-insensitive [288].
- The lithium niobate modulator is immune to radiation too. No transparency variation is observed at doses relevant to space [287, 289, 290]. Hypothetical variations of its electro-optic response are not an issue either as the FOG servo loop continuously adapts itself to the modulator.
- Passive optical components, such as couplers and isolators, react to irradiation (through RIA) as they each contain a few meters of optical fiber [291, 292]. Their transmission properties are then affected, but the involved fiber length in those components remains sufficiently small to be neglected if the selected fiber is a telecom-grade fiber such as the Corning SMF28. For cases where the FOG design imposes an exotic optical fiber associated

with higher RIA levels than SMF-28 fibers, the radiation response of those components will then become of importance. The transparency is not the only affected parameter during irradiation: spectral variations of those components due to RIA are detectable for the relevant space dose, but not strong enough to restrict the FOG design, even for high-precision varieties. With continuous improvements to FOG performance, this could become an interesting topic in the future.

- Optical coil: the Sagnac coil contains a length of PM fiber ranging from a few hundred meters to several kilometers, according to the required FOG performance. With such a fiber length, any RIA phenomenon quickly becomes a problem as the available optical power takes a hit and the FOG rotation noise rises. This excess of optical loss cannot be entirely mitigated by increasing the optical source power, implying the use of radiation-resistant optical fiber for the Sagnac coil. The fiber transmission is not the only affected parameter during irradiation: spectral variation occurs and affects the FOG scale factor performance. This spectral effect is negligible nowadays with radiation-resistant fibers and current high-end FOG performance, but as FOG performance is still increasing, this could still also become an interesting topic in the coming years. Radiation-induced birefringence variation could also theoretically affect the FOG, but this has not been observed today in existing commercial systems.

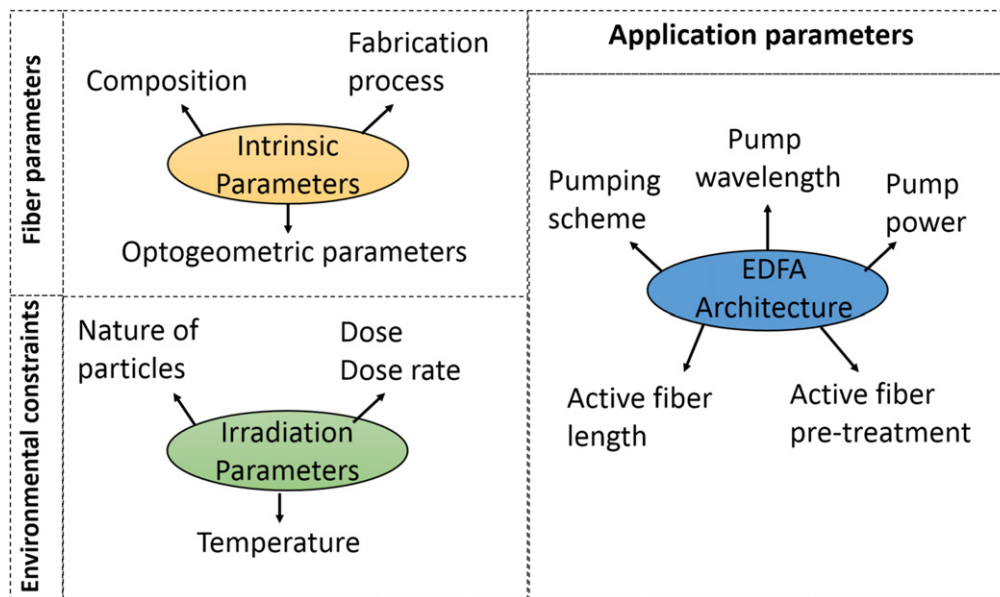


Figure 23. An illustration of the main parameters affecting the gain degradation of an EDFA or EYDFA under irradiation.

• Erbium-doped optical fiber: high-performance FOGs use EDFs as an ASE optical source. The fiber length ranges between 1 and 10 meters, while the power extracted at 1550 nm is in the 10 to 100 mW range. As already discussed, EDF is much more sensitive to RIA than passive optical fibers. As a consequence, this subpart of the FOG, albeit being far shorter in length than the Sagnac coil, is an important contributor to global FOG radiation degradation, and the use of radiation-hardened optical fibers appears mandatory. A radiation-induced optical spectrum change is inevitable, as the RIA changes the operating point of the ASE source, but does not limit the FOG scale factor performance today.

the requested optical performance. The second one corresponds to pre-treatment of the fibers in order to change (decrease) its number of precursor sites, reducing as a consequence the number of radiation-induced point defects. It is important to mention that today there exists no optimal composition, allowing the design of an optical fiber with a reduced RIA for all environments of interest. As an example, the so-called radiation-hardened pure silica core and fluorine-doped core fibers present the best radiation response in the infrared part of the spectrum under steady state γ -rays (high-energy physics facilities, nuclear power plants, etc) [75], whereas these fibers show the highest transient RIA after an x-ray shot (fusion by inertial confinement) [180].

4. Recent advances in radiation hardening

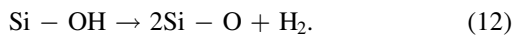
As more and more applications are envisaged for optical fibers in harsh environments, strongly extending their use to sensing, new approaches have to be followed to improve the radiation tolerance of optical fibers and fiber-based devices and to extend their lifetimes in harsh environments. In this part of the review, recent advances regarding the hardening of optical fibers, FBG and distributed sensors are given, with a particular focus on the technologies that have already been evaluated for space programs.

4.1. Optical fibers

Improving the radiation tolerance of optical fibers is possible by controlling the nature and concentrations of point defects in order to limit the RIA at the wavelengths of interest. For this, different approaches have been followed. The first one, called hardening-by-component, consists of tuning the fiber composition in order to decrease the RIA levels in the spectral domain of interest for a given environment, while maintaining

4.1.1. Hardening-by-component. Up to now, most research has been devoted to the identification of the best classes of optical fibers for operation either in the visible domain or in the infrared part of the spectrum and up to doses of a few MGy. This first class of fibers is of interest for the plasma diagnostics of the ITER facility, which require large core MMFs (above 100 μm) able to transmit light in the visible range. Numerous studies have been conducted in Europe [293], Russia [294] and Japan [209], allowing the best candidates for this application to be identified. These appear to be pure silica core (PSC) or fluorine-doped optical fibers. After that, several studies have focused on the hardening of these fibers to reduce the RIA levels in the visible domain. The first attempts were made to reduce the impurity levels in the fiber core and cladding. Two main classes of silica are available: the first one, also called ‘dry silica’, contains low levels (>1 ppm), but this is achieved by increasing the amount of chlorine in the glass. As a result, this kind of fiber presents a high transmission level in the IR but lower transmission in the UV range, compared to the second class of silica, ‘wet silica’, which contains high hydroxyl amounts (>100 ppm) and low chlorine concentration (< 1 ppm). For

ITER needs, wet silica is better adapted, but under irradiation these fibers are characterized by a strong RIA around 600–650 nm, which is related to the NBOHC, see figure 12. The high concentration of NBOHC is related to the presence of hydroxyl groups that act as precursor sites:



To overcome this limitation, a new class of glass has been made, mainly in Russia, combining both low hydroxyl group content (<1 ppm) and low chlorine impurity (<1 ppm) content. Radiation tests reveal that for these fibers, the strong diminution of precursor sites opens channels for the generation of less-studied unstable room-temperature defects, namely self-trapped holes (STHs). These defects have been studied in detail in [225], and are associated with absorption bands in the visible range (see figure 15), making it difficult for these fibers to qualify for the targeted applications. Another efficient way of minimizing the NBOHC concentration is to slightly dope the glass with fluorine. Adding this element does not induce the appearance of F-related defects, whereas it has demonstrated the ability to passivate some point defects such as NBOHCs. In addition to ITER studies, a complete investigation was performed by CERN to select the best optical fibers for the data links at the Large Hadron Collider (LHC) operating at 1310 nm. For these applications too, the fibers that are most tolerant to the considered dose of 100 kGy(SiO₂) are the fluorine-doped optical fibers from Fujikura [214]. These fibers present quite complex RIA growth kinetics at this wavelength, but the RIA levels remains below 5 dB km⁻¹ at a 100 kGy dose for the IR wavelengths 1310 nm and 1550 nm.

4.1.2. Hardening by pre-treatment. Another very efficient approach to reducing RIA due to NBOHC consists of loading the fiber core with gas, this gas being able to quickly react with radiation-induced point defects and passivate them. Hydrogen and deuterium are the most investigated, as fibers can be easily loaded with these gases. This treatment has been deeply studied by the fiber community in order to enhance the photosensitivity of germanosilicate optical fibers in view of their functionalization with FBGs. Several studies have reported that the hydrogen presence strongly changes the fiber radiation response, regardless of its composition [205, 295]. For PSC or F-doped optical fibers, the hydrogen presence improves their radiation hardness in the visible domain, thanks to the passivation of the NBOHCs [296], the drawback being that these defects are converted into hydroxyl groups absorbing in the IR part of the spectrum and in other defects causing an increase of induced losses in the UV part of the spectrum. The process at stake is the following:



This example clearly shows that the efficiency of this hardening technique strongly depends on the application needs, as the hydrogen presence will enhance the concentration of some defects, such as H(I), H(II) centers absorbing in

the ultraviolet, while passivating other defect structures. Using deuterium globally provides the same effect, although one difference concerns the spectral positions of the related D2 species, which differ from those of the hydrogen species, allowing for some applications to have less impact on the signal propagation [22]. One of the main concerns with this hardening solution is that the hydrogen diffuses out easily from the fiber at RT, and that without specific mitigation solutions, it is not possible to keep the gas inside the waveguide for more than a few days. This is of particular concern for long space missions and facilities with a long lifetime, and existing solutions will be detailed in section 4.4. More recent studies have investigated the potential of adding an excess of oxygen to the optical fibers, varying the manufacturing process, or by direct O₂ loading of the fiber at high temperature and high pressure [186, 187, 297]. Unlike hydrogen, oxygen is not mobile at RT and its concentration will remain constant during the fiber lifetime. Such treatment also strongly changes the defect equilibrium under irradiation, with a positive or negative impact on the RIA levels and kinetics depending on the considered signal wavelength. In [297], a larger RIA is reported in the UV and visible domain, whereas in [186, 187], the authors reported the positive impact of excess oxygen on the RIA levels in the IR part of the spectrum for PSC optical fibers. In addition to gas, other pre-treatment can change the nature and concentrations of point defects generated under irradiation. This is, for example, the case for pre-irradiation treatment, which can be used to convert the existing precursor sites into optically active point defects. If it is possible, e.g. by thermal treatment, to bleach these defects, the treated fiber can present a better radiation response when exposed to a second period of irradiation, as it contains a lower amount of precursor sites. Such an effect has been patented [208] and its efficiency to the response of PSC optical fibers was demonstrated in [207].

4.2. FBG

FBGs are affected by radiation through two phenomena: the decrease of FBG peak reflectivity and the radiation-induced Bragg wavelength shift (RI-BWS). The first one can be quite easily mitigated using several types of inscription methods. For the RI-BWS, since its amplitude and kinetics depend on so many parameters, the usual identification approach of the most tolerant FBG for a given application consists of testing each FBG technology at facilities reproducing the radiation constraints associated with the target application (see the 2013 review [240]).

Grobic *et al* showed that type I and II gratings, written with a femtosecond IR laser in unloaded Ge-doped or PSC fibers, are among the most radiation resistant under γ -rays at RT [298]. RI-BWSs of less than 15 pm were observed at the accumulated dose of 100 kGy. Even type I-IR FBGs are more radiation tolerant than those of type I-UV. This may be explained by the fact that the high laser peak power density values used to write the FBGs probably convert all the precursor sites into point defects during the grating inscription, reaching a stable state maintained during irradiation [106].

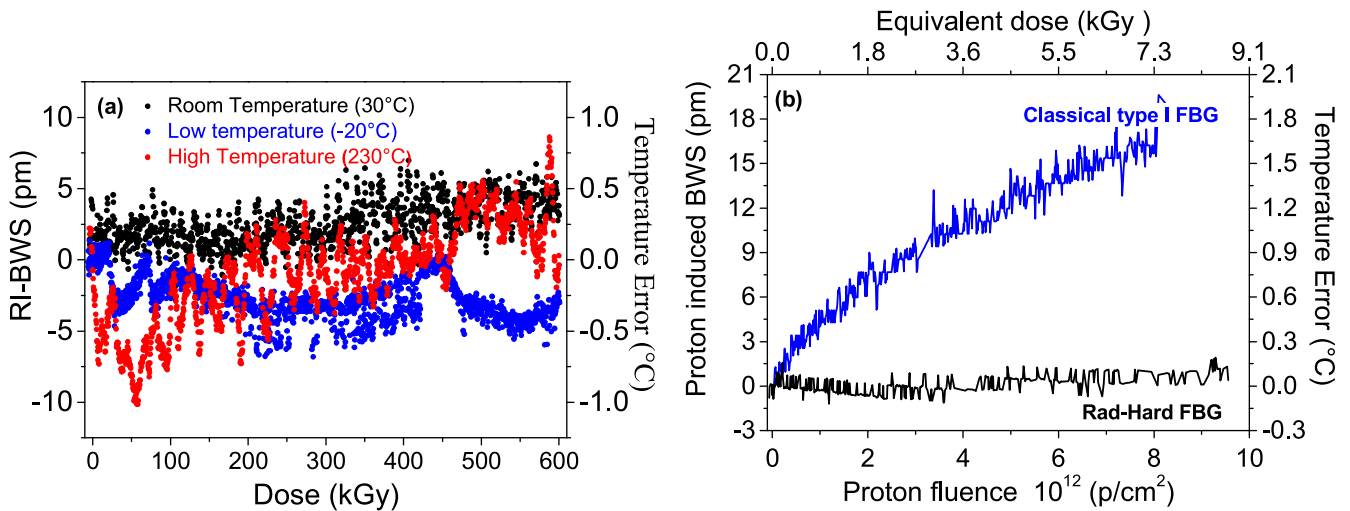


Figure 24. (a) BWS induced on rad-hard FBG by x-rays at different temperatures (30 °C—black points; –20 °C—blue points; 230 °C—red points), as a function of the TID, up to 600 kGy. (b) The proton-induced BWS of a classical type I-UV FBG (blue curve) and a rad-hard FBG (black curve) as a function of the proton fluence.

Morana *et al* recently patented a method for fabricating FBGs resistant to very harsh environments, mixing high doses and high temperatures [107, 299]. These gratings are written on radiation-hardened optical fibers (PSC or F-doped fibers), to ensure signal transmission, with a femtosecond IR laser (i.e. at 800 nm) and then subjected to thermal annealing treatment at 750 °C lasting at least 15 min. The laser power density has to be higher than the threshold needed to generate type II gratings; since thermal treatment at 750 °C will erase all type I components, only the type II variety resists such a high temperature. It is the post-thermal annealing performed on the gratings before irradiation that makes the FBGs more resistant. The robustness of these gratings has already been confirmed in several radiation environments, involving x-rays (up to a 3 MGy dose) or γ -rays (up to 200 kGy) and operating temperatures as high as 350 °C [300, 301], a total fast neutron fluence of $\sim 5 \cdot 10^{19}$ n cm⁻² and a total gamma dose of ~ 5 GGy [25], as well as high-energy protons (63 MeV) up to fluences of about 10^{13} p cm⁻² [302]. Figure 24(a) reports the response of such rad-hard gratings under x-rays at three different temperatures: low (–20 °C), room (30 °C) and high (230 °C). Independently of the irradiation temperature, the induced error on the temperature measurements is always lower than ± 1 °C. Figure 24(b) compares the responses of a classical type I-UV grating and that of a rad-hard FBG under a flux of about 3×10^{12} protons (cm⁻² · h⁻¹) at RT, up to a fluence of 10^{13} protons cm⁻², which corresponds to an equivalent TID of about 9 kGy(SiO₂). The Bragg peak of the classical FBG shifts by about 18 pm at the maximum TID, whereas the response of the rad-hard grating is not influenced by protons. As a consequence, such rad-hard FBGs will be efficient temperature and/or strain sensors in space, since they are insensitive to ionizing radiation at low and high temperatures and insensitive to TNID related to protons.

Recent studies [106, 246, 303] have focused on the radiation response of the void-gratings. They show complex

behavior under radiation: when the exposure is performed at RT, these gratings are as resistant as type II gratings (RI-BWS less than 5 pm at 1 MGy dose, for a void-FBG written in an F-doped fiber [246]); however, when these FBGs are exposed to the combined effects of radiation and temperature, the Bragg wavelength of the void-FBGs blue shifts, without showing saturating behavior with the accumulated dose [106, 246].

4.3. Distributed sensors

In this section, we discuss how the radiation tolerance of distributed sensors can be improved by making appropriate choices of component (fiber) or at the interrogation system level. Today, these different technologies are not being directly considered for use in space, to the best of our knowledge. Their integration remains limited by the interrogator parts of sensors that are not yet sufficiently miniaturized and radiation tolerant. In the near future, this limitation will probably be overcome thanks to the new generation of miniaturized integrators based on ASICs (application specific photonic integrated circuits). Such an on-chip interrogator already exists for FBG strain or temperature sensing [304]. However, DOF technologies are today of major interest in the ground environments associated with nuclear power plants, high energy physics facilities or radioactive waste repositories. For all these environments, the acquisition units can be stored in radiation-free zones, and the sole sensing fiber is exposed to harsh radiation constraints.

4.3.1. Rayleigh DOFS. Several papers have demonstrated that the fiber Rayleigh signature used by OFDR sensing technology is robust against radiation [305]. However, radiation affects the acrylate coating properties, and, by stabilizing the coating through pre-thermal treatments, the precision of the OFDR measurements is increased [221]. The

only remaining parameter to consider is then the RIA, which limits the available sensing length. As these sensors operate at telecom wavelengths, in the IR, the best fibers are usually PSC optical fibers or F-doped optical fibers, as shown in figure 20, allowing the use of fiber lengths exceeding 100 m under irradiation. In the future, the capabilities of Rayleigh-based sensors may be enhanced thanks to the development of a new generation of fibers—the so-called all-grating fibers [306]. These fibers contain densely spaced low reflective ($R < 0.1\%$) draw tower gratings (DTG@s) [306]. Combined with an OFDR interrogator, these fibers should greatly improve the measurement dynamics and then increase tolerance to RIA effects. By combining OFDR technology with a radiation-sensitive optical fiber, it appears possible to detect radiation and maybe to perform spatially resolved dose measurements with resolutions of 15 cm, but with a more difficult sensor calibration phase than for OTDR-based dosimetry systems [256].

4.3.2. Brillouin DOFS. For Brillouin-based sensing, two radiation effects have been observed that reduce sensor performance: RIA and the radiation-induced Brillouin frequency shift (RI-BFS). Although the microscopic origin of the RI-BFS is still not fully understood, the amplitude and growth kinetics of the RI-BFS with the dose clearly depend on the fiber composition. As a consequence, optimizing the fiber for sensing in harsh environments implies simultaneously reducing the RIA and RI-BFS levels. From today's knowledge, fluorine-doped fibers are the best candidates for such applications, having limited RIA levels at MGy dose levels (below 50 dB km^{-1} at 1550 nm) and a limited RI-BFS of a few MHz (equivalent to a temperature error of a few degrees Celsius). Regarding the RIA issues, some Brillouin sensor architectures allow greater dynamic measurements to be achieved than others, allowing the partial mitigation of RIA effects and the consideration of higher sensing distances at MGy dose levels [307].

4.3.3. Raman DOFS. For Raman-based sensing, two phenomena reduce sensor performance: RIA and differential RIA (ΔRIA). If an appropriate choice of fiber allows RIA-related constraints to be reduced, it appears very difficult to overcome the ΔRIA issue by tuning the fiber composition or its fabrication process. For this sensor, it is, however, possible to improve the radiation hardness by working on the architecture of the interrogator.

The first solution is to use a double-ended architecture that allows the ΔRIA to be compensated, but at the cost of doubling the RIA issues. With such architecture and as demonstrated in [82, 132, 250], it is possible to maintain the quality of the temperature measurements thanks to the correction made possible by probing the sensing fiber from its two ends. Using this scheme, in [253], the authors show that temperature measurements along a PSC optical fiber with a gold coating at 260°C are possible thanks to the positive combined effect of temperature and radiation on the fiber RIA.

Another solution, recently published in [308], allows a single-ended scheme to be kept (thus reducing RIA impact) while avoiding the negative impact of ΔRIA . This SE-RDTS architecture exploits two probing lasers at given wavelengths allowing the simultaneous recording of OTDR traces at the Stokes and anti-Stokes wavelengths in addition to Stokes and anti-Stokes traces. In this way, it is possible to correct these last traces for ΔRIA caused by radiation or the appearance of bending losses, and keep the temperature measurement precision. Associated with a radiation-sensitive optical fiber, this system could allow the dose (through RIA) and temperature distributions to be simultaneously recorded along a unique optical fiber [308].

4.4. Rare-earth-doped fiber amplifiers and sources

As previously discussed in section 3.4, the high radiation sensitivity of EDFA, EYDFA or sources is mainly explained by the high sensitivity of REDFs, either erbium-doped (EDF) or erbium-ytterbium-doped (EYDF). To improve the hardness of these amplifying systems, the first investigated solution involved enhancing the radiation tolerance of these active fibers to decrease the observed RIA levels at the pump (around 900 nm – $1 \mu\text{m}$) and signal wavelengths (around 1550 nm). Since 2010, several techniques have been described in the literature to achieve this goal, and they are schematically summarized in figure 25. In addition to these hardening-by-component approaches, it also appears possible to optimize the amplifier architecture (hardening-by-system) to reduce its radiation vulnerability, regardless of the fiber behavior. Finally by combining these two hardening approaches, it is today possible to conceive EDFAs and EYDFAs with optimized performance and reliability for a given space mission profile rather than for on-ground testing.

4.4.1. Hardening by component. As for the hardening of passive optical fibers for data transfer, several approaches have been followed to reduce the RIA in active optical fibers caused by P and/or Al-related defects. The first solution relies on a manufacturing process change, allowing the design of active fibers without using these dopants while still maintaining high amplification efficiency. Another approach could be to control the equilibrium between the various point defects created in silica under irradiation, trying to reduce the concentrations of those absorbing at pump and signal wavelengths. Such defect control can be achieved by the appropriate codoping of the fiber core or by pre-treatment.

The first approach was followed by Draka Comteq in 2012, and showed that active erbium-doped optical fibers with reduced amounts of Al can be produced by their patented nanoparticle doping process [311, 312]. This approach noticeably improves the radiation resistance of the fiber without degrading its amplification performance too much through quenching effects [313]. To the best of our knowledge, such a manufacturing process is not yet transposable to EYDFs. In figure 25(a), the advantage of using this technology is highlighted by comparing the performance of EDFA based on this fiber and on a conventional Al and/or

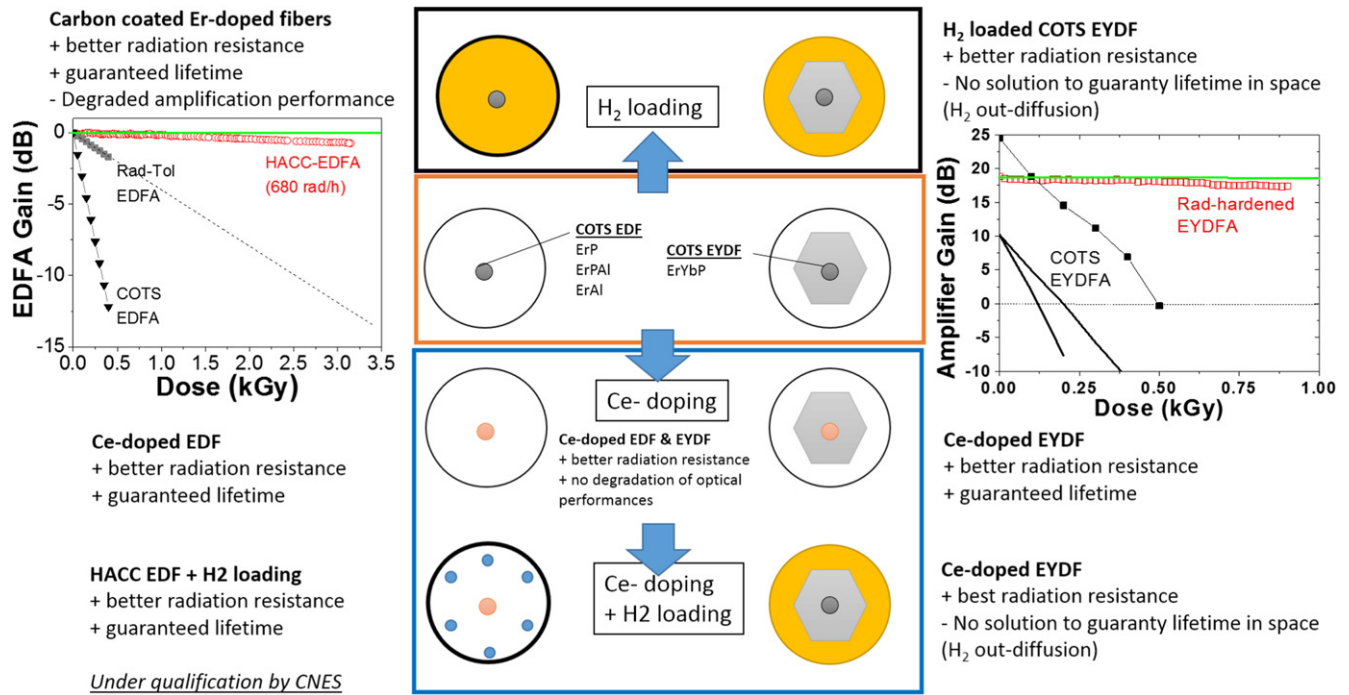


Figure 25. An illustration of the variety of hardening by the component solutions proposed in the literature to enhance the radiation tolerance of EDF and EYDFs. (a) A comparison between the gain degradation measured for a variety of EDFAs based on the different generations of EDFs; more details can be found in [309]. (b) A comparison between the gain degradation measured for a variety of EYDFAs based on different generations of EYDFs; more details can be found in [310].

P-doped fiber, tested under γ -rays in an OFF configuration (pumping only during the gain measurements), the conventional EDFA gain decrease is of about 100% after a 500 Gy dose, whereas it remains below 15% for an EDFA based on the nanoparticle EDF [218].

The same year, the codoping efficiency of the active fibers (EDF or EYDF) with cerium was demonstrated and patented by iXBlue Photonics [314]. Adding cerium to the fiber core does not modify the spectroscopic properties of erbium and ytterbium ions [315], or the EDFA performance, but strongly improves the fiber and EYDFA radiation resistance [310]. This can be explained by the positive impact of Ce^{3+} ions on the POHC and P1 defects, which are less efficiently produced in the presence of this element [83]. The positive impact of Ce-codoping on the radiation hardness of bulk optical materials has been known for years [316, 317] and exploited to manufacture radiation hardened glasses for optical space systems. This is also the case for Er-doped optical fibers and EDFA, even though the positive Ce impact seems less important than in the Er-Yb case from the published results [309]. The data of figure 25(a) shows that a Ce-doped EDF allows an EDFA to be built with a better radiation response than the nanoparticle EDF, with the gain decrease limited to 10% after 500 Gy. Figure 25(b) shows the strong positive impact of the Ce-codoping of the EYDF on the EYDFA performance. For this optimized EYDFA, the gain decrease is less than 5% after 500 Gy of γ -rays, whereas it reaches about 35% with a conventional EYDF [310].

In addition to these techniques, several authors have demonstrated that if the active fiber contains hydrogen in its

core, its radiation resistance and the corresponding EDFA or EYDFA is strongly increased [87, 218, 310, 318], with almost the complete bleaching of the Al and P-related absorption. By combining the two mitigation solutions (Ce-codoping and H₂-loading), it was demonstrated that both EDFA [218] and EYDFA [310] become very radiation resistant at high doses, exceeding those expected for future challenging space missions. This is also illustrated in figure 25 for the EDFA and EYDFA: the systems using gas-loaded fibers present almost no degradation of their gains (less than a few %) after a 500 Gy dose.

One of the difficulties with the practical use of an active fiber loaded with gas is that this gas will easily diffuse out of the fiber core at RT in a conventional fiber structure. Another challenge is that if the gas concentration is too high, the amplification properties of the active fiber are affected too, with a decrease of the achievable gain for the EDFA or EYDFA [144]. One solution for keeping the gas inside the fiber is to use a waveguide with a carbon layer of a few tens of nanometers between the fiber cladding and its coating [318]. Mobile hydrogen cannot go through this layer in normal conditions, but the loading of this carbon-coated fiber with hydrogen remains possible at elevated temperatures [319]. This solution is interesting but the loading procedure is complex, the amount of gas is difficult to control and usually the performance of the fibers is degraded by high-temperature treatment. An alternative approach was proposed in 2014 [218, 309] to overcome the observed limitation, namely through hole-assisted carbon coated (HACC) optical fibers. These fibers have holes in their cladding (see figure 26(a));

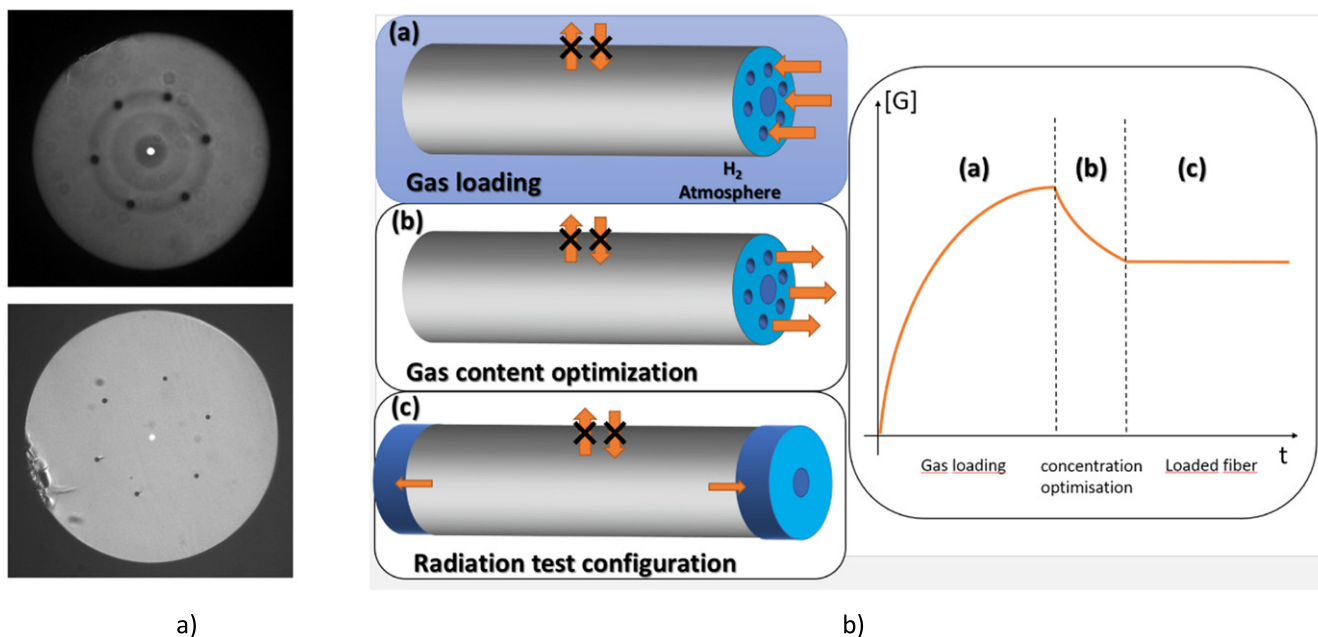


Figure 26. (a) An illustration of two different HACC fiber structures manufactured by iXBlue Photonics with holes of different sizes. (b) The principle of loading gas into these fibers; more details can be found in [218, 309]. During the first phase the gas is injected into the fiber through the holes at one of its ends, whereas the second end is closed. The gas diffuses into the fiber up to a certain concentration. The gas level is controlled in a second phase to ensure the best compromise between radiation hardness and amplifier gain. When the targeted amount is achieved, the fiber is spliced, and the out-diffusion kinetics of the gas at room temperature is decreased by a factor of more than 100, allowing the presence of hydrogen to be guaranteed during the lifetime of a space mission.

these holes have no impact on the fiber guiding properties (in contrast to MOFs), but allow the gas loading to have access to one fiber end only, according to the procedure described in figure 26(b).

Through this procedure, it is possible to control the amount of gas and achieve the best compromise between radiation hardness and the optical performance of the optical system. Using this approach, an EDFA based on this HACC fiber has been characterized under γ -ray doses up to 3.15 kGy(SiO_2) in an ON configuration where the active fiber is pumped during the whole irradiation test. The 31 dB amplifier is practically radiation insensitive, with a gain change of merely -2.2×10^{-4} dB Gy $^{-1}$ [218]. The irradiation of the same generation of EDFA with 63 MeV protons up to a fluence of 7.5×10^{11} p cm $^{-2}$ (equivalent dose of 1 kGy) confirms the excellent tolerance of this HACC-EDFA component, showing the limited decrease of ~ 0.6 dB of its ~ 27 dB gain [309].

4.4.2. Hardening-by-system approach. Various EDFA architectures can be realized to tune the amplifier performance (gain, noise figure) with respect to the targeted application requirements. For example, different pumping schemes can be used: forward, backward, double pumping, etc. Different pumping wavelengths can be selected (e.g. for EDFA 980 nm or 1480 nm), and the active fiber length needs to be optimized. All this optimization is usually performed by simulation as the physics of light amplification and the spectroscopy of various rare-earth ions is well-known today. State-of-the-art tools allow the amplifier architecture to be optimized to obtain the target performance. Recently, studies

have been initiated to implement the radiation effects in the code in order to optimize the system, not only for in-lab testing but rather for its operation during the space mission. In particular, the results of the optimization process will change by considering the radiation effects and their impact on the system characteristics and the resulting selected architecture will differ. The objective of such modeling is to optimize the full system for its operation profile-of-use with regards to the environmental constraints and not for on-ground tests before launch.

For the radiation effect module, the RIAs at the pump and signal wavelengths have to be considered since they are known to greatly affect the gain. However, the impact of radiation on rare-earth ions is less well studied and more difficult to investigate experimentally. To identify those parameters that could significantly modify amplifier behavior if they evolve under irradiation, a parametric simulation study was recently performed, varying each parameter by $\pm 20\%$ and evaluating its impact on the gain and noise figure of the system [90]. The outcomes of this study are that the energy transfer coefficient from Yb^{3+} to Er^{3+} ions can influence the EYDFA amplifier gain if the radiation changes its value by $\pm 20\%$, whereas the upper level lifetimes and up-conversion coefficient are not expected to affect the amplifier gain or noise figure [90]. At this time, two different categories of amplifiers have been investigated through the coupled experiment/simulation approaches.

- The first category concerns EYDFA with moderate output power (< 2 W) [310]. In this case, it has been shown that the measurements of the RIA at 915 nm and 1550 nm

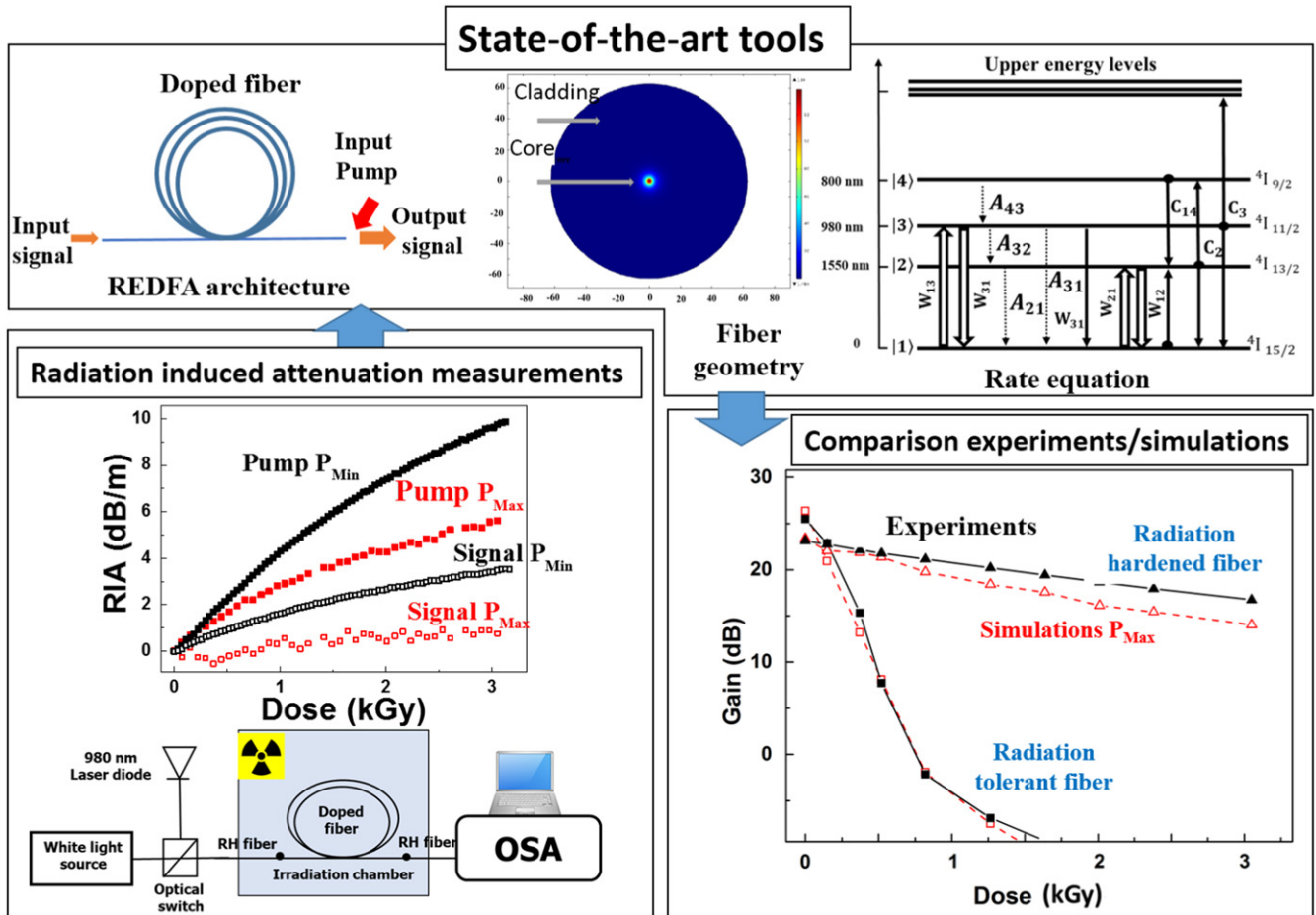


Figure 27. (a) An illustration of the RIA measurement setup allowing RIA levels to be obtained at the pump and signal wavelengths in the P_{MAX} and P_{MIN} configurations. (b) An illustration of the modeled architecture of EDFA and the considered model for the erbium ion spectroscopy. (c) A comparison between experimental and modeled EDFA gain degradations with a dose when rad-hard and COTS fibers are used.

through a classical measurement setup (white light source + spectrophotometer, PMIN configuration of figure 27) can be used as input parameters in the simulation tools and allow the observed EYDFA gain decrease under irradiation to be reproduced with good confidence. As a consequence, it was deduced that for such ErYb doped fibers, the photobleaching effects are negligible, as it was assumed by the limited gain recovery at the end of the γ -ray exposure and that all other radiation effects (on RE ions, etc) can be neglected at the first order. It should be noted that the modeling becomes more complex for high-power EYDFA (>10 W), for which combined photo and thermal issues will affect the RIA levels and kinetics.

- The second category concerns EDFA with output power on the order of 1 W. In this case, a recent work [144] reveals that a more complex approach has to be followed to evaluate the RIA levels at the pump (980 nm) and signal (1550 nm) wavelengths in order to reproduce the experimentally observed degradation of their gains with the dose. This is explained by the fact that for such optical fibers, there is a strong pump photobleaching effect on the RIA at both the pump and signal wavelengths and with

the PMIN configuration; the RIA levels are overestimated compared to those occurring in the pumped fiber of the EDFA. To reduce the error, the RIA measurements have to be done in conditions representative of the application. Today, the best solution (configuration PMAX) consists of pumping the fiber 80% of the time while the 20% remaining is used to measure the RIA values in a passive mode. In the figure we illustrate the different dose dependences of the RIA at 980 nm and 1550 nm measured with the two configurations: PMAX and PMIN. In the PMAX mode, the induced losses at 980 nm are reduced from 10 dB m^{-1} at 3.5 kGy (350 krad; PMIN down) to less than 6 dB m^{-1} , while at 1550 nm, the losses decrease from 3.5 dB m^{-1} to about 1 dB m^{-1} . Considering these new values for the RIA in the codes, it can be seen that the gain degradation is more efficiently reproduced, almost perfectly for the EDFA based on a COTS fiber. The error is larger for the EDFA based on the rad-hard fiber, especially at higher doses, and it is assumed that this is due to the fact that even if the PMAX configuration allows the positive impact of photobleaching to be better taken into account, its impact remains underestimated due to the 20% of time when the active

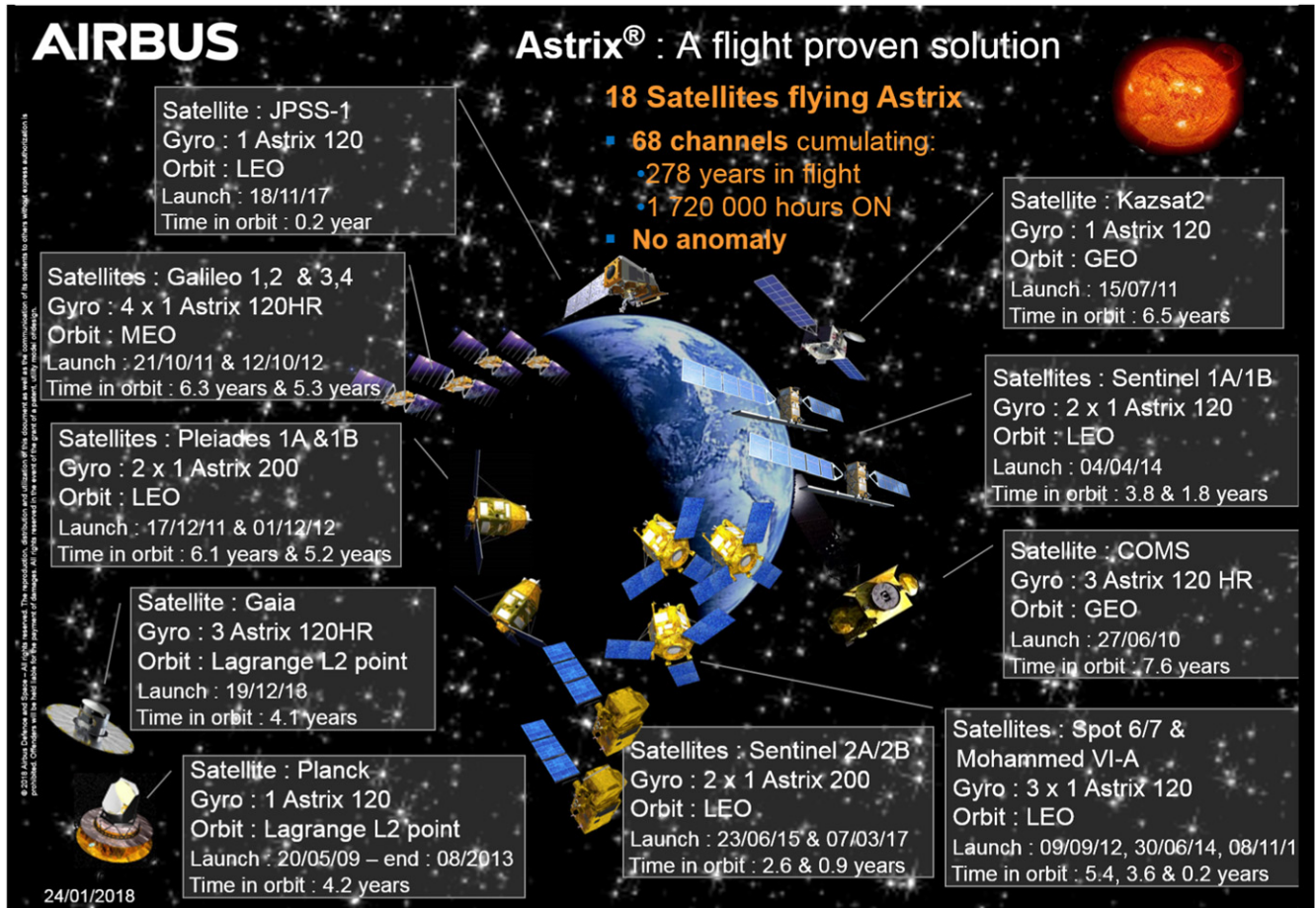


Figure 28. Astrix® fiber optic gyro space fleet (last update: 01/24/18). Image created by Airbus for this article. Used with permission.

fiber is not pumped. From these results, it clearly appears that for future missions, a model of the RIA dependence on dose and on injected power will have to be built to design prediction tools able to cover the variety of mission profiles in use.

4.5. Gyroscopes: recent advances

Four main mitigation strategies are followed to overcome radiation issues in commercial space FOGs. The first one remains the design of the targeted mission: adapting the orbit and optimizing the FOG localization inside the spacecraft are efficient mitigation mechanisms but are out of the scope of this topical review. Another way to decrease the radiation constraints is shielding (as discussed in section 1.2). Commercial FOGs indeed possess internal metallic shielding designed to decrease the level of TID dose on their sub-parts identified as the most radiation sensitive. Obviously, as inferred from the results and discussion presented in section 3.4, the third and most important mitigation approach consists of the identification and use of radiation-resistant optical fibers for both the optical source (REDFs) and for Sagnac’s coil (PSC PMF) [320, 321]. Another less-studied phenomenon to reduce the radiation impact is the photobleaching effect, which is partially able to recover the RIA in the FOG REDF and PMF fibers. This positive effect,

combined with low dose rate steady state irradiation and space temperature constraints, remains difficult to quantify in orbit, and its relative impact is also strongly fiber-dependent, so its contribution to the FOG response remains subject to speculation [322].

By combining all these approaches, it is possible to obtain high-performance FOGs able to operate in space. This is well demonstrated today by the recent data analysis of the ageing of several real in-orbit commercial FOGs of the Astrix® family. The analysis of this huge amount of in-flight data first reveals no anomaly over 1720 000 h of operation, and second shows no detectable impact of the RIA on the performance of radiation-hardened space FOGs after several years of navigation at LEO, MEO and GEO orbits [322]. These Astrix® FOGs cover a variety of space mission profiles (see figure 28) and have presented excellent results with very limited system degradation in terms of scale factor and noise, which is easily mitigated in-flight. An important outcome of this in-flight data, which is discussed in detail in [322], is that the degradation predictions that have been extrapolated from on-ground radiation tests lead to an overestimation of the observed changes in space. To the best of our current knowledge, this may be explained by the positive impact of the lower dose rate in space than during in-lab tests, and also because continuous in-orbit optical photobleaching is more efficient than expected in real conditions (varying temperature, etc). More studies on these effects will have to be

performed in the future to understand more precisely the basic mechanisms at stake.

5. Conclusions and perspectives

In this article, we review the main fiber-related technologies that are being used today or are under evaluation for integration in the harsh environments associated with low to extremely high levels of ionizing or nonionizing radiation. After describing the operation principles of the main technologies, we described the radiation response for each one, and if needed, the identified solutions to enhance its radiation tolerance. Generally, for a large amount of the targeted applications, optical fibers and fiber sensors (OFSs) present key advantages, and even if they are not immune to radiation, adequate solutions for each application can be found using either commercial telecom-grade fibers or commercially available radiation-hardened optical fibers. Considering the numerous intrinsic and extrinsic parameters affecting the fiber radiation response, it remains mandatory, before the implementation of fiber-based solutions, to evaluate their vulnerability with respect to the environmental constraints: radiation, the presence of gas, high operation temperature. Today, the response of an optical fiber or OFS remains too complex to be predictable by multi-scale simulation, and even if recent progress has been made on the atomic scale [323], accelerated radiation test experiments are still mandatory, sometimes with facilities covering only partially the characteristics of future environments (e.g. for megajoule-class lasers). Considering the increasing interest of industries in radiation-tolerant optical fibers, mitigation techniques (or radiation hardening techniques) of the radiation effects, mainly radiation-induced attenuation (RIA), have been developed. In particular, for space applications, very promising developments have been demonstrated, allowing radiation tolerant rare-earth-doped optical fibers, EDFA and EYDFA to be conceived for today's space missions. For future missions, such as JUICE missions, higher dose levels and larger operation temperature ranges are expected, pushing the development and qualification of even more radiation-tolerant devices and systems. In the future, driven by increasing free space optical communication needs, studies will also have to be performed on combined radiation and thermal effects in high-power fiber-based amplifiers (>10 W). In recent years, distributed OFS performance has strongly increased, making these sensors very attractive candidates for integration in nuclear facilities, high-energy physics facilities (CERN) or fusion-related facilities (ITER, NIF, LMJ). For these on-Earth applications, recent studies show that most of these sensors can operate in radiation-rich environments, even if for some of them, such as RDTS, specific mitigation techniques have to be applied at the system level to ensure measurement precision. Before these technologies can be used in satellites, progress is necessary on the integration and radiation hardening of the interrogation parts of these sensors.

This should be facilitated in the next year by the increasing performance of integrated photonic technologies such as ASPICSSs. As fiber-based applications are implemented in radiation environments more and more, future studies will also have to be devoted to establishing new guidelines and qualification procedures, considering the new generation of optical fibers and the diversity of fiber-related applications, to complete the existing reference documents [226].

Acknowledgments

The authors would like to thank N Richard, C Marcandella, J Baggio, P Paillet, M Gaillardin and M Raine; O Duhamel and M Martinez from CEA DAM (France), J-P Meunier, J-Y Michalon, B Tortech, J Bisutti, G Origlio, M Vivona, A Alessi, X Phéron, D Di Francesca, S Rizzolo, C Cangialosi, I Planes, I Reghioia, T Blanchet, C Sabatier, C Muller, T Allanche and V De Michele from the University of Saint-Etienne (France), and M Cannas, R Boscaino, F Gelardi and S Agnello from the University of Palermo, for the fruitful discussion about radiation effects on silica-based glasses.

ORCID iDs

Sylvain Girard  <https://orcid.org/0000-0002-9804-8971>

References

- [1] Barth J L 2003 Space and atmospheric environments: from low Earth orbits to deep space *Proc. 9th Int. Symp. on Materials in a Space Environment (Noordwijk, The Netherlands, 16–20 June)*
- [2] Miquel J-L, Lion C and Vivini P 2016 The Laser MegaJoule: LMJ & PETAL status and program overview *J. Phys.: Conf. Ser.* **688** 012067
- [3] Miller G H, Moses E I and Wuest C R 2004 The National Ignition Facility: enabling fusion ignition for the 21st century *Nucl. Fusion* **44** 228–38
- [4] Motojima O 2015 The ITER project construction status *Nucl. Fusion* **55** 104023
- [5] Sharp R E and Garlick D R 1994 Radiation effects on electronic equipment, a designers'/users' guide for the nuclear power industry *INIS* **25** 25067411
- [6] Ravotti F, Glaser M, Rosenfeld A B, Lerch M L F, Holmes-Siedle A G and Sarabayrouse G 2007 Radiation monitoring in mixed environments at CERN: from the IRRAD6 facility to the LHC experiments *IEEE Trans. Nucl. Sci.* **54** 1170–7
- [7] Friebele E J 1979 Optical fiber waveguides in radiation environments *Opt. Eng., Bellingham* **18** 186552
- [8] Golob J E, Lyons P B and Looney L D 1977 Transient radiation effects in low-loss optical waveguides *IEEE Trans. Nucl. Sci.* **24** 2164–8
- [9] Griscom D L 1985 Nature of defects and defect generation in optical glasses *Proc. SPIE* **0541** 38–59
- [10] Friebele E J, Askins C G, Gingerich M E, Marrone M J and Griscom D L 1985 Overview of radiation effects in fiber optics *Proc. SPIE* **0541** pp 70–80

- [11] Griscom D L 1985 Defect structure of glass: some outstanding questions in regard to vitreous silica *Non-Crystalline Solids* **73** 61–77
- [12] Griscom D L 1988 Intrinsic and extrinsic point defects in a-SiO₂ *The Physics and Technology of Amorphous* ed R A B Devine (New York: Plenum) pp 125–34
- [13] Wall J A and Bryant J F 1975 Radiation effects on fiber optics *Physical Sciences Research Papers AFCRI-TR-7* 5-0190 Physical Sciences Research Papers No. 627 Solid State Sciences Laboratory
- [14] Girard S, Baggio J and Bisutti J 2006 14 MeV neutron, gamma-ray, and pulsed x-ray radiation-induced effects on multimode silica-based optical fibers *IEEE Trans. Nucl. Sci.* **53** 3750–7
- [15] Benabdesselam M, Mady F, Girard S, Mebrouk Y, Duchez J B, Gaillardin M and Paillet P 2013 Performance of Ge-doped optical fiber as a thermoluminescent dosimeter *IEEE Trans. Nucl. Sci.* **60** 4251–6
- [16] Primak W 1958 Fast-neutron-induced changes in quartz and vitreous silica *Phys. Rev. B* **110** 1240–54
- [17] Rizzolo S *et al* 2017 Evaluation of distributed OFDR-based sensing performance in mixed neutron/gamma radiation environments *IEEE Trans. Nucl. Sci.* **64** 61–7
- [18] Cheymol G, Long H, Villard J F and Brichard B 2008 High level gamma and neutron irradiation of silica optical fibers in CEA OSIRIS nuclear reactor *IEEE Trans. Nucl. Sci.* **55** 2252–8
- [19] Barth J 2009 Evolution of the radiation environments *RADECS 2009 Short Course (Bruges, Belgium)*
- [20] Bourgade J L *et al* 2008 Present LMJ diagnostics developments integrating its harsh environment *Rev. Sci. Instrum.* **79** 10F301
- [21] Delepine-Lesoille S *et al* 2017 France's state of the art distributed optical fibre sensors qualified for the monitoring of the French underground repository for high level and intermediate level long lived radioactive wastes *Sensors* **17** 1377
- [22] Stone J 1987 Interactions of hydrogen and deuterium with silica optical fibres: a review *J. Lightwave Technol.* **5** 712–33
- [23] Røed K, Brugger M and Spiez G 2012 An overview of the radiation environment at the LHC in light of R2E irradiation test activities *CERN-ATS-Note-2011-077 TECH*
- [24] Yamamoto S *et al* 2000 Impact of irradiation effects on design solutions for ITER diagnostics *J. Nucl. Mater.* **283–287** 60–9
- [25] Remy L, Cheymol G, Gusarov A, Morana A, Marin E and Girard S 2016 Compaction in optical fibres and fibre Bragg gratings under nuclear reactor high neutron and gamma fluence *IEEE Trans. Nucl. Sci.* **63** 2317–22
- [26] Ferdinand P, Magne S and Laffont G 2013 Optical fiber sensors to improve the safety of nuclear power plants *Proc. SPIE* **8924** 89242G
- [27] O'Keefe S 2017 Optical fibres for radiation dosimetry *Fiber Optic Sensors: Current Status and Future Possibilities* ed I R Matias, S Ikezawa and J Corres (Berlin: Springer)
- [28] Agrawal G P 2010 *Fiber-Optic Communication Systems* 4th edn (New York: Wiley) (<https://doi.org/10.1002/9780470918524>)
- [29] Bourgade J L *et al* 2008 Diagnostic components in harsh environments: possible overlap in R&D requirements of IC and MF systems *Rev. Sci. Instrum.* **79** 10F304
- [30] Emslie C 2015 Fiber-optic components: harsh-environment optical fiber coatings: beauty is only skin deep *Laser Focus World*
- [31] Santin G, Truscott P, Gaillard R and Alia R G 2017 Radiation environments: space, avionics ground and below *RADECS 2017 Short Course Notebook*
- [32] Spjeldvik W N and Rothwell P L 1985 *Handbook of Geophysics And The Space Environment*
- [33] Sawyer D M and Vette J I 1976 AP-8 trapped proton environment for solar maximum and solar minimum *NASA TM-X-72605*
- [34] Vette J I 1991 The AE-8 trapped electron model environment *NSSDC/WDC-A-R&S* pp 91–24
- [35] Ginot G P *et al* 2013 AE9, AP9 and SPM: New models for specifying the trapped energetic particle and space plasma environment *Space Sci. Rev.* **179** 579–615
- [36] Robert Johnston W, O'Brien T P, Ginot G P, Huston S L, Guild T B and Fennelly J A 2014 AE9/AP9/SPM: new models for radiation belt and space plasma specification *Proc. SPIE* **9085** 908508
- [37] O'Brien P 2016 The AE9/AP9/SPM next generation radiation specification models *Progress Report, Proc. Space Radiation Modelling and Data Analysis, Workshop*
- [38] AE9/AP9/SPM (<https://vdl.afml.af.mil/programs/ae9ap9/>)
- [39] Boscher D, Sicard-Piet A, Lazaro D, Cayton T and Rolland G 2014 A new proton model for low altitude high energy specification *IEEE Trans. Nucl. Sci.* **61** 3401–7
- [40] ECSS Standard 2008 ECSS E-10-04 space environment standard *ESA/ESTEC, Technical Report*
- [41] Fourcault W, Léger J-M, Costes V, Fratter I and Mondin L 2010 Athermal fiber laser for the swarm absolute scalar magnetometer *Int. Conf. on Space Optics (ICSO) (Rhosse, Greece, 4–8 October)*
- [42] Seltzer S M 1980 SHIELDOSE: A computer code for space-shielding radiation dose calculations *National Bureau of Standards Technical Note* 1116
- [43] Seltzer S M 1979 Electron, electron-bremsstrahlung and proton dose depth data for space-shielding applications *IEEE Trans. Nucl. Sci.* **NS-26** 4896–904
- [44] Seltzer S M 1994 Updated calculations for routine space-shielding radiation dose estimates: SHIELDOSE2 *National Institute of Standards and Technology Report NISTIR* 5477
- [45] Ott M N 2010 Space flight applications of optical fiber: 30 years of space flight success *Invited paper, TuA2, IEEE Photonics Society Avionics, Fiber-Optics and Photonics Technology Conf. (AVFOP) (Denver, CO, 21–23 September)*
- [46] Reutlinger A, Glier M, Zuknik K-H, Hoffmann L, Müller M, Rapp S, Kurvin C, Ernst T, McKenzie I and Karafolas N 2017 Fiber optic sensing for telecommunication satellites *Proc. SPIE* **10566** 105661C
- [47] <https://escies.org/download/webDocumentFile?id=1622>
- [48] <https://spaceequipment.airbusdefenceandspace.com/avionics/fiber-optic-gyroscopes/astrix-120/>
- [49] COTS Fibre Optic Components in SMOS/MOHA—ESCIES (<https://escies.org/download/webDocumentFile?id=1606>)
- [50] McKenzie I SMOS—The 1st Deployment of an Optical Harness on a Deployment of an Optical Harness on a Satellite CCT CNES.
- [51] NASA facts 'Lunar Laser Communication Demonstration NASA's First Space Laser Communication System Demonstration' (https://www.nasa.gov/sites/default/files/llcdfactsheet.final_web_.pdf)
- [52] http://esa.int/Our_Activities/Telecommunications_Integrated_Applications/EDRS/Start_of_service_for_Europe_s_SpaceDataHighway
- [53] Kashyap R 2010 *Fiber Bragg Gratings* 2nd edn (New York: Elsevier)
- [54] Bao X and Chen L 2012 Recent progress in distributed fiber optic sensors *Sensors* **12** 8601–39
- [55] Measures R M 2001 *Structural Monitoring with Fiber Optic Technology* (San Diego, CA: Academic) ch 2
- [56] Hartog A H, Leach A P and Gold M P 1985 Distributed temperature sensing in solid-core fiber *Electron. Lett.* **21** 1061–2

- [57] Henschel H, Körfer M, Kuhnenn J, Weinand U and Wilf F 2004 Fibre optic radiation sensor systems for particle accelerators *Nucl. Instrum. Methods Phys. Res. A* **526** 537–50
- [58] Toccafondo I, Nannipieri T, Signorini A, Guillermain E, Kuhnenn J, Brugger M and Di Pasquale F 2015 Raman distributed temperature sensing at CERN *IEEE Photonics Technol. Lett.* **27** 2182–5
- [59] Dignonnet M J F 2001 Rare-earth-doped fiber lasers and amplifiers *Revised and Expanded* (Boca Raton, FL: CRC Press)
- [60] Lefevre H 2014 *The Fiber-Optic Gyroscope* (Norwood, MA: Artech House)
- [61] Stajanca P and Krebber K 2017 Radiation-induced attenuation of perfluorinated polymer optical fibers for radiation monitoring *Sensors* **17** 1959
- [62] O’Keeffe S, Fernandez-Fernandez A, Fitzpatrick C, Brichard B and Lewis E 2007 Real-time gamma dosimetry using PMMA optical fibres for applications in the sterilization industry *Meas. Sci. Technol.* **18** 3171–6
- [63] Henschel H, Kuhnenn J and Weinand U 2005 High radiation hardness of a hollow core photonic bandgap fiber *2005 8th European Conf. on Radiation and Its Effects on Components and Systems, Cap d’Agde* pp LN4-1–4
- [64] Girard S, Baggio J and Leray J L 2005 Radiation-induced effects in a new class of optical waveguides: the air-guiding photonic crystal fibers *IEEE Trans. Nucl. Sci.* **52** 2683–8
- [65] Olanterä L, Sigaud C, Troska J, Vasey F, Petrovich M N, Poletti F, Wheeler N V, Wooler J P and Richardson D J 2013 Gamma irradiation of minimal latency hollow-core photonic bandgap fibres *J. Instrum.* **8** C12010
- [66] European Space Agency 2013 Statement of Work ECI4: space validation of rad-hard erbium optical fibre amplifier at 1.55 μm *TEC-QTC/2013/ECI4-EEE41*
- [67] Monro T M and Ebendorff-Heidepriem H 2006 Progress in microstructured optical fibers *Annu. Rev. Mater. Res.* **36** 467–95
- [68] Russell P 2003 Photonic crystal fibers *Science* **17** 358–62
- [69] Fernandez-Fernandez A 1997 Photonics for nuclear environments from radiation effects to applications in sensing and data-communication *PhD Dissertation* Faculté Polytechnique de Mons, Mons
- [70] Friebele E J 1991 Correlation of single mode fiber fabrication factors and radiation response *Final Report NRL/MR/6505-92-6939* Naval Research Laboratories
- [71] Ott M 2002 Radiation effects data on commercially available optical fiber: database summary *Proc. IEEE NSREC Data Workshop* pp 24–31
- [72] Bisutti J 2010 Etude de la transmission du signal sous irradiation transitoire dans les fibres optiques *PhD Dissertation* Université de Saint-Etienne, Saint-Etienne, France
- [73] Uffelen M V 2001 Modélisation de systèmes d’acquisition et de transmission à fibres optiques destinés à fonctionner en environnement nucléaire *PhD Dissertation* Université de Paris XI, Paris
- [74] Girard S 2003 Analyse de la réponse des fibres optiques soumises à divers environnements radiatifs *PhD Dissertation* Université de Saint-Etienne, Saint-Etienne, France
- [75] Wijnands T, De Jonge L K, Kuhnenn J, Hoeffgen S K and Weinand U 2008 Optical absorption in commercial single mode optical fibers in a high energy physics radiation field *IEEE Trans. Nucl. Sci.* **55** 2216–22
- [76] Friebele E J, Lyons P B, Blackburn J, Henschel H, Taylor E W, Beauregard G T, West R H, Zagarino P and Smith D 1990 Interlaboratory comparison of radiation-induced attenuation in optical fibers: III. Transient exposures *J. Lightwave Technol.* **8** 977–89
- [77] Friebele E J, Taylor E W, Beauregard G T, Wall J and Barnes C 1988 Interlaboratory comparison of radiation-induced attenuation in optical fibers: I. Steady state exposures *J. Lightwave Technol.* **6** 165–71
- [78] Taylor E W, Friebele E J, Henschel H, West R H, Barnes C and Krinski J A 1990 Interlaboratory comparison of radiation-induced attenuation in optical fibers: II. Steady state exposures *J. Lightwave Technol.* **8** 967–76
- [79] Borgermans P 2001 Spectral and kinetic analysis of radiation induced optical attenuation in silica: towards intrinsic fiber optic dosimetry? *PhD Dissertation* Vrije Universiteit, Brussels
- [80] Deparis O 1997 Etude physique et expérimentale de la tenue des fibres optiques aux radiations ionisantes par spectrométrie visible-infrarouge *PhD Dissertation* Faculté Polytechnique de Mons, Mons
- [81] Brichard B 2008 Systèmes à fibres optiques pour infrastructures nucléaires: du durcissement aux radiations à l’application *PhD Dissertation* IES—Institut d’Electronique du Sud, Montpellier
- [82] Cangialosi C 2016 Performances of Raman and Brillouin fiber-based sensing of temperature and strain in harsh environments *PhD Dissertation* University of Saint-Étienne, Saint-Etienne
- [83] Francesca D D 2015 Roles of dopants, interstitial O₂ and temperature in the effects of irradiation on silica-based optical fibers *PhD Dissertation* University of Saint-Étienne, Saint-Etienne
- [84] Origlio G 2009 Properties and radiation response of optical fibers: role of dopants *PhD Dissertation* University of Saint-Étienne, Saint-Etienne
- [85] Morana A 2013 Gamma-rays and neutrons effects on optical fibers and Bragg gratings for temperature sensors *PhD Dissertation* University of Saint-Étienne, Saint-Etienne
- [86] Tortech B 2008 Effets des radiations sur des fibres optiques dopées erbium *PhD Dissertation* University of Saint-Étienne, Saint-Etienne
- [87] Zotov K V, Likhachev M E, Tomashuk A L, Bubnov M L, Yashkov M V, Guryanov A N and Klyamkin S N 2008 Radiation-resistant erbium-doped fiber for spacecraft applications *IEEE Trans. Nucl. Sci.* **55** 2213–5
- [88] Fox B P 2013 Investigation of ionizing-radiation-induced photodarkening in rare-earth-doped optical fiber amplifier materials *PhD Dissertation* University of Arizona
- [89] Jérémie T 2013 Impact de la nanostructuration des fibres dopées erbium sur leurs performances: application aux contraintes du spatial *PhD Dissertation* University of Montpellier
- [90] Ayoub L 2017 Rare earth doped optical fibers and amplifiers for space applications *PhD Dissertation* University of Saint-Étienne
- [91] Likhachev M E, Bubnov M M, Zotov K V, Tomashuk A L, Lipatov D S, Yashkov M V and Guryanov A N 2013 Radiation resistance of Er-doped silica fibers: effect of host glass composition *J. Lightwave Technol.* **31** 749–55
- [92] Henschel H, Kohn O, Schmidt H U, Kirchof J and Unger S 1998 Radiation-induced loss of rare earth doped silica fibres *IEEE Trans. Nucl. Sci.* **45** 1552–7
- [93] Jean-Bernard D 2015 Étude du noircissement dans les fibres optiques dopées ytterbium: interaction entre photo- et radio-noircissement *PhD Dissertation* University of Nice
- [94] Lezius M *et al* 2012 Radiation induced absorption in rare earth doped optical fibers *IEEE Trans. Nucl. Sci.* **59** 425–33
- [95] Friebele E J, Brambani L A, Gingerich M E, Hickey S J and Onstott J R 1989 Radiation-induced attenuation in polarization maintaining fibers: low dose rate response, stress, and materials effects *Appl. Opt.* **28** 5138–43
- [96] Chamorovskii Y K, Butov O V, Ivanov G I, Kolosovskii A A, Voloshin V V, Vorob’ev I L and Golant K M 2009 N-doped-silica-core polarization maintaining fibre for gyros and other sensors for application in space industry *Proc. SPIE* **7503** 75036T

- [97] Taylor E W, Wilson V R, Vigil M L, Lemire R A and Thompson E E 1989 Ionization-induced nonequivalent absorption in a birefringent silica fiber *IEEE Photon. Technol. Lett.* **1** 248–9
- [98] Girard S, Yahya A, Boukenter A, Ouerdane Y, Meunier J-P, Kristiansen R E and Vienne G 2002 Gamma radiation-induced attenuation in photonic crystal fibre *IEE Electron. Lett.* **38** 1169–71
- [99] Kosolapov A F, Nikolin I V, Tomashuk A L, Semjonov S L and Zabezhaïlov M O 2004 Optical losses in as prepared and gamma-irradiated microstructured silica-core optical fibers *Inorg. Mater.* **40** 1229–32
- [100] Girard S, Ouerdane Y, Bouazaoui M, Marcandella C, Boukenter A, Bigot L and Kudlinski A 2011 Transient radiation-induced effects on solid core microstructured optical fibers *Opt. Express* **19** 21760–7
- [101] Hill K O and Meltz G 1997 Fiber Bragg grating technology: fundamentals and overview *J. Lightwave Technol.* **15** 1263–76
- [102] Hill K O, Fujii Y, Johnson D C and Kawasaki B S 1978 Photosensitivity in optical fiber waveguides: application to reflection filter fabrication *Appl. Phys. Lett.* **32** 647–9
- [103] Malo B, Hill K O, Bilodeau F, Johnson D C and Albert J 1993 Point by point fabrication of micro-Bragg gratings in photosensitive fibre using single excimer pulse refractive index modification techniques *Electron. Lett.* **29** 1668–9
- [104] Hill K O, Malo B, Bilodeau F, Johnson D C and Albert J 1993 Bragg gratings fabricated in monomode photosensitive optical fiber by UV exposure through a phase mask *Appl. Phys. Lett.* **62** 1035–7
- [105] Kersey A D, Davis M A, Patrick H J, LeBlanc M, Koo K P, Askins C G, Putnam M A and Friebel E J 1997 Fiber grating sensors *J. Lightwave Technol.* **15** 1442–63
- [106] Morana A *et al* 2015 Influence of photo-inscription conditions on the radiation-response of fiber Bragg gratings *Opt. Express* **23** 8659–69
- [107] Morana A, Girard S, Marin E, Marcandella C, Paillet P, P erisse J, Mac e J-R, Boukenter A, Cannas M and Ouerdane Y 2014 Radiation tolerant fiber Bragg gratings for high temperature monitoring at MGy dose levels *Opt. Lett.* **39** 5313–6
- [108] Tam T T, Trung D Q, Vu T A, Minh L H and Chung D N 2007 Investigation of the embedded fiber Bragg grating temperature sensor *VNU J. Sci. Math. Phys.* **23** 237–42
- [109] Erdogan T, Mizrahi V, Lemaire P J and Monroe D 1994 Decay of ultraviolet-induced fiber Bragg gratings *J. Appl. Phys.* **76** 73–80
- [110] Baker S R, Rourke H N, Baker V and Goodchild D 1997 Thermal decay of fiber Bragg gratings written in boron and germanium codoped silica fiber *J. Lightwave Technol.* **15** 1470–7
- [111] Barber D A and Rizvi N H 2003 Practical study of the effects of exposure conditions on the quality of fibre Bragg gratings written with excimer and argon-ion lasers *Proc. SPIE* **4941** 494110
- [112] Mihailov S J, Smelser C W, Lu P, Walker R B, Grobncic D, Ding H, Henderson G and Unruh J 2003 Fiber Bragg gratings made with a phase mask and 800-nm femtosecond radiation *Opt. Lett.* **28** 995–7
- [113] Tsai T-E, Williams G M and Friebel E J 1997 Index structure of fiber Bragg gratings in Ge-SiO₂ fibers *Opt. Lett.* **22** 224–6
- [114] Mihailov S J, Smelser C W, Grobncic D, Walker R B, Lu P, Ding H and Unruh J 2004 Bragg gratings written in All-SiO₂ and Ge-doped core fibers with 800 nm femtosecond radiation and a phase mask *J. Lightwave Technol.* **22** 94–1002
- [115] Smelser C W, Mihailov S J and Grobncic D 2004 Hydrogen loading for fiber grating writing with a femtosecond laser and a phase mask *Opt. Lett.* **29** 2127–9
- [116] Archambault J-L, Reekie L and Russell P S J 1993 100% reflectivity Bragg reflectors produced in optical fibers by single excimer laser pulses *Electron. Lett.* **29** 453–5
- [117] Smelser C W, Mihailov S J and Grobncic D 2005 Formation of type I-IR and type II-IR gratings with an ultrafast IR laser and a phase mask *Opt. Express* **13** 5377–86
- [118] Liu Y, Williams J A R, Zhang L and Bennion I 2002 Abnormal spectral evolution of fiber Bragg gratings in hydrogenated fibers *Opt. Lett.* **27** 586–8
- [119] Dong L, Liu W F and Reekie L 1996 Negative-index gratings formed by a 193 nm excimer laser *Opt. Lett.* **21** 2032–4
- [120] Pissadakis S and Konstantaki M 2005 Type IIA gratings recorded in B-Ge codoped optical fibre using 213 nm Nd:YAG radiation *31st European Conf. on Optical Communication* 3, pp 563–4
- [121] Lindner E, Canning J, Chojetzki C, Bruckner S, Becker M, Rothhardt M and Bartelt H 2011 Thermal regenerated type IIA fiber Bragg gratings for ultra-high temperature operation *Opt. Commun.* **284** 183–5
- [122] Martinez A, Dubov M, Khrushchev I and Bennion I 2006 Photo-induced modifications in fiber gratings inscribed directly by infrared femtosecond irradiation *IEEE Photonics Technol. Lett.* **18** 2266–8
- [123] Martinez A, Khrushchev I and Bennion I 2005 Thermal properties of fiber Bragg gratings inscribed point-by-point by an infrared femtosecond laser *Electron. Lett.* **41** 176–7
- [124] Agrawal G P 2012 *Nonlinear Fiber Optics* 5th edn (New York: Academic)
- [125] Sakaguchi S, Todoroki S-I and Shibata S 1996 Rayleigh scattering in silica glasses *J. Am. Ceram. Soc.* **79** 2821–4
- [126] Dakin J P 1993 Distributed optical fiber sensors *Proc. SPIE* **1797** 179733
- [127] Li Y, Zhang F and Yoshino T 2003 Wide temperature-range Brillouin and Rayleigh optical-time-domain reflectometry in a dispersion-shifted fiber *Appl. Opt.* **42** 3772–5
- [128] Gifford D K, Soller B J, Wolfe M S and Froggatt M E 2005 Distributed fiber-optic temperature sensing using Rayleigh backscatter *31st European Conf. on Optical Communication (ECOC 2005)* 3, 511–2
- [129] Th evenaz L 2010 Novel schemes for optical signal generation using laser injection locking with application to Brillouin sensing *Front. Optoelectron. China* **3** 13–21
- [130] Kurashima T, Horiguchi T and Tateda M 1990 Distributed-temperature sensing using stimulated Brillouin scattering in optical silica fibers *Opt. Lett.* **15** 1038–40
- [131] Ferraro J R, Namamoto K and Brown C W 2003 *Introductory Raman Spectroscopy* (New York: Academic)
- [132] Fernandez Fernandez A, Rodeghiero P, Brichard B, Berghmans F, Hartog A H, Hughes P, Williams K and Leach A P 2005 Radiation-tolerant Raman distributed temperature monitoring system for large nuclear infrastructures *IEEE Trans. Nucl. Sci.* **52** 2689–94
- [133] Failliau G, Beaumont O, Razouk R, Delepine Lesoille S, Landolt M, Courthial B, H enault J M, Martinot F, Bertrand J and Hay B 2018 A metrological comparison of Raman-distributed temperature sensors *Measurement* **116** 18–24
- [134] Delepine-Lesoille S, Planes I, Landolt M, Hermand G and Perrochon O 2017 Compared performances of Rayleigh Raman and Brillouin distributed temperature measurements during concrete container fire test *Optical Fiber Sensors Conf. (OFS) 25th* pp 1–4
- [135] Delepine-Lesoille S *et al* 2012 Industrial qualification process for optical fibers distributed strain and temperature sensing in nuclear waste repositories *J. Sensors* **2012** 369375
- [136] Cornwell D 2016 Space-based laser communications break threshold *Optics Photonics News* **27** 24–31
- [137] Dreischer T, Thieme B, Bacher M and Buchheim K 2012 OPTEL- μ : A compact system for optical downlink from LEO satellites *SpaceOps* **1** 789–98

- [138] Yamakawa S, Chishiki Y, Sasaki Y, Miyamoto Y and Kohata H 2015 JAXA's optical data relay satellite programme *ICSOS*
- [139] Muehlnikel G, Kämpfner H, Heine F, Zech H, Troendle D, Meyer R and Philipp-May S 2012 The alphasat GEO laser communication terminal flight acceptance tests *Proc. Int. Conf. on Space Optical Systems and Applications (ICSOS) 2012* pp 1–4
- [140] Chishiki Y, Yamakawa S, Takano Y, Miyamoto Y, Araki T and Kohata H 2016 Overview of optical data relay system in JAXA *Proc. SPIE* **9739** 97390D
- [141] Qian S-E 2016 *Optical Payload for Space Missions* (New York: Wiley)
- [142] Kehayas E, Stampoulidis L, Henderson P, Robertson A, Van Dijk F, Achouche M, Le Kernec A, Sotom M, Schuberts F and Brabant T 2017 The European project HIPPO high-power photonics for satellite laser communications and on-board optical processing *Proc. SPIE* **10563** 105635C
- [143] Ladaci A, Girard S, Mescia L, Robin T, Laurent A, Cadier B, Boutillier M, Ouerdane Y and Boukenter A 2017 Optimization of rare-earth-doped amplifiers for space mission through a hardening-by-system strategy *Proc. SPIE* **10096** 100960F
- [144] Ladaci A, Girard S, Mescia L, Robin T, Laurent A, Cadier B, Boutillier M, Ouerdane Y and Boukenter A 2017 Optimized radiation-hardened erbium doped fiber amplifiers for long space missions *J. Appl. Phys.* **121** 163104
- [145] Mescia L, Girard S, Bia P, Robin T, Laurent A, Prudenzano F, Boukenter A and Ouerdane Y 2014 Optimization of the design of high power Er³⁺/Yb³⁺-codoped fiber amplifiers for space missions by means of particle swarm approach *IEEE J. Sel. Top. Quantum Electron.* **20** 3100108
- [146] Girard S *et al* 2013 Design of radiation-hardened rare-earth doped amplifiers through a coupled experiment/simulation approach *J. Lightwave Technol.* **31** 1247–54
- [147] Stampoulidis L, Edmunds J, Kechagias M, Stevens G, Farzana J, Welch M and Kehayas E 2017 Radiation-resistant optical fiber amplifiers for satellite communications *Proc. SPIE* **10096** 100960H
- [148] Engin D, Kimpel F, Burton J, Cao H, McIntosh B, Storm M and Gupta S 2013 Highly efficient and athermal 1550 nm-fiber-MOPA-based high power down link laser transmitter for deep space communication *Proc. SPIE* **8610** 86100G
- [149] Stampoulidis L, Kehayas E, Kehayas M, Stevens G, Henwood-Moroney L, Hosking P and Robertson A 2014 Radiation-hard mid-power booster optical fiber amplifiers for high-speed digital and analogue satellite laser communication links *Proc. SPIE* **10563** 1056327
- [150] Li M, Jiao W, Song Y, Zhang X and Chang L 2015 Self-adaptive high anti-radiation EDFA for space optical communication systems *J. Lightwave Technol.* **33** 4513–6
- [151] MacDougall J, Henderson P, Naylor P, Elder J, Norman A, Turner I, Stampoulidis L and Kehayas E 2017 Transmission and pump laser modules for space applications *Proc. SPIE* **10096** 100960I
- [152] Wright M W, Yao H and Marciante J R 2012 Resonant pumping of Er-doped fiber amplifiers for improved laser efficiency in free-space optical communications *IPN Prog. Rep.* **42** 189
- [153] Lefèvre H 2014 *The Fiber-Optic Gyroscope* (Norwood, MA: Artech House)
- [154] Lefèvre H 2012 The fiber optic gyroscope: achievement and perspective *Gyroscopy Navig.* **3** 223–6
- [155] Post E J 1967 Sagnac effect *Rev. Mod. Phys.* **39** 475–94
- [156] Arditty H J and Lefèvre H C 1981 Sagnac effect in fiber gyroscopes *Opt. Lett.* **6** 401–3
- [157] Sagnac G 1913 *Comptes rendus à l'Académie des Sciences* **95** 708–10
- [158] Fesler K A, Kalman R F, Dignonnet M J F, Kim B Y and Shaw H J 1989 Behavior of broadband fiber sources in a fiber gyroscope *Proc. SPIE* **1171** 346–52
- [159] Wysocki P F, Kalman R F, Dignonnet M J F and Kim B Y 1990 1.55 μm broadband fiber sources pumped near 980 nm *Proc. SPIE* **1373** 66–77
- [160] Ashley P R, Temmen M G and Sanghadasa M 2002 Applications of SLDs in fiber optical gyroscopes *Proc. SPIE* **4648** 464812
- [161] Ezekiel S and Udd E 1991 *Fiber Optic Gyro: 15th Anniversary Conf.*, *SPIE Proc.* vol 1585
- [162] Suchocky P G, Findakly T K T K and Leonberger F L 1988 LiNbO₃ integrated optical components for fiber-optic gyroscopes *Proc. SPIE* **993** 240–3
- [163] Ulrich R 1980 Fiber-optic rotation sensing with low drift *Opt. Lett.* **5** 173–5
- [164] Lefevre H, Martin P, Morisse J, Simonpietri P, Vivenot P and Arditty H 1991 High dynamic range fiber gyro with all-digital signal processing *Proc. Vol 1367, Fiber Optic and Laser Sensors VIII*
- [165] Girard S and Marcandella C 2010 Transient and steady state radiation responses of solarization-resistant optical fibers *IEEE Trans. Nucl. Sci.* **57** 2049–55
- [166] Skuja L 1998 Optically active oxygen-deficiency-related centers in amorphous silicon dioxide *J. Non-Cryst. Solids* **239** 16–48
- [167] Johan A, Azaïs B, Malaval C, Raboisson G and Roche M 1989 ASTERIX, un nouveau moyen pour la simulation des effets de débit de dose sur l'électronique *Ann. Phys.* **14** 379–93
- [168] Capoen B, El Hamzaoui H, Bouzaoui M, Ouerdane Y, Boukenter A, Girard S, Marcandella C and Duhamel O 2016 Sol-gel derived copper-doped silica glass as a sensitive material for x-ray beam dosimetry *Opt. Mater.* **51** 104–9
- [169] Girard S *et al* 2017 Potential of copper- and cerium-doped optical fiber materials for proton beam monitoring *IEEE Trans. Nucl. Sci.* **64** 567–73
- [170] Primak W 1958 Fast-neutron-induced changes in quartz and vitreous silica *Phys. Rev. B* **110** 1240–54
- [171] Lell E, Hensler N J, Hensler J R and Burke J 1966 Radiation effects in quartz, silica and glasses *Progr. Ceramic Sci.* vol. 4 (New York: Pergamon) pp 3–93
- [172] León M, Giacomazzi L, Girard S, Richard N, Martín P, Martín-Samos L, Ibarra A, Boukenter A and Ouerdane Y 2014 Neutron irradiation effects on the structural properties of KU1, KS-4V and I301 silica glasses *IEEE Trans. Nucl. Sci.* **61** 1522–30
- [173] Skuja L 2000 Optical properties of defects in silica *Defects in and Related Dielectrics: Science and Technology (NATO Science Series II)* ed G Pacchioni, L Skuja and D L Griscom (Dordrecht: Kluwer) pp 73–116
- [174] Cannas M 1998 Point defects in amorphous SiO₂: optical activity in the visible, UV and vacuum-UV spectral regions *PhD Dissertation* Università di Palermo, Palermo, Italy
- [175] Agnello S 2000 Gamma ray induced processes of point defect conversion in silica *PhD Dissertation* Università di Palermo, Palermo, Italy
- [176] Girard S, Vincent B, Meunier J-P, Ouerdane Y, Boukenter A and Boudrioua A 2004 Spatial distribution of the red luminescence in pristine, gamma-rays and ultraviolet-irradiated multimode optical fibers *Appl. Phys. Lett.* **84** 4215–7
- [177] Torteche B, Girard S, Régnier E, Ouerdane Y, Boukenter A, Meunier J-P, Van Uffelen M, Gusarov A, Berghmans F and Thienpont H 2008 Core versus cladding effects of proton irradiation on erbium-doped optical fiber: micro-luminescence study *IEEE Trans. Nucl. Sci.* **55** 2223–8

- [178] Reghioia I *et al* 2016 Cathodoluminescence investigation of Ge-point defects in silica-based optical fibers *J. Lumin.* **179** 1–7
- [179] Reghioia I *et al* 2017 Cathodoluminescence characterization of point defects in optical fibers *IEEE Trans. Nucl. Sci.* **64** 2318–24
- [180] Girard S, Keurinck J, Boukenter A, Meunier J-P, Ouerdane Y, Azaïs B, Charre P and Vié M 2004 Gamma-rays and pulsed x-ray radiation responses of nitrogen, germanium doped and pure silica core optical fibers *Nucl. Instrum. Methods Phys. Res. B* **215** 187–95
- [181] Beauvois G 2017 Projet DROÏD: étude et développement d'un dosimètre distribué à fibre optique *PhD Dissertation* Université de Perpignan Via Domitia, Perpignan
- [182] Girard S, Keurinck J, Ouerdane Y, Meunier J-P and Boukenter A 2004 Gamma-rays and pulsed x-ray radiation responses of germanosilicate single-mode optical fibers: influence of cladding codopants *J. Lightwave Technol.* **22** 1915–22
- [183] Skuja L, Kajihara K, Smits K, Silins A and Hosono H 2017 Luminescence and Raman detection of molecular Cl₂ and ClCIO molecules in amorphous SiO₂ matrix *J. Phys. Chem. C* **121** 5261–6
- [184] Tanimura K, Itoh C and Itoh N 1988 Transient optical absorption and luminescence induced by band-to-band excitation in amorphous SiO₂ *J. Phys. C: Solid State Phys.* **21** 1869–76
- [185] Sasajima Y and Tanimura K 2003 Optical transitions of self-trapped holes in amorphous SiO₂ *Phys. Rev. B* **68** 014204–014204
- [186] Tomashuk A L, Salgansky M Y, Kashaykin P F, Khopin V F, Sultangulova A I, Nishchev K N, Borisovsky S E, Guryanov A N and Dianov E M 2014 Enhanced radiation resistance of silica optical fibers fabricated in high O₂ excess conditions *J. Lightwave Technol.* **32** 213–9
- [187] Kashaykin P F, Tomashuk A L, Yu. Salgansky M, Guryanov A N and Dianov E M 2017 Anomalies and peculiarities of radiation-induced light absorption in pure silica optical fibers at different temperatures *J. Appl. Phys.* **121** 213104
- [188] Origlio G, Cannas M, Girard S, Boscaino R, Boukenter A and Ouerdane Y 2009 Influence of the drawing process on the defect generation in multistep-index germanium-doped optical fibers *Opt. Lett.* **34** 2282–4
- [189] Girard S, Marcandella C, Alessi A, Boukenter A, Ouerdane Y, Richard N, Paillet P, Gaillardin M and Raine M 2012 Transient radiation responses of optical fibers: influence of MCVD process parameters *IEEE Trans. Nucl. Sci.* **59** 2894–901
- [190] Watanabe Y, Kawazoe H, Shibuya K and Muta K 1986 Structure and mechanism of formation of drawing- or radiation-induced defects in SiO₂:GeO₂ optical fiber *Japan. J. Appl. Phys.* **25** 425–31
- [191] Alessi A, Girard S, Cannas M, Agnello S, Boukenter A and Ouerdane Y 2012 Influence of drawing conditions on the properties and radiation sensitivities of pure-silica-core optical fibers *J. Lightwave Technol.* **30** 1726–32
- [192] Brichard B, Borgermans P, Fernandez A F, Lammens K and Decréton A 2001 Radiation effect in silica optical fiber exposed to intense mixed neutron-gamma radiation field *IEEE Trans. Nucl. Sci.* **48** 2069–73
- [193] Griscom D L, Gingerich M E and Friebele E J 1994 Model for the dose, dose-rate and temperature dependence of radiation-induced loss in optical fibers *IEEE Trans. Nucl. Sci.* **41** 523–6
- [194] Griscom D L 2001 Fractal kinetics of radiation-induced point-defect formation and decay in amorphous insulators: application to color centers in silica-based optical fibers *Phys. Rev. B* **64** 174201
- [195] Henschel H, Köhn O and Schmidt H U 1991 Influence of dose rate on radiation induced loss in optical fibres *Proc. SPIE* **1399** 49–63
- [196] Friebele E J, Askins C G and Gingerich M E 1984 Effect of low dose rate irradiation on doped silica core optical fibers *Appl. Opt.* **23** 4202–8
- [197] Mady F, Benabdesselam M, Duchez J-B, Mebrouk Y and Girard S 2013 Global view on dose rate effects in silica-based fibers and devices damaged by radiation-induced carrier trapping *IEEE Trans. Nucl. Sci.* **60** 4241–348
- [198] Girard S *et al* 2013 Combined high dose and temperature radiation effects on multimode silica-based optical fibers *IEEE Trans. Nucl. Sci.* **60** 4305–13
- [199] Blue T 2012 Testing of performance of optical fibers under irradiation in intense radiation fields when subjected to high temperature *Reactors Concept RD&D* Project No. 09-81
- [200] Regnier E, Flammer I, Girard S, Gooijer F, Achten F and Kuyt G 2007 Low-dose radiation-induced attenuation at infrared wavelengths for P-doped, Ge-doped and pure silica-core optical fibres *IEEE Trans. Nucl. Sci.* **54** 1115–9
- [201] Henschel H and Kohn O 2000 Regeneration of irradiated optical fibres by photobleaching? *IEEE Trans. Nucl. Sci.* **47** 699–704
- [202] Mori H, Suzuki Y and Hirai M 1994 Selective photobleaching of radiation-induced absorption in a-SiO₂ *Nucl. Instrum. Meth. Phys. Res. B* **91** 391–4
- [203] Friebele E J and Gingerich M E 1981 Photobleaching effects in optical waveguide *Appl. Opt.* (<https://doi.org/10.1364/AO.20.003448>)
- [204] Nagasawa K, Hoshi Y, Ohki Y and Yahagi K 1985 Improvement of radiation resistance of pure silica core fibers by hydrogen treatment *Japan. J. Appl. Phys.* **24** 1224–8
- [205] Shelby J E 1979 Radiation effects in hydrogen impregnated vitreous silica *J. Appl. Phys.* **50** 3702–6
- [206] Brichard B, Tomashuk A L, Ooms H, Bogatyrvov V A, Klyamkin S N, Fernandez A F, Berghmans F and Decréton M 2007 Radiation assessment of hydrogen-loaded aluminium-coated pure silica core fibres for ITER plasma diagnostic applications *Fusion Eng. Des.* **82** 2451–5
- [207] Griscom D L 1997 Radiation hardening of pure-silica-core optical fibers: reduction of induced absorption bands associated with self-trapped holes *Appl. Phys. Lett.* **71** 175–7
- [208] Griscom D L 1995 Radiation hardening of pure silica core optical fibers and their method of making by ultra-high-dose gamma ray pre-irradiation *Patent US 5574820 A*
- [209] Shikama T, Kakuta T, Shamoto N, Narui M and Sagawa T 2000 Behavior of developed radiation-resistant silica-core optical fibers under fission reactor irradiation *Fusion Eng. Des.* **51–52** 179–83
- [210] Wijnands T, Aikawa K, Kuhnenn J, Ricci D and Weinand U 2011 Radiation tolerant optical fibers: from sample testing to large series production *J. Lightwave Technol.* **29** 3393–400
- [211] Dianov E M, Golant K M, Khrapko R R, Kurkov A S and Tomashuk A L 1995 Low-hydrogen silicon oxynitride optical fibers prepared by SPCVD *J. Lightwave Technol.* **13** 1471–4
- [212] Tomashuk A L, Dianov E M, Golant K M, Khrapko R R and Spinov D E 1998 Performance of special radiation-hardened optical fibers intended for use in the telecom spectral windows at a megagray level *IEEE Trans. Nucl. Sci.* **45** 1566–9
- [213] Lancry M, Hari Babu B, Ollier N and Poumellec B 2017 Radiation hardening of silica glass through fictive temperature reduction *Int. J. Appl. Glass Sci.* **8** 285–90
- [214] <https://fujikura.co.uk/products/medical-industrial-optical-fibre/radiation-resistant-fibre/>
- [215] <https://photonics.ixblue.com/products-list-detail/rad-hard-harsh-environment-custom-passive-fibers>

- [216] https://prysmiangroup.com/en/en_fibre_speciality-drakaelite_radhard_radhard2.html
- [217] Alessi A, Girard S, Marcandella C, Agnello S, Cannas M, Boukenter A and Ouerdane Y 2011 X-ray irradiation effects on a multistep Ge-doped fiber produced using different drawing conditions *J. Non-Cryst. Solids* **357** 1966–70
- [218] Girard S, Laurent A, Pinsard E, Robin T, Cadier B, Boutillier M, Marcandella C, Boukenter A and Ouerdane Y 2014 Radiation-hard erbium optical fiber and fiber amplifier for both low- and high-dose space missions *Opt. Lett.* **39** 2541–4
- [219] Henschel H, Hoeffgen S K, Krehber K, Kuhnenn J and Weinand U 2008 Influence of fiber composition and grating fabrication on the radiation sensitivity of fiber Bragg gratings *IEEE Trans. Nucl. Sci.* **55** 2235–42
- [220] Blanchet T *et al* 2018 X-rays, protons and electrons radiation effects on type I fiber Bragg gratings *IEEE Trans. Nucl. Sci.* accepted (<https://doi.org/10.1109/TNS.2018.2823771>)
- [221] Rizzolo S, Marin E, Morana A, Boukenter A, Ouerdane Y, Cannas M, Perisse J, Bauer S, Mace J-R and Girard S 2016 Investigation of coating impact on OFDR optical remote fiber-based sensors performances for their integration in high temperature and radiation environments *J. Lightwave Technol.* **34** 4460–5
- [222] Gilard O, Caussanel M, Duval H, Quadri G and Reynaud F 2010 New model for assessing dose, dose rate, and temperature sensitivity of radiation-induced absorption in glasses *J. Appl. Phys.* **108** 093115
- [223] Mashkov V A, Austin W R, Zhang L and Leisure R G 1996 Fundamental role of creation and activation in radiation-induced defect production in high-purity amorphous SiO₂ *Phys. Rev. Lett.* **76** 2926–9
- [224] Griscom D L 2004 γ -ray-induced visible/infrared optical absorption bands in pure and F-doped silica-core fibers: are they due to self-trapped holes? *J. Non-Cryst. Solids* **349** 139–47
- [225] Griscom D L 2006 Self-trapped holes in pure-silica glass: a history of their discovery and characterization and an example of their critical significance to industry *J. Non-Cryst. Solids* **352** 2601–17
- [226] FOTP-64 Procedure for Measuring Radiation-Induced Attenuation in Optical Fibers and Optical Cables, TIA-455-64 1998 Edition, 1998
- [227] IEC 60793-1-54:2018 2018 *Optical Fibres—Part 1–54: Measurement Methods and Test Procedures—Gamma Irradiation*
- [228] Lu Valle M J, Friebele E J, Dimarcello F V, Miller G A, Monberg E M, Wasserman L R, Wisk P W, Yan M F and Birch E M 2006 Radiation-induced loss predictions for pure silica core polarization-maintaining fibers *Proc. SPIE* **6193** 61930J
- [229] Williams G M, Wright B M, Mack W D and Friebele E J 1999 Projecting the performance of erbium-doped fiber devices in a space radiation environment *Proc. SPIE* **3848** 271–80
- [230] Mescia L *et al* 2018 Temperature dependent modelling of cladding-pumped Er³⁺/Yb³⁺-codoped fiber amplifiers for space applications *J. Lightwave Technol.* **36** 3594–602
- [231] Friebele E J and Griscom D L 1979 Radiation effects in glass *Treatise on Materials Science and Technology* ed M T Doremus (New York: Academic)
- [232] Devine R A B 1990 On the physical models of annealing of radiation induced defects in amorphous SiO₂ *Nucl. Instrum. Meth. Phys. Res. B* **46** 261–4
- [233] Liu D T H and Johnston A R 1994 Theory of radiation-induced absorption in optical fibers *Opt. Lett.* **19** 548–50
- [234] Kyoto M, Chigusa Y, Ohe M, Go H, Watanabe M, Matsubara T, Yamamoto T and Okamoto S 1992 Gamma-ray radiation hardened properties of pure silica core single-mode fiber and its data link system in radioactive environments *J. Lightwave Technol.* **10** 289–94
- [235] Levy P W 1985 Overview of nuclear radiation damage processes phenomenological features of radiation damage in crystals and glasses *Proc. SPIE* **0541** 2–24
- [236] Gilard O, Thomas J, Troussellier L, Myara M, Signoret P, Burov E and Sotom M 2012 Theoretical explanation of enhanced low dose rate sensitivity in erbium-doped optical fibers *Appl. Opt.* **51** 2230–5
- [237] Friebele E J, Gingerich M E and Griscom D L 1992 Survivability of optical fibers in space *Proc. SPIE* **1791** 177–88
- [238] Vasiliev S A, Dianov E M, Golant K M, Medvedkov O I, Tomashuk A L, Karpov V I, Grekov M V, Kurkov A S, Leconte B and Niay P 1998 Performance of Bragg and long-period gratings written in N- and Ge-doped silica fibers under γ -radiation *IEEE Trans. Nucl. Sci.* **45** 1580–3
- [239] Niay P *et al* 1994 Behavior of Bragg gratings, written in germanosilicate fibers, against γ ray exposure at low dose rate *IEEE Photon. Technol. Lett.* **6** 1350–2
- [240] Gusarov A I and Hoeffgen S K 2013 Radiation effects on fiber gratings *IEEE Trans. Nucl. Sci.* **60** 2037–53
- [241] Gusarov A I, Brichard B and Nikogosyan D N 2010 Gamma-radiation effects on Bragg gratings written by femtosecond UV laser in Ge-doped fibers *IEEE Trans. Nucl. Sci.* **57** 2024–8
- [242] Gusarov A I and Doyle D B 2001 Modeling of gamma-radiation impact on transmission characteristics of optical glasses *Proc. SPIE* **4547** 78–85
- [243] Lin S, Song N, Jin J, Wang X and Yang G 2011 Effect of grating fabrication on radiation sensitivity of fiber Bragg gratings in gamma radiation field *IEEE Trans. Nucl. Sci.* **58** 2111–7
- [244] Gusarov A I, Berghmans F, Fernandez Fernandez A, Deparis O, Defosse Y, Starodubov D, Décreton M, Mégret P and Blondel M 2000 Behavior of fibre Bragg gratings under high total dose gamma radiation *IEEE Trans. Nucl. Sci.* **47** 688–92
- [245] Fernandez Fernandez A, Brichard B, Berghmans F and Décreton M 2002 Dose-rate dependencies in gamma-irradiated fiber Bragg grating filters *IEEE Trans. Nucl. Sci.* **49** 2874–7
- [246] Morana A, Girard S, Marin E, Lancry M, Grelin J, Marcandella C, Paillet P, Boukenter A and Ouerdane Y 2018 Dependence of the voids-fiber Bragg grating radiation response on temperature, dose and dose-rate *IEEE Trans. Nucl. Sci.* at press (<https://doi.org/10.1109/TNS.2017.2778882>)
- [247] Henschel H, Hoeffgen S K, Kuhnenn J and Weinand U 2010 Influence of manufacturing parameters and temperature on the radiation sensitivity of fiber Bragg gratings *IEEE Trans. Nucl. Sci.* **57** 2029–34
- [248] Faustov A, Safari P, Koutsides C, Gusarov A, Wuilpart M, Mégret P, Kalli K and Zhang L 2012 Highly radiation sensitive type IA FBGs for future dosimetry applications *IEEE Trans. Nucl. Sci.* **59** 1180–5
- [249] Di Francesca D, Li Vecchi G, Girard S, Alessi A, Reghioua I, Boukenter A, Ouerdane Y, Kadi Y and Brugger M 2018 Radiation induced attenuation in single-mode phosphosilicate optical fibers for radiation detection *IEEE Trans. Nucl. Sci.* **65** 126–31
- [250] Jensen F B H, Takada E, Nakazawa M, Kakuta T and Yamamoto S 1998 Consequences of radiation effects on pure-silica-core optical fibers used for Raman-scattering-based temperature measurements *IEEE Trans. Nucl. Sci.* **45** 50–8
- [251] Cangialosi C, Girard S, Boukenter A, Cannas M, Delepine-Lesoille S, Bertrand J, Paillet P and Ouerdane Y 2015 Effects of radiation and hydrogen-loading on the performances of Raman distributed temperature fiber sensors *J. Lightwave Technol.* **33** 2432–8

- [252] Cangialosi C, Girard S, Cannas M, Boukenter A, Marin E, Agnello S, Delepine-Lesoille S, Marcandella C, Paillet P and Ouerdane Y 2016 On-line characterization of gamma radiation effects on single-ended Raman based distributed fiber optic sensor *IEEE Trans. Nucl. Sci.* **63** 2051–7
- [253] Lecomte P 2017 Mesure haute température en environnement irradié par fibre optique utilisant l'effet Raman *Thèse de Doctorat* Université de Perpignan via Domitia
- [254] Alasia D, Fernandez A F, Abrardi L, Brichard B and Thévenaz L 2006 The effects of gamma-radiation on the properties of Brillouin scattering in standard Ge-doped optical fibres *Meas. Sci. Technol.* **17** 1091–4
- [255] Phéron X, Girard S, Boukenter A, Brichard B, Delepine-Lesoille S, Bertrand J and Ouerdane Y 2012 High γ -ray dose radiation effects on the performances of Brillouin scattering based optical fiber sensors *Opt. Express* **20** 26978–85
- [256] Faustov A 2014 Advanced fibre optics temperature and radiation sensing in harsh environments *PhD Thesis* University of Mons, Belgium
- [257] Rizzolo S, Boukenter A, Marin E, Cannas M, Perisse J, Bauer S, Macé J-R, Ouerdane Y and Girard S 2015 Vulnerability of OFDR-based distributed sensors to high γ -ray doses *Opt. Express* **23** 18997–9009
- [258] Rizzolo S, Marin E, Cannas M, Boukenter A, Ouerdane Y, Perisse J, Macé J-R, Bauer S and Girard S 2015 Radiation effects on optical frequency domain reflectometry fiber-based sensor *Opt. Lett.* **40** 4571–4
- [259] Rizzolo S *et al* 2015 Radiation hardened optical frequency domain reflectometry distributed temperature fiber-based sensors *IEEE Trans. Nucl. Sci.* **62** 2988–94
- [260] Faustov A, Gusarov A, Mégret P, Wuilpart M, Zhukov A, Novikov S G, Svetuhin V V and Fotiadi A A 2015 The use of optical frequency-domain reflectometry in remote distributed measurements of the gamma-radiation dose *Tech. Phys. Lett.* **41** 412–5
- [261] Faustov A, Gusarov A, Mégret P, Wuilpart M, Zhukov A, Novikov S G, Svetuhin V V and Fotiadi A A 2016 Application of phosphate doped fibers for OFDR dosimetry *Results Phys.* **6** 86–7
- [262] Zaghoul M A S, Yan A, Chen R, Li M-J, Flammang R, Heibel M and Chen K P 2017 High spatial resolution radiation detection using distributed fiber sensing technique *IEEE Trans. Nucl. Sci.* **64** 2569–77
- [263] Henschel H, Körfer M, Wittenburg K and Wulf F 2000 Fiber optic radiation sensing systems for TESLA *TESLA Report No.* 2000-26
- [264] Toccafondo I, Marin Y E, Guillermain E, Kuhnenn J, Mekki J, Brugger M and Pasquale F D 2017 Distributed optical fiber radiation sensing in a mixed-field radiation environment at CERN *J. Lightwave Technol.* **35** 3303–10
- [265] Rizzolo S *et al* 2016 Optical frequency domain reflectometer distributed sensing using microstructured pure silica optical fibers under radiations *IEEE Trans. Nucl. Sci.* **63** 2038–45
- [266] Rizzolo S, Périssé J, Boukenter A, Ouerdane Y, Marin E, Macé J-R, Cannas M and Girard S 2017 Real time monitoring of water level and temperature in storage fuel pools through optical fibre sensors *Sci. Rep.* **7** 8766
- [267] Williams G M, Putnam M A, Askins C G, Gingerich M E and Friebele E J 1992 Radiation effects in erbium-doped optical fibres *Electron. Lett.* **28** 1816–8
- [268] Girard S *et al* 2009 Radiation effects on ytterbium-and ytterbium/erbium-doped double-clad optical fibers *IEEE Trans. Nucl. Sci.* **56** 3293–9
- [269] Fox B P, Simmons-Potter K, Thomes W J and Kliner D A V 2010 Gamma-radiation-induced photodarkening in unpumped optical fibers doped with rare-earth constituents *IEEE Trans. Nucl. Sci.* **57** 1618–25
- [270] Girard S *et al* 2007 Proton- and gamma-induced effects on erbium-doped optical fibers *IEEE Trans. Nucl. Sci.* **54** 2426–34
- [271] Williams G M and Friebele E J 1998 Space radiation effects on erbium doped fiber devices: sources, amplifiers, and passive measurements *IEEE Trans. Nucl. Sci.* **45** 1531–6
- [272] Ott M 2004 Radiation effects expected for fiber laser/amplifier and rare earth-doped optical fibers *Parts, Packaging and Assembly Technologies Office Survey Report* NASA GSFC
- [273] Xing Y, Zhao N, Liao L, Wang Y, Li H, Peng J, Yang L, Dai N and Li J 2015 Active radiation hardening of Tm-doped silica fiber based on pump bleaching *Opt. Express* **23** 24236–45
- [274] Gusarov A, Van Uffelen M, Hotoleanu M, Thienpont H and Berghmans F 2009 Radiation sensitivity of EDFAs based on highly Er-doped fibers *J. Lightwave Technol.* **27** 1540–5
- [275] Ma J, Li M, Tan L, Zhou Y, Yu S and Ran Q 2009 Experimental investigation of radiation effect on erbium-ytterbium co-doped fiber amplifier for space optical communication in low-dose radiation environment *Opt. Express* **17** 15571–7
- [276] Rose T S, Gunn D and Valley G C 2001 Gamma and proton radiation effects in erbium-doped fiber amplifiers: active and passive measurements *J. Lightwave Technol.* **19** 1918–23
- [277] Li M, Ma J, Tan L Y, Zhou Y P, Yu S Y, Yu J J and Che C 2009 Investigation of the irradiation effect on erbium-doped fiber amplifiers composed by different density erbium-doped fibers *Laser Phys.* **19** 138–42
- [278] Ainslie B J 1991 A review of the fabrication and properties of erbium-doped fibers for optical amplifiers *J. Lightwave Technol.* **9** 220–7
- [279] Griscom D L, Friebele E J and Long K J 1983 Fundamental defect centers in glass: electron spin resonance and optical absorption studies of irradiated phosphorus-doped silica glass and optical fibers *J. Appl. Phys.* **54** 3743–62
- [280] Deschamps T, Vezin H, Gonnet C and Ollier N 2013 Evidence of AIOHC responsible for the radiation-induced darkening in Yb doped fiber *Opt. Express* **21** 8382–92
- [281] Pukhkaya V, Goldner P, Ferrier A and Ollier N 2015 Impact of rare earth element clusters on the excited state lifetime evolution under irradiation in oxide glasses *Opt. Express* **23** 3270–81
- [282] Ladaci A *et al* 2017 X-rays, γ -rays, electrons and protons radiation-induced changes on the lifetimes of Er^{3+} and Yb^{3+} ions in silica-based optical fibers *J. Lumin.* **195** 402–7
- [283] Zotov K V, Likhachev M E, Tomashuk A L, Kosolapov A F, Bubnov M M, Yashkov M V, Guryanov A N and Dianov E M 2008 Radiation resistant Er-doped fibers: optimization of pump wavelength *IEEE Photonics Technol. Lett.* **20** 1476–8
- [284] Gusarov A, Uffelen M V, Hotoleanu M, Thienpont M and Berghmans F 2009 Radiation sensitivity of EDFAs based on highly Er-doped fibers *J. Lightwave Technol.* **27** 1540–5
- [285] Dardaillon R, Thomas J, Myara M, Blin S, Pastouret A, Gonnet C and Signoret P 2017 Broadband radiation-resistant erbium-doped optical fibers for space applications *IEEE Trans. Nucl. Sci.* **64** 1540–8
- [286] Duchez J-B, Mady F, Mebrouk Y, Ollier N and Benabdesselam M 2014 Interplay between photo- and radiation-induced darkening in ytterbium-doped fibers *Opt. Lett.* **39** 5969–72
- [287] Johnston A 2003 Radiations effect in light-emitting and laser diodes *IEEE Trans. Nucl. Sci.* **50**
- [288] Buret T 2006 Fibre optic gyroscopes for space application *OSA Technical Digest* (<https://doi.org/10.1364/OFS.2006.MC4>)

- [289] Thomes W J 2007 Investigation of hermetically sealed commercial LiNbO₃ optical modulator for use in laser/LIDAR space-flight applications *Proc. SPIE* **6713** 67130T
- [290] Taylor E W 2002 Radiation effects in LiNbO₃ *Properties of Lithium Niobate* ed K K Wong (London: INSPEC) pp 359–71
- [291] Henschel H, Kohn O and Schmidt H 1992 Radiation sensitivity of fiber optic couplers *Proc. SPIE* **1791** 151–63
- [292] Gutierrez R, Swift G, Dubovitsky S, Bartman R, Barnes C and Dorsky L 1994 Radiation effects on fused biconical paper wavelength division multiplexer *IEEE Trans. Nucl. Sci.* **41** 1950–7
- [293] Brichard B *et al* 2004 Radiation-hardening techniques of dedicated optical fibres used in plasma diagnostic systems in ITER *J. Nucl. Mater.* **329–333** 1456–60
- [294] A Ivanov I A, Tugarinov S N, Kaschuck Y A, Krasilnikov A V and Bender S E 2000 *In situ* radiation testing of KU and KS-4V optical fibers in a reactor environment *Fusion Eng. Des.* **51–52** 973–8
- [295] Faile S P, Schmidt J J and Roy D M 1967 Irradiation effects in glasses: suppression by synthesis under high pressure hydrogen *Science* **156** 1593–5
- [296] Brichard B, Tomashuk A L, Ooms H, Bogatyryov V A, Klyamkin S N, Fernandez A F, Berghmans F and Decréton M 2007 Radiation assessment of hydrogen-loaded aluminum-coated pure silica core fibres for ITER plasma diagnostic applications *Fusion Eng. Des.* **82** 2451–5
- [297] Di Francesca D, Agnello S, Girard S, Marcandella C, Paillet P, Boukenter A, Ouerdane Y and Gelardi F M 2014 Influence of O₂ loading pre-treatment on the radiation response of pure and fluorine doped silica-based optical fibers *IEEE Trans. Nucl. Sci.* **61** 3302–8
- [298] Grobnc D, Henschel H, Hoeffgen S K, Kuhnenn J, Mihailov S J and Weinand U 2009 Radiation sensitivity of Bragg gratings written with femtosecond IR lasers *Proc. SPIE* **7316** 731611
- [299] AREVALaboratoire Hubert Curien 2013 Procédé de fabrication d'une fibre optique traitée pour capteur de température résistant aux radiations *France Brevet* **13** 62691
- [300] Morana A *et al* 2016 Radiation-hardened fiber Bragg grating based sensors for harsh environments *IEEE Trans. Nucl. Sci.* **64** 68–73
- [301] Kuhnenn J *et al* 2017 Gamma radiation tests of radiation-hardened fiber Bragg grating based sensors for radiation environments *IEEE Trans. Nucl. Sci.* **64** 2307–11
- [302] Morana A *et al* 2016 Radiation-hardened fiber Bragg gratings for space missions *Photonics and Fiber Technology 2016 (ACOFT, BGPP, NP) OSA 2016, paper JT4A.25*
- [303] Ams M, Pal A, Williams R J, Sen R, Withford M J, Sun T and Grattan K T V 2014 Fibre Bragg grating sensors for radiation insensitive measurements *OECC/ACOFT 2014 (Melbourne, Australia)*
- [304] Evenblij R and Leijtens J A P 2014 Space gator: a giant leap for fiber sensing *Presented at Int. Conf. on Space Optics, ICSSO 2014 (Tenerife, Spain)* pp 7–10
- [305] Rizzolo S 2016 Advantages and limitations of distributed optical frequency-domain reflectometry for optical fiber based sensors in harsh environments *PhD Dissertation Université de Saint-Etienne, Saint-Etienne*
- [306] FBGS website: <http://fbgs.com/>
- [307] Morana A, Planes I, Girard S, Cangialosi C, Delepine-Lesoille S, Marin E, Boukenter A and Ouerdane Y 2018 Steady-state radiation-induced effects on the performances of BOTDA and BOTDR optical fiber sensors *IEEE Trans. Nucl. Sci.* **65** 111–8
- [308] Di Francesca D *et al* 2017 Radiation hardened architecture of a single-ended Raman-based distributed temperature sensor *IEEE Trans. Nucl. Sci.* **64** 54–60
- [309] Girard S *et al* 2014 Proton irradiation response of hole-assisted carbon coated erbium-doped fiber amplifiers *IEEE Trans. Nucl. Sci.* **61** 3309–15
- [310] Girard S, Vivona M, Laurent A, Cadier B, Marcandella C, Robin T, Pinsard E, Boukenter A and Ouerdane Y 2012 Radiation hardening techniques for Er/Yb doped optical fibers and amplifiers for space application *Opt. Express* **20** 8457–65
- [311] Thomas J, Myara M, Troussellier L, Burov E, Pastouret A, Boivin D, Mélin G, Gilard O, Sotom M and Signoret P 2012 Radiation-resistant erbium-doped-nanoparticles optical fiber for space applications *Opt. Express* **20** 2435–44
- [312] Pastouret A, Gonnet C and Burov E 2010 Amplifying optical fiber and production method *Patent US* 2010135627
- [313] Boivin D, Fohn T, Burov E, Pastouret A, Gonnet C, Cavani O, Collet C and Lempereur S 2010 Quenching investigation on new erbium doped fibers using MCVD nanoparticle doping process *Proc. SPIE* **7580** 75802B
- [314] Cadier B, Laurent A, Robin T, Girard S and Marcandella C 2013 Radiation-resistant rare-earth-doped optical fiber and method of radiation-hardening a rare-earth-doped optical fiber *US Patent* 20130101261 A1
- [315] Vivona M, Girard S, Robin T, Cadier B, Vaccaro L, Cannas M, Boukenter A and Ouerdane Y 2012 Influence of Ce³⁺ + codoping on the photoluminescence excitation channels of phosphosilicate Er/Yb doped glasses *IEEE Photonics Technol. Lett.* **24** 509–11
- [316] Stroud J S 1965 Color-center kinetics in cerium-containing glass *J. Chem. Phys.* **43** 2442–50
- [317] Stroud J S 1962 Color centers in a cerium-containing silicate glass *J. Chem. Phys.* **37** 836–41
- [318] Zotov K V, Likhachev M E, Tomashuk A L, Bubnov M M, Yashkov M V and Gur'yanyov A N 2007 Radiation-resistant erbium-doped silica fibre *Quantum Electron.* **37** 946–9
- [319] Rehman S and Norin L 2010 Specialty optical fibers for harsh environments *Photonics Spectra* October issue
- [320] Pinsard E, Laurent A, Robin T, Cadier B, Ferrand S, Bonnefois J-J, Moluçon C and Boutillier M 2012 Radiation resistant erbium doped fiber for ASE source and fiber gyroscope application *9th Int. Conf. on Space Optics (ICSSO) (Ajaccio, France)*
- [321] Di Francesca D, Girard S, Agnello S, Alessi A, Marcandella C, Paillet P, Richard N, Boukenter A, Ouerdane Y and Gelardi F 2016 Radiation response of Ce-codoped germanosilicate and phosphosilicate optical fibers *IEEE Trans. Nucl. Sci.* **63** 2058–64
- [322] Paveau A, Cros G, Mangeret R, Mariojous S and Bonnefois J J 2017 Robustness of Astrix fiber optic gyros in space radiative environment *Proc. of American Astronautical Society, Guidance Navigation and Control Conference, Breckenridge, AAS-17-111*
- [323] Richard N *et al* 2014 Coupled theoretical and experimental studies for the radiation hardening of silica-based optical fibers *IEEE Trans. Nucl. Sci.* **61** 1819–25